Calibrated fMRI in the normal, aged and diseased human brain

Thesis submitted in accordance with the requirements of the University of Liverpool for the degree of Doctor in Philosophy

by

Jonathan Alan Goodwin

January 2009

UNIVERSITY OF LIVERPOOL

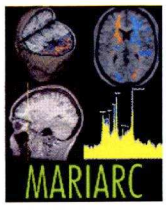

Calibrated fMRI in the normal, aged and diseased human brain

Jonathan Alan Goodwin

Abstract

Calibrated functional magnetic resonance (fMRI) has received growing interest in recent years, becoming recognized as a viable technique for quantitatively examining both the cerebral blood flow (CBF) and oxygen metabolism ($CMRO_2$) changes associated with neural activation. It offers a relatively novel approach for examining the physiological effects of ageing and disease in the brain, which if measured by the blood oxygen level dependent (BOLD) signal alone, may be difficult to interpret. Traditionally, a *hypercapnia* calibration technique involving the inhalation of a carbon dioxide gas mixture during arterial spin labelling (ASL) MRI scanning has been the method of choice. However, other techniques such as *breath-hold* induced hypercapnia, and the comparatively new *hyperoxia* calibration technique involving the inhalation of high concentration oxygen gas, have also been explored as viable alternatives.
In this thesis each of these calibration approaches are applied during fMRI, to assess the neurovascular changes in normal, aged and diseased human brains.

We first tested the precision and viability of the Q2TIPS ASL sequence for obtaining simultaneous BOLD and CBF signal changes during sensory stimulation.

The use of the breath hold calibration technique was tested in a combined reproducibility and ageing study using visual and motor stimuli, and found that the calibrated fMRI measurements were less reproducible, and less accurate than previously documented studies using the CO_2 gas hypercapnia approach.

In a separate study, CO_2 gas hypercapnia and hyperoxia calibration techniques were compared across an ageing population using a visual stimulus. A good agreement between the techniques was observed if a *fixed* value of 5% was used in the hyperoxia model for CBF reduction during hyperoxic periods during. However, the use of measured CBF values during hyperoxia was found to be detrimental to the model due to the low signal to noise ration (SNR). Unlike the hypercapnia method, no significant age related effects were observed when using hyperoxia calibrated measurements, which may be the result of using a fixed value for CBF reduction.

The use of hyperoxia calibration with a cognitive Stroop task was assessed in a reproducibility study. The reproducibility of the calibrated measurements was lower than a previous hypercapnia reproducibility study during visual activation. We attributed this in part to the lower SNR of BOLD and CBF measurement obtained from the frontal cortex regions, compared to the visual cortex. We found consistent intra-subject regional activation between the two runs, but less so for inter-subject. The same methodology was applied in two further studies: a comparison of young and old groups, as well as an ongoing clinical study into neurovascular changes and cognitive decline associated with cerebral small vessel disease (cSVD), for which preliminary results are presented.

Acknowledgements

First and foremost, I would like to thank my supervisor, colleague and friend Dr. Laura Parkes; one of the nicest and most talented people I have met, and with whom it has been my privilege to work with over the last few years.

I would also like to thank my fellow colleagues from MARIARC, past and present who have offered their time and expertise over the years; former second supervisor Prof. Neil Roberts, current second supervisor Dr. Graham Kemp, senior radiographer Valerie Adams, Bill Bimson, Roozbeh Rezaie, Satomi Higuchi, Rishma Vidyasagar, Guy Lumley and Andrew Irwin.

A big thanks to my collaborators at the Human Brain Research Center at Kyoto University; Prof. Hidenao Fukuyama, Kenji Aso and especially Shin Ichi Urayama, for all his help with recruiting volunteers, translating, ordering food, and explaining to the barber how I want my hair cut.
I would also like to acknowledge Unilever R&D, Vlaardingen for their financial support of my PhD research, without which, none of it would have been possible.

A final thanks to my friends and family, particularly my parents, for their encouragement and ongoing support.

Table of contents

List of figures

List of tables

Publications

PAPERS

1. **Goodwin JA**, Urayama S, Aso K, Higuchi S, Fukuyama H, Parkes LM 'A Comparison of hypercapnia and hyperoxia calibration techniques for fMRI'. Submitted to Neuroimage [2009]

2. **Goodwin JA**, Vidyasagar R, Balanos G, Bulte D, Parkes LM, 'Quantitative fMRI using Hyperoxia Calibration: Reproducibility during a cognitive stroop task'. Submitted to Neuroimage [2008] – *in review*)

ABSTRACTS

1. Parkes LM, Lumley G, Mohtasib RS, Emsley H, **Goodwin JA** 'Calibrated fMRI reveals altered neurovascular coupling with age during a cognitive Stroop task' ISMRM Honolulu [2009].

2. **Goodwin JA**, Lumley G, Irwin A, Emsley H, Parkes LM 'Hyperoxia calibrated fMRI of cerebral small vessel disease during a cognitive Stroop task' ISMRM Honolulu [2009].

3. **Goodwin JA**, Urayama S, Aso K, Higuchi S, Fukuyama H, Parkes LM 'Quantitative fMRI during visual activation: comparison of hypercapnia and hyperoxia calibration techniques and the effects of age. ISMRM –British Chapter, Newcastle [2008]

4. **Goodwin JA**, Urayama S, Aso K, Fukuyama H, Parkes LM 'Comparison of hypercapnia and hyperoxia BOLD calibration techniques' ESMRMB, Valencia [2008].

5. **Goodwin JA**, Urayama S, Aso K, Higuchi S, Fukuyama H, Parkes LM 'Quantitative measures of BOLD, CBF and $\Delta CMRO_2$ during visual activation using hypercapnia and hyperoxia BOLD calibration' ESMRMB, Oral Presentation Valencia [2008].

6. **Goodwin JA**, Vidyasagar R, Balanos GM, Bulte D, Parkes LM 'Quantitative fMRI using Hyperoxia Calibration: Reproducibility during a cognitive task' ESMRMB, Oral Presentation Valencia [2008].

7. **Goodwin JA**, Parkes LM 'Reproducibility of BOLD and perfusion data during visual, motor and hypercapnia experiments at 3T' British Chapter of the ISMRM, Birmingham [2007]. Poster presentation.

8. **Goodwin JA**, Ho L, Roberts N, Parkes LM, 'Combining CBF and BOLD measurements of motor activity to determine individual differences in neurovascular coupling' Human Brain Mapping conference poster, Florence [2006].

Chapter 1. Introduction

The primary focus of the experimental work contributing to this thesis is the application of magnetic resonance imaging in the study of functional changes in the human brain, to investigate how these changes vary across brain regions and across people. By way of an introduction to this topic, chapter 1 offers an overview of the basic anatomical and physiological features of the human brain, as well as the physical principles of magnetic resonance imaging.

1.1 The human brain

1.1.1 Introduction to neuroanatomy

The basic functional cells within the brain are neurones. They communicate with each other through the transmission of electrical *action potentials* and neurotransmitters, via a network of axonal fibres and synaptic junctions. Areas in the brain that are rich in either nerve cell bodies or fibres constitute grey and white matter, respectively.
The brain is comprised of several anatomically distinct regions: *forebrain* (cerebral hemispheres and thalamus), *midbrain,* and *hindbrain* (pons, medulla oblongata and cerebellum). The midbrain, pons and medulla oblongata collectively form the brainstem.(Wilkinson, 1992).

The region most associated with information processing and cognition, which is of particular interest in most functional MRI studies, is the cerebral cortex, which forms the top layer of the cerebral hemispheres. The surface of this structure is covered by a series of furrows known as *sulci*, with the intervening ridges known as *gyri.* It is further divided into a number of anatomical regions (Figure 1.1), each of which has evolved to perform particular functions. This organisation, sometimes referred to by a numbered cytoarchitectural map known as *Brodmann's areas*, is largely consistent between people.

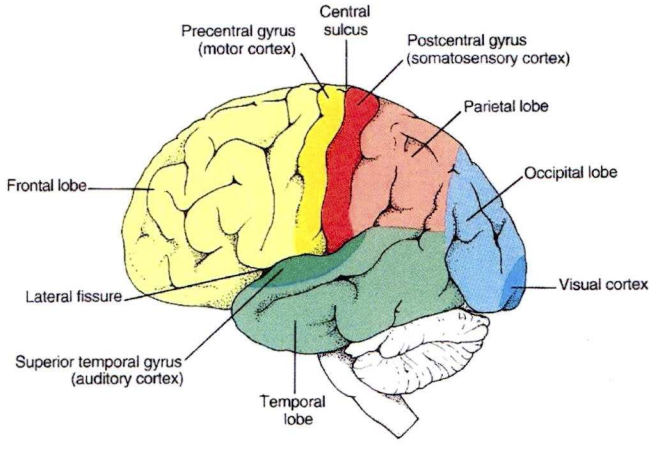

Figure 1.1 Lateral view of the brain. Illustrating sub-divisions of the cerebral cortex, with some of the principal gyri, sulci and functional areas. (Crossman et al., 1998).

1.1.2 Blood supply to the brain

Blood is supplied to the brain through two pairs of arteries; the *vertebral* and *common carotid* arteries (Figure 1.2), from which the later bifurcates to form the *external* and *internal* carotid arteries within the brain. The internal carotid arteries follow a series of characteristic bends know as the *carotid siphon*, and continue upward to the surface of the brain, along the way giving rise to a series of preterminal branches. The vertebral arteries meanwhile, converge between medulla and pons to form the *basilar artery*, with a number of branches supplying the brain stem, cerebellum and occipital lobe.

The internal carotid and vertebrobasilar systems are joined by two thin vessels known as the *posterior communicating arteries,* which form a contiguous network know as the *Circle of Willis* (Figure 1.3). In the event of narrowing or obstruction of the cerebral arteries, the arrangement of vessels in the circle of Willis is such that any insufficiency in perfusion as a result of the obstruction, may be compensated for blood flow through the communicating arteries (Crossman et al., 1998). From the anterior, middle and posterior cerebral arteries, which connect with the circle of Willis, are a network of small vessels known as *pial* arteries, which run along the surface of the brain

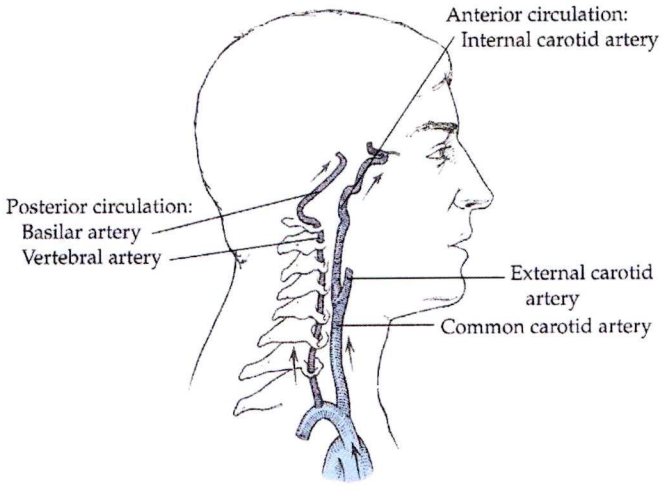

Figure 1.2 Extracranial and cranial courses of the vertebral, basilar and carotid arteries (Martin, 2003).

These vessels penetrate the cortical surface and branch further to form a dense capillary bed within the grey matter, which engulf the large network of neurones and other cellular constituents of cortex such as glia cells, supplying the required oxygen, metabolites and warmth to sustain adequate function.

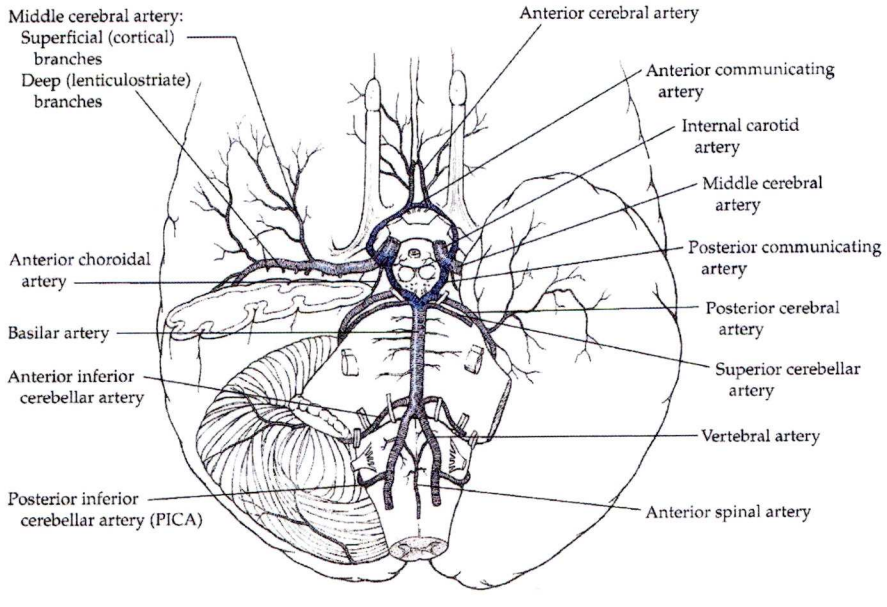

Figure 1.3 Diagram of the ventral surface of the brain stem and cerebral hemispheres, illustrating key components of anterior (carotid) and posterior (vertebral-basilar) circulation. The circle of Willis is shown in dark blue. (Martin, 2003).

1.1.3 Blood flow and metabolism

In 1890 Roy and Sherrington found that functional activity increased blood flow and conjectured that this was somehow governed by metabolic demands (Roy et al., 1890). Although at the time the mechanism behind this relationship was not well understood, the basic premise remains true and in fact provides the physiological basis for functional magnetic resonance imaging (fMRI). However, with over a century of research since Roy and Sherrington's observations, it is fair to say that the exact mechanisms behind the vascular changes that occur in response to neural activation, the so called *neurovascular coupling*, are not completely understood.

It is thought that the primary role of the increase in blood flow that occurs during functional activity is to compensate for the increased metabolic demand of oxygen and glucose, used for the production of ATP. But perhaps what is not certain is why the main cellular or functional processes driving the increase in metabolism, trigger an increase in blood flow which appears to be disproportionately large, relative to the metabolic demands.

It is generally accepted that initial transitory vasodilation occurs as a result of increased K^+ in extracellular space, which diffuses out of neuron terminals during action potentials. But the role of K^+ during sustained dilation and how this relates to ATP depletion, and uncompensated increases in oxygen extraction by active neurons is less clear. Evidence also suggests that a glutamate evoked Ca^{2+} influx in postsynaptic neurons plays a part in local vasodilation, reflecting the activity of the presynaptic neurons, and the level of depolarisation of the postsynaptic cell (Attwell et al., 2002). This suggests that a significant portion of the haemodynamic response may be triggered from local, energetically expensive neurotransmitter events (Logothetis et al., 2001), reflecting local dendritic activity. Although, a number of other *classical* neurotransmitters associated with neuromodulation rather than neurotransmission, have been shown to have a considerable effect of CBF (Logothetis, 2008).

Despite some uncertainties regarding the biophysical mechanisms of neurovascular coupling, it well accepted that local changes in blood flow, glucose and oxygen metabolism do occur in regions of increased neural activity, and it is the relationship between these changes, which will be investigated in this thesis, through the use of fMRI.

1.2 The physical basis for Magnetic Resonance Imaging

The development of MRI, like any scientific endeavour, is based on an accumulation of insights and observations, leading to progressive understanding and exploitation of physical phenomena, which in the case of MRI is the phenomenon of Nuclear Magnetic Resonance (NMR). In 1938 the Austrian born physicist Isidor Isaac Rabi, documented the first observation of NMR during a molecular beam experiment (Rabi et al., 1938), and was followed soon after by the work of Bloch and Purcell, whom were later awarded the Nobel Prize in physics "for their development of nuclear magnetic precision measurements, and discoveries in connection therewith". In the seven decades subsequent to Rabi, Bloch and Purcell's seminar work, there have been a number of significant developments in the application of NMR, perhaps none more so than the work of Lauterbur (Lauterbur, 1973) and Mansfield (Mansfield et al., 1973), who in the 1970's utilized the principles of NMR to establish Magnetic Resonance Imaging, for which they also received a Nobel Prize in 2003, and which formed the basis of MRI as we know it today.

This section provides a brief overview of the physical principles behind MRI. A more detailed account can be found in standard texts (Haacke et al., 1999; Kuperman, 2000; McRobbie et al., 2003).

1.2.1 Spin and precession

Protons and neutrons exhibit a property known as *spin*. Atomic nuclei with an odd number of protons and neutrons have a *net* spin and a magnetic dipole moment ($\vec{\mu}$) that is proportional to their spin angular momentum ($\vec{S}$).

$$\vec{\mu} = \gamma \vec{S} \qquad [1.1]$$

where γ is the gyromagnetic ratio constant for a specific nucleus type.

An example of an atomic nucleus with a net spin, which is also the most abundant element in the human body, and the element typically utilized in MRI, is the hydrogen atom (^{1}H), consisting of one proton, with a value of 'spin one-half'. In the absence of orbital motion, the total angular momentum of the proton results from the intrinsic spin, the magnitude of which is given by:

$$S^2 = s(s+1)\hbar^2 \qquad [1.2]$$

Where $\hbar = \frac{h}{2\pi}$ and h is Planks constant [1.3]

With a spin quantum value of s=1/2 for a proton,

And subsequently a magnetic quantum number $m_s = \pm\frac{1}{2}$ [1.4]

Relating to the Z direction of the spin vector, which is by convention the direction of the external magnetic field, through:

$$S_z = m_s\hbar \qquad [1.5]$$

This leads to the energy associated with the proton magnetic moment in the presence of the external field, which can be derived from the classical equation, to give the quantum equivalent *discretized* energy:

$$E = -\vec{\mu}\cdot\vec{B} = -\mu_z B_z = -\gamma m_s \hbar B_z \qquad [1.6]$$

The quantized nature of this phenomenon is such that distinct energy levels exist for the hydrogen proton in the presence of the external magnetic field. These two values represent lower and upper energy levels, which will be either aligned or anti-aligned with the external field (Figure 1.4).

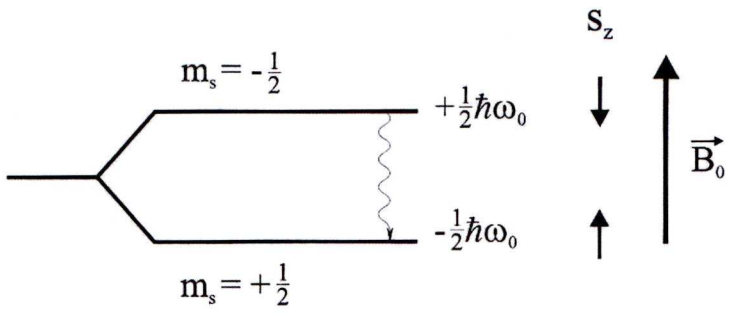

Figure 1.4 The Zeeman energy levels for a spin one-half system and positive gyromagnetic ratio (Haacke 1999).

Transition of a proton from one spin state or energy level to another is accompanied by photon emission or absorption. From equation [1.6] we can see that the energy difference is equal to $\gamma\hbar B_z$, and can be expressed as:

$$\Delta E = \hbar\omega_0 \qquad [1.7]$$

Where (from equation 1.6) $$\omega_0 = \gamma B_0 \qquad [1.8]$$

The distribution of spin systems between the two energy levels is referred to as the population difference, and is a product of both magnetic field strength and ambient temperature:

$$\frac{N_u}{N_l} = e^{-\frac{\Delta E}{kT}} \qquad [1.9]$$

Where N_u and N_l represent the relative numbers of Nuclei in the upper and lower energy bands respectively. With ω_0 and therefore ΔE proportional to magnetic field strength, equation 1.9 shows that an increased proportion of nuclei will reside in the lower energy state, parallel with the magnetic field, as the field strength increases, thereby increasing the *net magnetization* of the system. Conversely, an increase in thermal energy would provide additional energy to the system, allowing more nuclei to reside in the high energy, anti parallel state, which would therefore reduce the net magnetization of the system.

The parameter ω_0 is known as the Larmor frequency, and represents the energy of photons released in a downward transition, as well as the energy required to stimulate an upward transition. The classical conception of the Larmor frequency is the precession rate of the spin around the external magnetic field.

To derive equation 1.8 classically, we begin by considering the equation describing the torque experienced by a nucleus in precession around a magnetic field, and how this acts on the angular momentum over time:

$$\tau = \vec{\mu} \times \vec{B}_0 = \frac{d\vec{S}}{dt} = \frac{1}{\gamma}\frac{d\mu}{dt} \qquad [1.10]$$

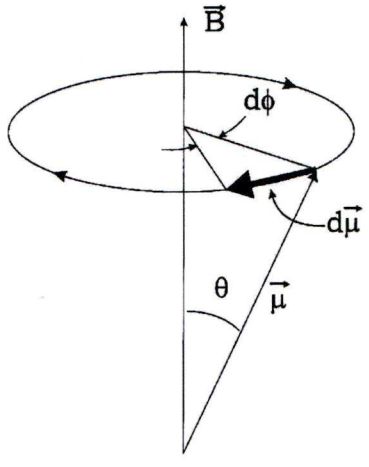

Figure 1.5 *Larmor precession.* Precession of a dipole around a magnetic field.

This 'equation of motion' describes how the magnetic moment of a dipole ($\vec{\mu}$) precesses when placed in an external magnetic field, shown graphically in Figure 1.5. The radial distance from $\vec{B}$ to the dipole moment $\vec{\mu}$ is $\mu \sin\theta$. The magnetic moment of the dipole is a vector quantity, which is varying in angular direction (rather than magnitude) in the transverse plane ($d\phi$) with time, performing a left hand rotation about the external field $\vec{B}_0$

i.e. $$d\mu = \mu \sin\theta \, d\phi \qquad [1.11]$$

$$\vec{\mu} \times \vec{\beta} = \mu B \sin\theta \qquad [1.12]$$

From equations [1.10] and [1.12] we obtain:

$$d\mu = \gamma \mid \vec{\mu} \times \vec{B}_0 \mid dt = \gamma \mu B_0 \sin\theta \, dt \qquad [1.13]$$

When compared with equation [1.11] we find that $\gamma B_0 \; dt = d\phi$, which leads to the angular frequency, or Larmor frequency for precession around B_0: $\omega_0 = \frac{d\phi}{dt} = \gamma B_0$

1.2.2 Radio frequency excitation and relaxation

In the previous section, the concept of net magnetization was introduced, which is typically denoted as M_0. This concept applies to the macro behavior of hydrogen atoms in a sample of water, in the presence of the external field B_0, and represents an equilibrium state of magnetization. The net magnetization that develops in the sample is the result of a relatively small fraction of total atoms aligning with the field. This is due to the overwhelming effects of ambient thermal temperature. However, it is the net magnetization that is exploited in MRI imaging.

The net magnetization vector is aligned with the external field during equilibrium, however if we apply an oscillating RF electromagnetic field (B_1) at the Larmor frequency for hydrogen (~ 128 MHz at 3 Tesla), perpendicular to B_0 in the transverse X-Y plane, the precessing nuclei will be brought into phase and their classical net magnetization vector will begin to precess around B_1, tipping the vector towards the x-y plane. In a magnetic field free environment, application of RF energy at the resonant frequency of the nuclei will result in an increased number of transitions between energy states, in both directions, with equal probability. However, because of the initial net magnetization that exists in the direction of B_0, the absorption of RF energy during resonance will act to reduce the M_0 magnitude. If the oscillating field is sufficiently long enough to cause half the excess B_0 aligned nuclei to become anti-aligned, the net magnetization vector in the longitudinal plane will reduce to zero, and the net

magnetization will revolve or 'flip' into the X-Y plane, perpendicular to the oscillating transverse field B_1. The angle θ to which the magnetization vector M is flipped is arbitrary and is determined by the magnitude and duration of the RF pulse.

$$\theta = \gamma B_1 t_p \qquad [1.14]$$

Where B_1 represents the strength of the oscillating magnetic field, and t_p represents the duration of the RF pulse. The rate of change of θ, the spin precession frequency due to the circularly polarized field B_1, is generally termed ω_1.

The emission of electromagnetic photon energy by the protons during transition to a lower energy state will cause a changing magnetic flux, which can be detected by measuring emf (electromotive force) induced currents in a tuned RF coil placed in the X or Y plane. The frequency of the measured signal will be equal to the Larmor frequency, and the amplitude will be determined by the magnitude of the transverse component of the net magnetization vector (i.e. maximum at $\theta = \frac{\pi}{2}$ radians), which in turn is proportional to the proton density. Although the release of photon energy by the excited protons occurs during the application of the RF pulse, it is only after the cessation of the pulse that the corresponding emf induced current is measured.

1.2.3 Relaxation and the Bloch equations

The equilibrium magnetization condition (M_0) is characterized by a net magnetization in the z or B_0 field direction, and represents the lowest energy state of the spin system. Any perturbation of the net magnetization vector from this low energy state will be short lived, as the system tries to recover its equilibrium.

The Bloch Equation

The evolution of magnetization during excitation and relaxation can be described by the so called Bloch equation:

$$\frac{d\vec{M}}{dt} = \gamma \vec{M}_{\perp} \times \vec{B} + \frac{1}{T_1}(M_0 - M_z)\vec{z} - \frac{1}{T_2}\vec{M}_{\perp} \qquad [1.15]$$

For a constant external field, without the addition of an oscillating RF field, we have $\vec{B} = B_0\vec{z}$, which gives:

$$\frac{dM_x}{dt} = \omega_0 M_y - \frac{M_x}{T_2} \qquad [1.16]$$

$$\frac{dM_y}{dt} = -\omega_0 M_x - \frac{M_y}{T_2} \qquad [1.17]$$

$$\frac{dM_z}{dt} = \frac{M_0 - M_z}{T_1} \qquad [1.18]$$

T_1 (Spin-lattice) Relaxation

This form of relaxation refers to the gradual recovery of longitudinal magnetization in alignment with B_0 through the return to thermal equilibrium between protons and the surrounding 'lattice', that is, the surrounding volume in which neighboring atoms are arranged. The duration of the longitudinal recovery of magnetization is field dependent, with higher field strength resulting in higher T_1 values, and is described by the equation:

$$\frac{dM_z}{dt} = \frac{1}{T_1}(M_0 - M_z) \qquad [1.19]$$

Where Curie's law states $M_0 = C\frac{B_0}{T}$ [1.20]

and C is a constant relating to spin state, and spin density, and T is absolute temperature in degrees Kelvin.

The rate of change of longitudinal magnetization M_z is proportional to the difference between M_z and the equilibrium value M_0. The equilibrium recovery is an exponential process, becoming asymptotic as $M_z \rightarrow M_0$ and $t \rightarrow \infty$. In practice, T_1 is the time taken for the magnetization to recover 63% of its equilibrium value.

Table 1.1 Relaxation parameters in human tissue. Superscripts a - h refer to independently validated studies. (See (McRobbie et al., 2003))

	T_1(ms)			T_2(ms)		
Tissue	0.5 T	1.5 T	3.0 T	0.5 T	1.5 T	3.0 T
White matter	520[f]	560[a]	832[i]	107[b]	82[c]	110[i]
Grey matter	780[f]	1100[a]	1331[i]	110[b]	92[c]	80[i]
CSF	–	2060[e]	3700	–	–	–
Muscle	560[g]	1075[d]	898[h]	34[g]	33[g]	29[h]
Fat	192[b]	200[b]	382[h]	108[b]	–	68[h]
Liver	395[b]	570[e]	809[h]	96[b]	–	34[h]
Spleen	760[b]	1025[e]	1328[h]	140[b]	–	61[h]

The variation in T_1 throughout the human body reflects variation in the local lattice surrounding the hydrogen nuclei. Randomly fluctuating fields caused by vibrational and rotational motion of molecules within the lattice, leads to interaction between magnetic moments of hydrogen nuclei, through the so called *intra-molecular dipole-dipole interaction*. If the frequency of the fluctuating magnetic fields is at or near the Larmor frequency, then an exchange of energy that results in a transition of spin states and leads to T_1 relaxation will occur, and continue until thermal equilibrium is reached between spins and the lattice. Thus the rate of *tumbling* of the spins or surrounding molecules is a critical determinant of T_1 relaxation time. The most efficient environment for thermal interactions and therefore rapid T_1 relaxation is where the hydrogen nuclei have an intermediate level of binding, and can tumble at the Larmor frequency, thereby releasing energy to the surrounding lattice.

T_2 (Spin – spin) Relaxation

This represents the loss of coherence of the transverse component of the net magnetization. It is the result of dipole-dipole interactions and the influence of local magnetic fields associated with the magnetic moment of neighboring protons, and leads to a loss of phase coherence due to variations in precession frequency. This can be thought of as the result of inhomogeneities in the local magnetic field resulting from molecular motion. The fact that different tissue has different T_2 times reflects the ease

with which local molecular motion can occur. If a molecule is able to 'tumble' freely, then the inhomogeneity in the local field experienced by a dipole can change very rapidly, and effectively average out over a few milliseconds. This phenomenon known as 'motional averaging' will create a relatively homogeneous field around the proton, which will lead to a longer T_2 time. Conversely, protons that are bound will have shorter T_2 times.

The change in the transverse component of the net magnetization is given by:

$$\frac{d\vec{M}_{\perp}}{dt} = \gamma \vec{M}_{\perp} \times \vec{B} - \frac{1}{T_2}\vec{M}_{\perp} \qquad [1.21]$$

Where $\vec{M}_{\perp}$ represents the net magnetization vector in the transverse plane.

Table 1.1 shows a summary for T_1 and T_2 relaxation parameters for different body tissue.

T_2^* Relaxation

The reduction in transverse magnetization due to loss of signal coherence is also affected by small inhomogeneities in the main external magnetic field. This causes variations in precession frequencies across a sample, leading to signal dephasing at a faster rate than during T_2 relaxation alone. It is expressed as:

$$\frac{1}{T_2^*} = \frac{1}{T_2} + \frac{1}{T_2'} \qquad [1.22]$$

Where T_2' is an external field induced parameter that is both machine and sample dependent.

1.2.4 Image Formation

Slice selection

Typically, the acquisition of MRI data involves collecting a series of 2 dimensional image slices, which can later be combined to form a 3 dimensional image volume.

The technique for acquiring discrete slices within a sample, is based on the work of Lauterbur in the 1970's (Lauterbur, 1973). It involves the use of 'gradient coils' to generate magnetic field gradients of B_0 in any of the *x, y* or *z* direction.

This causes a modulation of field strengths within the sample, and because the Larmor frequency is proportional to field strength, a distribution of proton precession frequencies will exist.
If the gradient is applied in unison with the RF pulse, it is possible it excite a particular slice of interest by varying the RF pulse frequency, to excite the protons that are precessing at the equivalent frequency, which will be unique to that spatial dimension due to the modulated gradient. For example, if a slice selective gradient G_{ss} was applied in the *z* direction, in parallel with the main field, an RF frequency band can be chosen, which will excite a particular slice of interest that lies parallel to the x-y plane.

The width of this slice will be proportional to the bandwidth, and indirectly proportional to the amplitude of the applied gradient. By applying a Fourier Transform of the measured signals, the relative magnitudes of the different frequencies can be obtained, which correspond to the proton density, or amount of sample, and the relaxation parameters at a particular position within the gradient.

Phase encoding

After selectively exciting spins in the desired *x-y* plane, it is possible to gain additional information about spin position within this plane by applying an additional gradient, known as the *phase encode* gradient. This can be applied either immediately, or after a sufficient time for a required echo time, perpendicular to the slice selection gradient, and immediately prior to a r*ead out* gradient. This is achieved by sequentially inducing variations in the phase of the precessing protons in the slice, by applying progressively larger or smaller gradient amplitudes during each acquisition sequence, which will be greatest for protons positioned at the ends of the gradient. The data is accumulated in a matrix where the variations in phase occur at a known position. Applying a Fourier

transform along the phase encode direction (y axis) for each x column, allows the changes in phase and associated signal amplitude to be correlated with a specific position in the phase encode direction.

Frequency encoding

The frequency encode gradient, also known as the *read out* gradient, is applied perpendicular to the phase encoding gradient, which for a transverse x-y slice would be either the x or y axis. It is applied before and during signal *echo* readout, and generates a spatial distribution of proton frequencies along the direction of the gradient, which when subtracted from the main field precession frequency, gives a range of frequency values ($-f_{max}$ to f_{max}), which can be applied to the Fourier transform to assign a specific spatial position, due to the known relationship between frequency and position of the gradient.

k –space

In simple terms, k-space is a 2 dimensional matrix containing the raw, already encoded MR signals, where each point in space represents a spatially sampled location. The space is defined by two axes, representing spatial frequencies k_x (k_{FE}) and k_y (k_{PE}). The line spacing in k space (Δk) determines the field of view (FOV), whereby the narrower the spacing, the larger the field of view, according to:

$$\Delta k = \frac{2\pi}{FOV} \qquad [1.23]$$

The spatial resolution of the image (Δx) is given by: $\frac{FOV}{N}$ where N is the number of increments of Δk.

$$k_{\max} = \Delta k \cdot \frac{N}{2} \qquad \text{similarly} \qquad k_{\min} = \Delta k \cdot \frac{-N}{2} \qquad [1.24]$$

or

$$k_{\max} = \frac{\pi}{\Delta x} \qquad [1.25]$$

i.e. spatial resolution of the image is inversely related to the extent of k-space sampled.

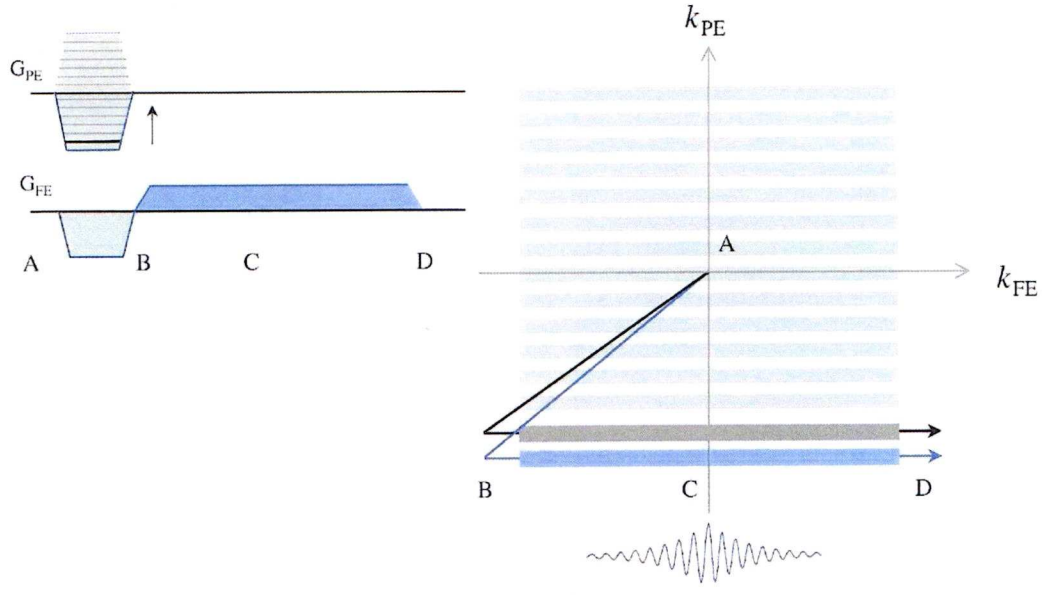

Figure 1.6 K-space path for a pair of frequency and phase encode gradients. Prior to application of gradients, the signal is at the centre of k-space. (McRobbie et al., 2003)

Application of phase and frequency encoding gradients defines a path or trajectory through k-space (Figure 1.6), and corresponds to a summation of the measured signal. The trajectory is generally organized to pass through the central region of k-space at the peak of the echo, and so represents the maximum acquired signal. It is defined by low spatial frequency and represents the high contrast and gross signal that will be present in the resulting image. Higher spatial frequencies define edge definition in the image; therefore a large k-space comprising both low and high spatial frequencies is desirable.

Echo planar imaging (EPI)

EPI is an imaging sequence that allows the collection of a complete 2 dimensional image, through the sampling of all k-space, with only one excitation pulse. High gradient amplitudes, fast gradient switching and fast sampling mean that this process occurs before the measureable signal has fully decayed.

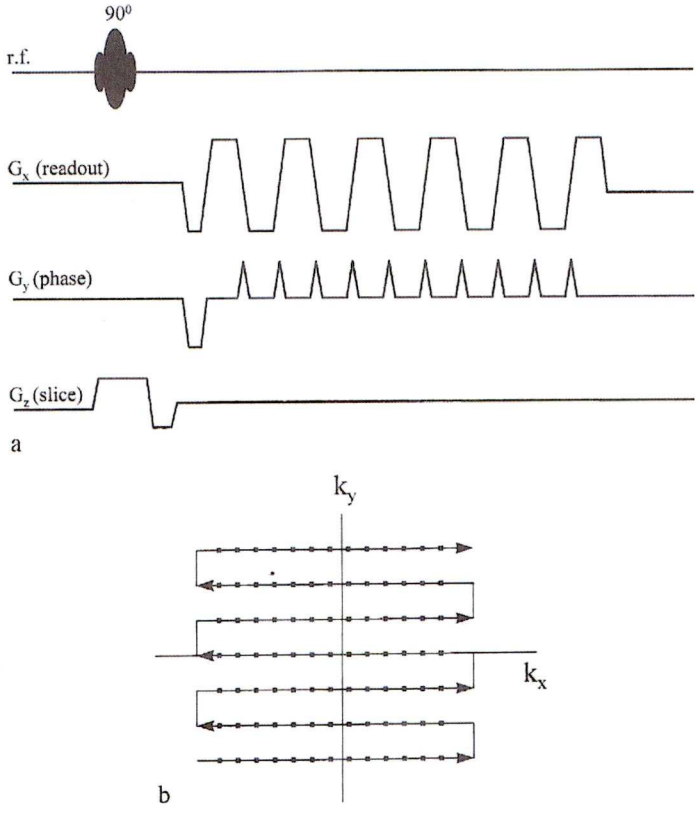

Figure 1.7 Typical EPI pulse sequence with corresponding k-space trajectory. (Kuperman, 2000).

The key features of the EPI k-space trajectory, as shown in Figure 1.7b, are the reversing trajectory of k_x, which results from switching the polarity of readout encode gradient, and the *blipped* phase encode gradient, which causes the k_y trajectory in increase between each polarity switch of the readout gradient.

Gradient echo EPI

The use of reversing polarity gradients to dephase and rephase transverse magnetization, such as this, is an example of gradient echo EPI, which has the effect of creating an attenuated, meaningful signal. The dephasing of spins which occurs in this process is the result of the applied gradient itself, and does not correct for the dephasing resulting from local magnetic field inhomogeneities or tissue susceptibilities. Therefore the measured intensity of the MR signal is affected by T_2^* relaxation.

Spin Echo EPI

To minimize the T_2^* effects that exist in Gradient echo EPI sequences, the Spin echo technique was introduced, which has the effect of removing signal loss that results from additional phase shifts due to macroscopic field inhomogeneities. It involves the same sequence as that mentioned above, but with an additional 180° pulse after the first 90° pulse, also in the presence of the slice selection gradient. The dephasing that occurs after the initial pulse is removed when the 180° causes rotation around the *y* axis, and signal rephasing is established. This is then followed by the standard *blipped* phase encode gradient, and alternating readout gradient as with gradient echo EPI, with the exception that the effects of field inhomogeneity and static tissue susceptibility gradients have been removed, and the intensity of the acquired image is dependent on T_2 relaxation.

Chapter 2. Arterial Spin Labelling

2.1 Comparison of ASL techniques

Arterial Spin Labelling (ASL) refers to a class of MRI pulse sequence that is used primarily to obtain measures of cerebral blood flow (CBF). It can be further divided into two sub-classes known as *Continuous* ASL (CASL) and *Pulsed* ASL (PASL).
In contrast to other techniques for measuring blood flow, such as bolus tracking of paramagnetic contrast agents using MRI, and radionuclide based modalities such as SPECT and PET, ASL is completely non invasive and non-ionising. Instead it utilizes the magnetic properties of the blood itself, to obtain image contrast. This involves magnetically *tagging* inflowing blood to the brain, and imaging it some short time later. If a second image is also acquired in the same region without the tagging of inflowing blood (*control*), the difference between the two images (*control – tag*) will result in what is generally termed a *perfusion* weighted image, which will be representative of the blood flow into the imaging region. That is, any static signal resulting from tissue itself will be measured during both tag and control images, and will be removed upon subtraction of the two images. The *tag- label* method is the most conventional approach, but several different subtraction techniques exist (Liu et al., 2005). The perfusion weighted images have a low signal to noise ratio (SNR), and require a number of averages (~30 images) to generate a useable perfusion weighted image. Once the required number of images has been obtained, quantitative estimates of CBF are made with the application of a kinetic model, of which there are more than one type, which will be covered later in this chapter.

2.1.1 Continuous ASL

In CASL the magnetisation of arterial blood is continuously inverted by constant radiofrequency radiation (usually over a period $\approx$2-3 sec.) in the presence of a constant gradient as it flows across the tagging plane. This is the same process that applies in slice selection, except that the image is not acquired in the region excited by the RF energy (*tagging or labelling plane*), but instead is acquired in a region above (*imaging plane or imaging* slices) into which the inflowing tagged blood has perfused (Figure 2.1).

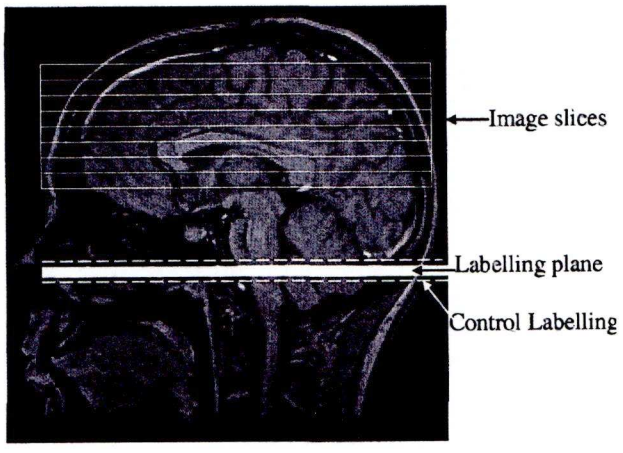

Figure 2.1 CASL – typical slice positions. Inflowing hydrogen protons in blood are magnetically tagged as they pass through the labelling plane. Control labelling uses a double inversion to leave inflowing blood *un-tagged.* Subtraction of images (control – tag) gives perfusion weighted images.

The magnetic field gradient G is applied effectively in parallel with the direction of blood flow through carotid and vertebral arteries, which allows a labelling plane to be selected with a low power RF field (B_1) that is perpendicular to the direction of flow. As inflowing hydrogen protons pass through G their precession frequency is altered, such that the applied RF energy will excite the proton spins to a higher energy state, and cause a magnetisation inversion if the following condition is met:

$$\frac{1}{T_1}, \frac{1}{T_2} << \frac{Gv}{B_1} << \gamma B_1 \qquad [2.1]$$

Where T_1 and T_2 are spin-lattice and spin-spin relaxation times, B_1 is the RF field strength, G is the magnetic gradient field strength, v is the linear velocity of the inflowing spins and γ is the gyromagnetic ratio for protons (Williams et al., 1992). The efficiency of this inversion process is largely determined by the relative values for G and B_1. These parameters would generally be kept constant across subject scans, and the only likely variable to contribute toward inefficiency is the blood velocity, which may vary between people, perhaps more so in certain clinical populations. However, it has been shown that doubling or halving the velocity only changes the efficiency by 2% (Maccotta et al., 1997), which suggests that it is unlikely to amount to a large source of error.

As the tagged blood flows out of the labelling plane and into the imaging plane, it undergoes spin-lattice relaxation, which causes the magnetisation M_z, parallel with the main field to become progressively less negative. However, relative to the surrounding tissue, the net longitudinal magnetisation of the blood is still reduced, which has the effect of lowering the overall longitudinal magnetization within the imaging slices (Tofts, 2003), and is the basis for measureable difference between tagged and control images. The duration of RF labelling field is sufficiently long enough to allow the magnetisation in the imaging plane to reach a steady state. However, the application of the RF field for this length of time (2-3 seconds), introduces the problem known as *magnetisation transfer* (MT) (Wolff et al., 1989); a phenomena that can lead to reduced magnetization in the labelled images. The problem relates to magnetization in static tissue rather than flowing blood, specifically protons which are bound to macromolecules such as proteins, which may be present in myelin sheaths surrounding neurons, or in cells (Tofts, 2003). Unlike freely moving protons such as those in water, which have a narrow spectral line and therefore narrow resonance bandwidth, these protons have a comparatively broad bandwidth and are resonant over a larger band of RF frequencies, with a short T_2 value that is effectively invisible to standard MR images. As such, these protons can be sensitive to off-resonant RF pulses despite not being in the labelling plane, and by dipole-dipole or direct chemical transfer with the freely moving protons, the magnetisation in the imaging plane may be reduced.

As this effect results from the application of an RF field, it is present during the images acquired after labelling, whereas no RF field is required during the control imaging. And so the underlying detrimental effect that MT can pose to CASL imaging is the difference in measured signal originating from static tissue in control and tagged images. Subtraction of the two images would lead to an inaccurate representation of CBF, and so it is desirable to have the same magnetization transfer effects in both tagged and control images. There are a number of ways to achieve this; in the case of single slice imaging, it is possible to apply an equivalent RF pulse above the head, equidistant from the imaging plane as the labelling plane. This has the effect of inducing the same MT effects within the imaging plane, but without tagging the inflowing blood (Detre et al., 1992). This technique would not work with multi-slice acquisition as the MT effects are

position dependent, and so at best the control RF pulse could only be equidistant for one of the slices. Instead, two other techniques can be applied when using multi- slice acquisition. One of them involves the use of an additional surface coil for spin labelling, which is placed on the neck, and provides better spatial discrimination of the RF pulse and avoids contamination of macromolecules in the imaging slices, thereby preventing MT effects during labelling (Zhang et al., 1995).

This technique involves specialist hardware and may not always be practicable, and so a more favourable technique involves the use of amplitude modulated *double* inversion pulses, which stimulate the required MT effects in the labelling slices, but because of the double inversion the in flowing blood remains effectively un-labelled. The position of the inversion, or *control labelling* planes are shown in Figure 2.1.

2.1.2 Pulsed ASL

There are a number of PASL techniques available, but the defining feature that distinguishes them from CASL, is the use of a *tagging volume*, which is larger and applied for shorter time duration than the CASL tagging slice. Typically, PASL sequences are divided into two main types:

EPISTAR *(Echo planar imaging and signal targeting with alternating radiofrequency)*
Consists of a tagging volume inferior to imaging slices, whereby a 180° pulse is applied in the presence of a field gradient to invert the longitudinal magnetization of the hydrogen protons within that region. After a specified inversion time, which is sufficiently long to allow for adequate perfusion into the tissue within the imaging slices, EPI acquisition is used to obtain images within those slices. To eliminate MT effects, a control labelled volume is positioned superior to the imaging slices, where any inflowing blood entering the imaging slices is assumed to be negligible. To avoid direct magnetization effects on the blood or tissue within the imaging slices as a result of the imperfect slice profile of the RF inversion pulse, a gap is placed inferior and superior to the imaging slices for to separate it from them from the tag and control inversion pulses. (Figure 2.2a) (Edelman et al., 1994).

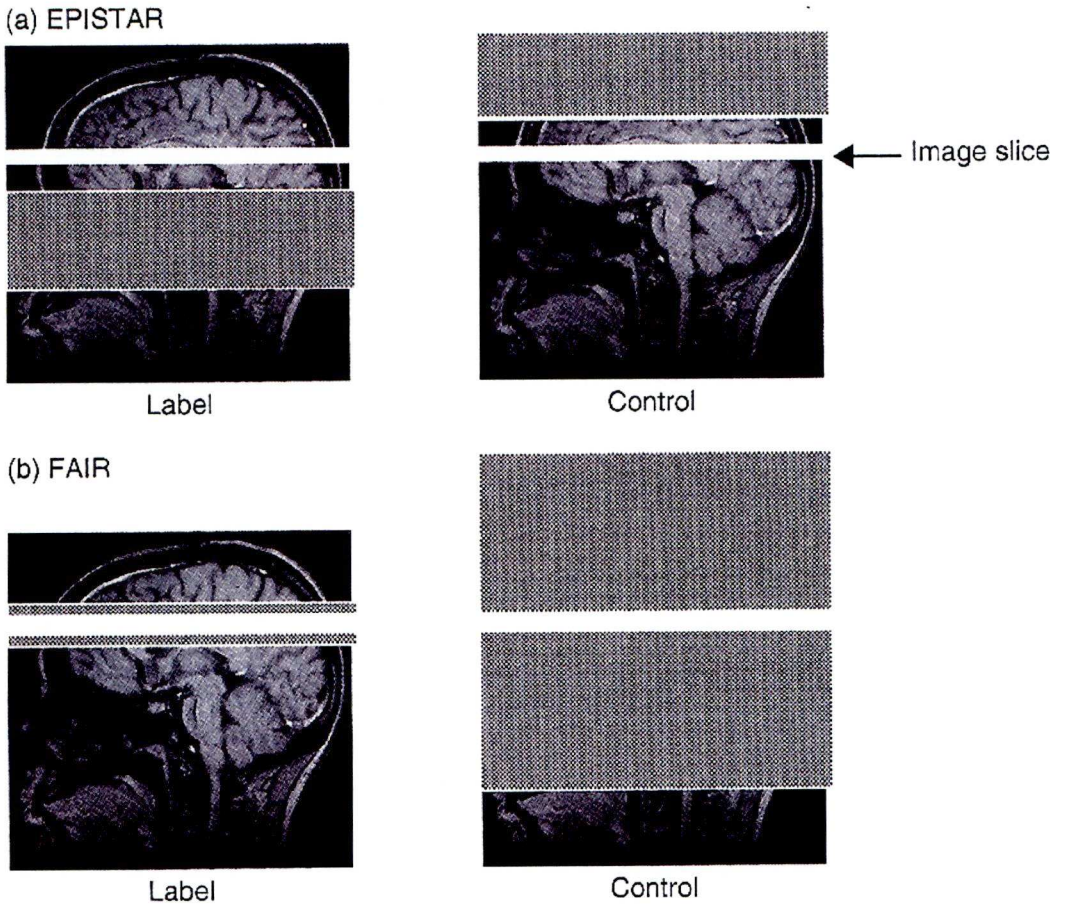

Figure 2.2 The two main techniques of PASL imaging, with labelling or tagging planes shown in grey, and imaging planes shown in white. (Parkes, chapter 13, (Tofts, 2003))

PICORE *(Proximal inversion with a control for off-resonance effects)* (Wong et al., 1997) is a variation of the EPISTAR method, which uses the same tagging technique as EPISTAR, but with an off resonance RF pulse during the control phase, in the absence of an applied gradient.

FAIR *(Flow sensitive alternating inversion recovery)*

This technique utilizes a non-selective inversion pulse across the whole of the RF coil coverage, in the absence of an applied gradient, to obtain the control image, which is sometimes referred to as the tag image, however we define it here as control, as is the case in Figure 2.2b. The tag image however, has an inversion volume covering a region

only slightly larger that the imaging slices. On subtraction of these images, the signal measured in the imaging volume is a measure of the volume of blood from both above and below that has flowed into the imaging slices (Kim, 1995; Kwong et al., 1995; Schwarzbauer et al., 1996).

2.1.3 Inaccuracies of PASL

There are two potential sources of inaccuracy that exist with the previously mentioned PASL techniques. Firstly, vessels passing through the imaging slices can potentially lead to overestimation of perfusion in some voxels, due to the labelled blood in large vessels. This is referred to as *intravascular spin* artefact, and is dealt with by introducing *flow dephasing* or *crusher* gradients into the PASL sequence (Wong et al., 1997; Ye et al., 1997), which are bi-polar gradient pulses used to dephase the magnetization of flowing spins in the larger vessels that pass through the imaging slices.

The second source of inaccuracy is known as the *transit time effect,* which is the effect of underestimated perfusion resulting from labelled spins that are still in transit from the labelling to image plane, when the image acquisition commences. This effect is more significant in CASL where the labelling slice is further away from the imaging plane, but is still relevant in PASL sequences. To combat the effects of transit time, a number of modifications have been introduced, to use in conjunction with exiting PASL techniques such as EPISTAR, PICORE and FAIR sequences. These are detailed as follows:

QUIPSS (Quantitative imaging of perfusion using a single subtraction)
The QUIPSS sequence addresses the issue of transit time by applying an additional saturation pulse to the imaging volume at a time TI_1 after the initial RF labelling pulse, and the images are acquired at a time TI_2 after a delay time ΔTI_1. If the chosen TI_1 time is less than the minimum transit delay time, the labelled spins will have already started to enter the imaging plane, and if ΔTI_1 is less than the time width of the tagged bolus, a consistent flow of labelled spins will be entering the imaging plane during the period of ΔTI_1. Therefore despite apparently saturating some of the labelled spins, the sequence is

now effectively invariant to transit time; instead using well defined inversion times to quantify CBF.

QUIPSSII

A modification of the original QUIPSS sequence, applies the same principle but rather than applying the saturation pulse to the imaging plane at time TI_1, it is instead applied to the labelling plane, meaning that only spins that have already left the labelling plane at time TI_1 will be included in the measurement, which effectively cuts the tail end of the labelled bolus. If the ΔTI_1 time is greater than the minimum transit time, the time width to the bolus is equal to TI_1.

Q2TIPS

A variation on the QUIPSSII, which offers improved accuracy of CBF measurement, and is the PASL imaging sequence used for the experimental work of this thesis, is known as Q2TIPS (QUIPSII with thin-slice TI_1 periodic saturation) (Luh et al., 1999). The basic difference between the two imaging sequences is that the saturation pulse, which is applied to the tagging region at time TI_1 in QUIPSSII, is replaced with a train of thin-slice saturation pulses at the distal end of the tagging region (Figure 2.3).
This addresses two sources of residual error, which are known to occur when using QUIPSSII, namely; the incomplete saturation of spins in the tagging plane after time TI_1 due to B_1 inhomogeneity when using sinc-shaped pulses, the result of which is an overestimation of perfusion.
The second source of error arises from spatial mismatch of the distal edge of the saturation and inversion slice profiles. The use of a sech inversion pulse for tagging provides a highly selective region of magnetization, with well defined boundaries.

However, the applied sinc-tagging pulse does not have such well defined boundaries, and therefore results in a discrepancy between the locations of the two pulses. By using thin rather than a thick pulse for saturation, the B_1 inhomogeneity is improved and therefore the error of incomplete saturation is improved, as well as a reduced spatial mismatch between tagging and saturation regions.

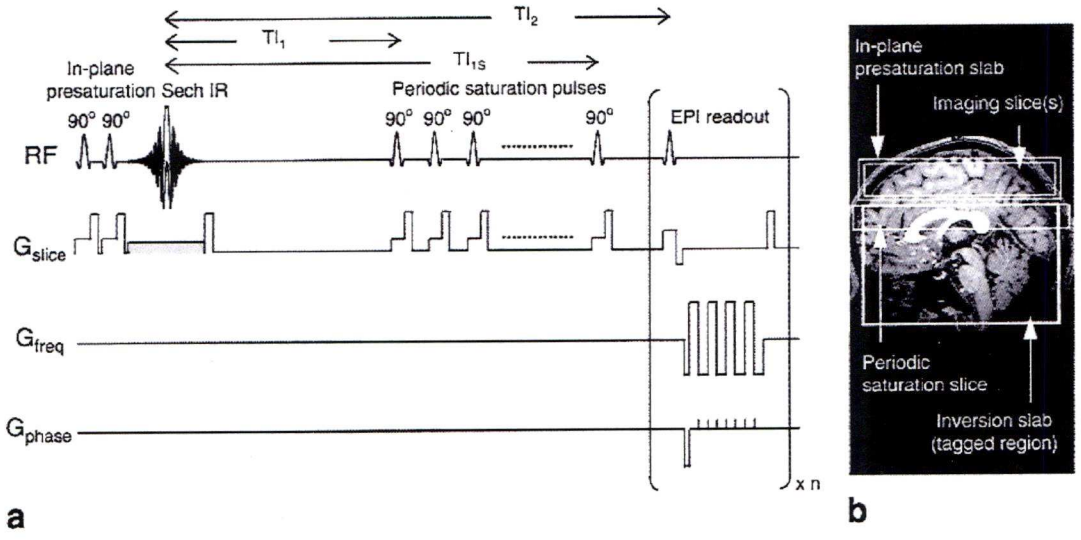

Figure 2.3 The Q2TIPS pulse sequence. The gradient lobe shown in grey is applied alternatively to generate tag and control images. 90° periodic saturation pulses applied between TI_1 and TI_{1stop} to the distal end of the tagging region, with each followed by a crusher gradient. (Luh et al., 1999)

2.2 Quantification of CBF using PASL

Obtaining estimates of CBF from measured differences in magnetisation between tagged and control images in ASL, involves the implementation of a kinetic model to provide a physiological basis for the measured magnetisation differences. In this section, the two main kinetic models that have up until now been used to quantify CBF will be discussed.

2.2.1 The single compartment model

The simplest and most applicable model for ASL acquired images is the single compartment model, whereby we start with the assumption that the imaging voxel is a single, well-mixed compartment with intra- and extra-vascular water in perfect communication (Figure 2.4) (Parkes et al., 2002). There are a number of approaches to using the single compartment model in CBF quantification, the most common of which is to modify the Bloch equations:

$$\frac{dM(t)}{dt} = \frac{M_0 - M(t)}{T1} + f(m_a(t) - m_v(t)) \qquad [2.2]$$

Where $M(t)$ is the total magnetization in a tissue voxel of the difference image, m_a is the arterial magnetisation in the difference image, m_v is the venous magnetisation in the difference image, $T1$ is the longitudinal relaxation of the magnetisation in the tissue voxel, and f is the CBF.

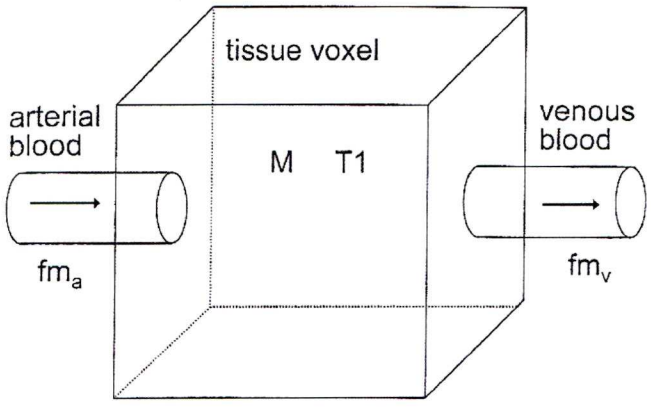

Figure 2.4 Single compartment model. The measured tissue voxel has magnetization M and relaxation time T1. (Parkes, 2005)

This approach works on the assumption that the capillary walls have infinite permeability to water, and that the magnetisation of venous blood as it leaves the voxel, is equal to the magnetisation of the whole voxel, weighted by the equilibrium ratio of water in brain compared to blood (λ). That is $m_v(t) = M(t)/\lambda$.

If we consider the difference between tagged and control images (Δ), and assume the parameters f, $T1$, M_0 and λ are constant in both images, the equation reduces to:

$$\frac{d\Delta M(t)}{dt} + \frac{\Delta M(t)}{T1_{app}} = f\Delta M_a(t) \qquad [2.3]$$

Where

$$\frac{1}{T1_{app}} = \frac{1}{T1} + \frac{f}{\lambda} \qquad [2.4]$$

Equation [2.3] can be solved if the difference between arterial magnetization $\Delta m_a(t)$ of label and control images in known. The form this parameter takes depends on the

labeling sequence used. For Q2TIPS $\Delta m_a = 0$ for $t < t_a$ and for $t > TI_1 + t_a$ (i.e. before bolus arrives and after it has been crushed).

$$\Delta m_a(t) = 2m_a^0 \alpha e^{(-\frac{t}{T1b})} \quad \text{for } t_a < t < TI_1 + t_a \quad \text{(exponential decay with } T1_b\text{)} \qquad [2.5]$$

Where m_a^0 is the equilibrium magnetization of arterial blood, α is the inversion efficiency of labeling, and $T1_b$ is the T1 of blood. The difference in magnetization between control and label images is *twice* the equilibrium magnetization at t=0, which accounts for the factor 2 in equation. The exponential component of the equation accounts for the fact that T_1 decay begins before the tagged blood leaves the tagging region.

2.2.2 The single blood compartment

The main difference between the single blood compartment model (Figure 2.5) and the previously described single compartment model is the assumption that labelled water does not leave the blood compartment during the imaging time, and the parameter m_v in equation [2.3] is assumed to be zero. In a Q2TIPS experiment, the typical time between labelling and image collection (TI2) is less ~ 2 seconds, so this assumption is likely to be valid.

An additional assumption of this model is that that none of the labelled water leaves the tissue voxel during the imaging time. This assumption applies to perfusing water only, where labelled water in larger vessels should have time to flow through and out of the voxel, and is therefore disregarded in this model.

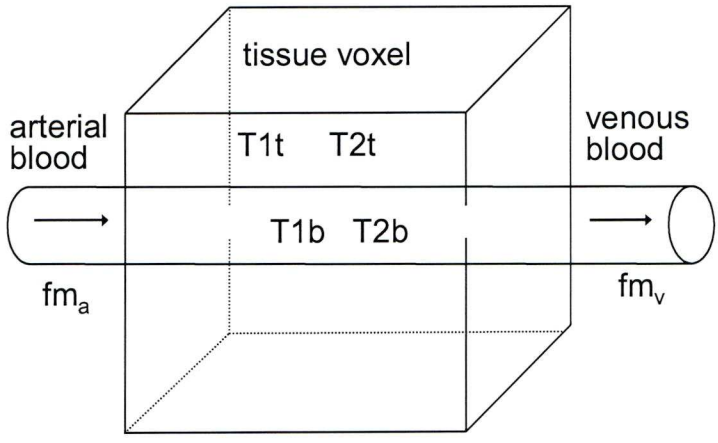

Figure 2.5 The single blood compartment model: where m_a is the arterial magnetization in the difference image. m_v is the venous magnetization in the difference image. T1b and T1t are the longitudinal relaxations of the magnetization in the intravascular and extravascular space respectively. T2b and T2t are the transverse relaxations of the magnetization in the intravascular and extravascular space respectively, and f is perfusion.

By substituting equation [2.5] in to equation [2.3], solving for ΔM gives:

$$\Delta M = 2fm_a^0 \alpha TI_1 e^{-(\frac{t}{T1b})} \qquad [2.6]$$

The parameter M represents the value at the time the measurement is made. However, because the acquisition of multiple slices does not occur simultaneously, the value for M will be slightly different for each slice due to the time taken to image the slices. Therefore a slice time correction is usually applied to the parameter *t*, to account for time between slice collections.

The actual measured signal (S) is also the product of an unknown gain factor (G), therefore, equation [2.6] is more accurately presented as:

$$S = 2fGm_a^0 \alpha TI_1 e^{-(\frac{t}{T1b})} \qquad [2.7]$$

Using an estimated value for alpha (~0.97) and literature values for $T1_b$ (~1.6s), leaves the remaining unknown parameters Gm_a^0, the equilibrium magnetisation of arterial blood multiplied by the unknown gain factor for the sequence. To obtain a measure of

these unknown values, a calibration scan is performed, whereby an EPI image with the same parameters as the control and label images is acquired, but with the labelling pulses turned off and the TR increased to ~10s, allowing sufficient time for full magnetisation equilibrium.

The signal, S_C in the calibration scan (and the control perfusion scans, i.e. those without labelling) is given by the equation:

$$S_C = Gm_0 \qquad [2.8]$$

The equilibrium magnetisation for tissue, m_0, is related to the equilibrium magnetisation for arterial blood, m_a^0 by the brain: blood partition coefficient λ:

$$\lambda = \frac{m_0}{m_a^0} \qquad [2.9]$$

Where λ describes the relative water content of brain to blood. Therefore;

$$Gm_a^0 = G\frac{m_0}{\lambda} \qquad [2.10]$$

The assumption that most of the tagged water molecules remain intravascular during the measurement time necessitates the use of a corrected brain: blood partition co-efficient λ, to account for the relative T2* decay of water in tissue and blood (Buxton et al., 1998a). Essentially, after a time TE when the measurement is obtained, the transverse magnetisation of the water in the two compartments has decayed according to their relative relaxations times T2*. Therefore the resultant correction to λ is:

$$\lambda' = \lambda e^{(\frac{TE}{T2_b^*} - \frac{TE}{T2_t^*})} \qquad [2.11]$$

Therefore, the final form of the equation used to calculate values for CBF using the single blood compartment model and Q2TIPS sequence, is obtained from substituting equations [2.10] and [2.11] into equation [2.7]. After rearranging in terms of the CBF variable *f*, we find:

$$f = \frac{S\lambda e^{\frac{t}{T1_b}} e^{(\frac{TE}{T2_b^*} - \frac{TE}{T2_t^*})}}{2\alpha G m_0 TI_1} \qquad [2.12]$$

2.2.3 The two compartment model

In addition to the single compartment models mentioned in the previous section, a number of more complex models exist, which attempt to address inaccuracies in the single compartment model (Alsop et al., 1996). The *two-compartment model* was developed to correct for two inaccuracies, the first of which is known as the 'T_1' effect. It was assumed in the single-compartment model that when water enters the tissue voxel, the magnetisation relaxes with the T_1 value of tissue. However, it first relaxes with the T_1 value of blood, before moving into the extra-vascular space. By not accounting for the difference in the T_1 values of blood and tissue, an overestimation of perfusion will be made due to the fact that the T_1 of blood is longer than the T_1 of tissue.

The second inaccuracy of the single-compartment model is due to the so called 'outflow effect'. It was assumed in this model that there is a total exchange of water between blood and tissue, and that an equilibrium condition occurs between the two. However, some of the labelled water will pass directly out of the vasculature without exchanging with tissue, thus giving a greater venous magnetisation than would be expected when using the relation $m_v = M(t)/\lambda$. The result of this is an underestimation of perfusion.

One approach to correct for the T_1 effect is through the introduction of an arterial compartment within the tissue voxel. In this model, water enters the arterial compartment within the tissue voxel, relaxing with the T_1 of blood. It then moves into the tissue compartment with an exchange time T_{ex}. However, this technique is complicated by the difficulty of defining an exchange time.

An alternative approach is to include the use of *permeability surface* area product (PS) (Alsop et al., 1996; Zhou et al., 2001), which accounts for the semi-permeable nature of the vascular wall, where exchange of labelled blood from the vascular to the extra-vascular environment is uni-directional.

In practice, the accuracy of the various CBF quantification models is dependent on factors such as tissue type, measurement time, field strength, and perfusion rate (Parkes, 2005). The most practicable quantification model for the experimental work in this thesis, which is to some extent constrained by the requirement of measurements of CBF change over time, is the single blood compartment model; requiring only one inversion

time, with no dependency on arrival time or vessel wall permeability. It has been shown to give a fairly high level of accuracy (<10% error) (Parkes et al., 2002) in CBF estimates in grey matter, which is the primary region of interest for this thesis.

2.3 Applications of ASL

2.3.1 Clinical applications

The development of ASL techniques over the last two decades has seen an increasing number of clinical applications; however, as a method for obtaining robust CBF measurements, it has failed to make the impact of other imaging modalities, perhaps largely due to the comparatively low SNR. However, it is becoming increasingly recognised as a viable alternative to more established methods, particularly from a health perspective, where techniques that involve ionizing radiation or contrast injection may not be ideal for repeat measurements. The contrast injection method also requires a period of time for the agent to equilibrate in the system before a repeat measurement is possible, making it difficult to track CBF over time with non ASL techniques. As such, there have been a variety of different applications in recent years using ASL to measure CBF. Ranging from the assessment of cerebrovascular diseases and the effect of stenoses (Detre et al., 1998; Detre et al., 2001), CBF changes in hyperacute stroke (Chalela et al., 2000; Detre, 2001) and multiple sclerosis (Rashid et al., 2004) as well as in the assessment of tumoral related disease, including diagnosis and biopsy guidance (Tourdias et al., 2008). A recent publication highlights a variety of other applications of clinical neuroimaging using ASL (Wolf et al., 2007), which also include the measurement of CBF in neurodegenerative disorders, epilepsy and neuropsychiatric diseases.

2.3.2 ASL in functional MRI

There has been a great deal of interest in recent years in the study of functional changes in the brain using MRI, usually in response to certain stimuli. This is generally referred to as functional MRI (fMRI), and is typically achieved using EPI to measure the BOLD (Blood Oxygen Level Dependent) signal, which essentially is a measure of the changes

in magnetisation that occur in response to varying levels of deoxyhaemoglobin content in the blood, which have been found to occur in regions associated with increased or decreased neural activity. However, similar information can also be extracted from PASL acquired images. That is, instead of subtracting tagged images from control images, the images can be *added*, or just the control images themselves can be used to obtain measurements of the BOLD signal. Therefore PASL has the added benefit of being able to acquire two measurements simultaneously.

The previously highlighted clinical applications rely on making repeated measurements or averages over several minutes, in order to obtain a perfusion weighted image with sufficiently high SNR to generate a robust baseline CBF measurements or maps. However, the fact that simultaneous BOLD measurements can be acquired makes it particularly beneficial for applications in fMRI, where it is possible to measure relative local changes in CBF and BOLD signal in response to a given neural stimulus. And by obtaining these two measures simultaneously, it is also possible to obtain estimates for local changes in oxygen metabolism, which occur during the given stimulus. The application of PASL and in particular Q2TIPS in fMRI is central to the work presented in this thesis; the theory of which will be further detailed in the next chapter.

Chapter 3. Functional MRI

3.1 Introduction to fMRI

The introduction of MRI saw an imaging modality that was, and still is an unrivalled technique for obtaining high detail anatomical images, with minimal detriment to safety. But it is perhaps the development of functional MRI and its application in the study of the human brain that really demonstrates the versatility of this technology.
The foundation for fMRI as a dedicated research area was established in the early 1990's, when it was observed that the paramagnetic deoxyhaemoglobin in venous blood could be used as a naturally occurring contrast agent. It was found that with high field strengths and a gradient-echo imaging sequence, the paramagnetic effects of deoxyhaemoglobin could be accentuated to obtain in vivo images of brain microvasculature (Ogawa et al., 1990).This had obvious implications as a technique for mapping blood oxygenation changes, which occur in response to neural demand.

At around the same time, a technique was being developed to measure cerebral blood volume (CBV) changes using an injection of gadolinium based contrast agent, which could be mapped using gradient echo EPI sequences (Rosen et al., 1991a; Rosen et al., 1991b). This technique was soon applied to a human during photic stimulation, and functional maps were produced showing increased blood volume during visual activation (Belliveau et al., 1991).

It was soon after this work by Belliveau et al. that the concept of functional activation maps using a contrast agent was applied to the earlier observations by Ogawa et al. whereby changes in deoxyhaemoglobin concentration could be measured in response to local changes in CBF, CBV and oxygen metabolism ($CMRO_2$).
In fact, several independent research groups simultaneously demonstrated functional mapping using the Blood Oxygen Level Dependent (BOLD) signal, with signal time courses corresponding to sensory stimulation paradigms, which were measured in brain regions known to be associated with the given tasks (Bandettini et al., 1992; Kwong et al., 1992; Ogawa et al., 1993).

This was sufficient evidence to suggest that by measuring the BOLD signal in response to a given stimulus, during a predetermined experimental paradigm, it was possible to obtain a map of functional activity, reflecting regions of the brain which were metabolically active in response to the stimulus.

3.1.1 Coupling of neuronal activity to the haemodynamic response

It was observed by Ogawa et al. that neural activation in the brain, was accompanied by changes in CBV, CBF and blood oxygenation (Ogawa et al., 1993). The relationship between these physiological variables had previously been studied using positron emission tomography (Fox et al., 1986), where it was hypothesised that CBF changes were somehow regulated by neuronal or biochemical changes, independently of oxygen metabolism. Later fMRI studies showed that during neural activation, an increase in oxygen usage occurs, and is accompanied within a few seconds by an increase in CBF and CBV (Malonek et al., 1997). This relationship between metabolic demand and blood flow had been proposed a long time before the intervention of fMRI (Roy et al., 1890), but exactly what mechanisms couple the supply and demand for energy, and which cells types generate this demand, remain open questions (Logothetis, 2007). To simplify this issue, we need to try and address two fundamental issues: what is the purpose of CBF increase? And what triggers a CBF increase?

The energy required for normal brain function is in the form of the metabolite ATP, the production of which involves the process of glycolysis; that is the breakdown of glucose to pyruvate, lactate and ATP. Under normal conditions, this is achieved aerobically in mitochondria within cells, in the presence of oxygen (Matthews, 2001). This is the main source of energy production in the brain, and accounts for around 90% of the metabolised oxygen in the brain (Gjedde et al., 2002). As such, one of the primary purposes of CBF in the brain is to supply a sufficient quantity of glucose and oxygen to meet with metabolic demands, necessary for maintaining homeostasis. This is also true for increases in CBF in response to increased metabolic activity during neural activation. However, one curious aspect of the CBF increase is the apparent disparity between O_2

supply and demand. A disproportionally large change in CBF occurs, and therefore supply of O_2, relative to the rate of oxygen metabolism.
It has been proposed that this is the result of *diffusion-limited delivery* of oxygen to brain tissue (Buxton et al., 1997), and is based on two assumptions: a) That all of the brain capillaries are perfused at rest, and (b) Essentially all the O_2 that leaves the capillaries is metabolized. The implications of these physiological assumptions are that if the capillaries are fully perfused at rest, then an increase in CBF is accompanied by increased blood velocity in the capillaries. The second implication is that the O_2 extraction fraction must decrease as flow increases and therefore a relatively large change in flow is required to support a small increase in O_2 metabolism. This suggests that despite the apparent disproportionality between CBF and $CMRO_2$, they are in fact tightly coupled. This physical description has been used to form the basis for modelling the BOLD response (Buxton et al., 1998a; Friston et al., 2000).

If we accept that one of the primary roles of CBF increase is to meet with the increased demand for oxygen and glucose, we need to understand what mechanism triggers this response. The oxygen used during neural activation must co-localise with the activity. However, the regions where increased blood flow occurs, subsequent to neural activity are substantially larger, which suggests that it is controlled by factors other than a lack of energy. The available evidence suggests that a glutamate evoked Ca^{2+} influx in postsynaptic neurons activates the production of nitric oxide (NO), adenosine and arachidonic acid metabolites. The effect of these chemicals is a local vasodilation, reflecting the activity of the presynaptic neurons, and the level of depolarisation of the postsynaptic cell (Attwell et al., 2002).

Vasodilation has also been shown to occur as a result of increased extracellular K^+ concentrations (Iadecola et al., 1991). The effect is not as substantial as that derived from neural activity, and could be largely the result of K^+ depolarizing neurons, leading to NO release through the release of glutamate or evoking Ca^{2+} influx via voltage gated channels (Dreier et al., 1995).

It has also been found that neurally evoked increases in CBF do not relate to the firing of the cerebellar principle output neurons; the *Purkinje* cells (Attwell et al., 2002). If we consider the role of CBF increase in terms of response to metabolic demand, then this observation is further supported by a recent publication where simultaneous and co-localized measurements of oxygen partial pressure and electrical activity, were made in the visual cortex of the cat (Viswanathan et al., 2007). The results of the experiment showed a high level of coupling between local field potentials (LFP's, generated by integrated local dendritic events), and changes in tissue oxygen concentration. The same coupling was not observed between action potentials and tissue oxygen concentration. These results would suggest that the increase in $CMRO_2$ and subsequent increase in CBF, which give rise to the BOLD signal in fMRI, most likely reflect input neurotransmitter signaling events and intra-cortical processing rather than the output from that area. However, it has also been suggested that the establishment of an increased CBF level may be to support the increased oxidative energy metabolism in the so called *afferent* phase, associated with projection from the area of activation (Gjedde et al., 2002).
The mechanisms responsible for the neurovascular coupling, although not completely understood, can be thought of conceptually as two independent processes, both associated with neural activity. On the one hand there is increased energy consumption, resulting in increased oxygen metabolism through aerobic glycolysis, and on the other hand there is an associated increase in CBF due to the vasodilatory effects associated with neurotransmitter signaling events. Understanding these physiological events seems critical for accurate interpretation of fMRI data. However, the interpretation of the BOLD signal is to some degree confounded by the assumptions that are made, such as the diffusion limited model, regarding the biophysical origin of that signal.

3.2 Modeling the BOLD signal change

3.2.1 Deoxyhaemoglobin dilution model

The sensitivity of MRI to the blood oxygen level is based on the T_2^* effects of deoxyhaemoglobin, which is paramagnetic and causes attenuation of local image intensity. The uptake of O_2 from blood in the capillary network, leads to a subsequent

increase in deoxyhaemoglobin in the venous network, which leads to reduced signal intensity in that region. As mentioned earlier in this chapter, the metabolism of oxygen is closely followed with an increase in CBF and CBV. The increased blood flow leads to an increase in venous oxygen saturation (SvO_2), and a relative decrease in deoxyhaemoglobin within the tissue voxel. The SvO_2 changes associated with CBF increase, and the resultant increase in signal intensity, represents the dominant effect that gives rise to the measured BOLD signal.

In attempting to understand quantitatively how changes in CBF, CBV are coupled with changes in $CMRO_2$, a model was introduced which describes the measured BOLD signal change in terms of the transverse relaxation rate ΔR_2^*, which is linearly dependent on the blood volume fraction, and dependent on magnetic susceptibility difference between blood and tissue, which is proportional to deoxyhaemoglobin content of the venous blood (Davis et al., 1998). This so called *deoxyhaemoglobin dilution model* has been the basis for a large number of quantitative fMRI studies, including the experimental work in this thesis.

Soon after the introduction of this model by Davis et al. a revised version was published by Hoge et al, which presents the model in what has become a more established form (Hoge et al., 1999a). The basis for the models is made from the observation that transverse relaxation rate due to deoxyhaemoglobin is related to CBV in the form:

$$R_2^*|_{dHb} = A \cdot CBV \cdot [dHb]_v^{\beta} \qquad \text{(Boxerman et al., 1995)} \qquad [3.1]$$

The parameter A is a proportionality constant, dependent on field strength and imaging sample. The value β is a simulated value referring to the power law relationship $R \propto \Delta B^{\beta}$ as detailed by Davis et al, representing the magnitude of field distortion. For a mixture of vessel sizes, β=1.5 is a good approximation for B =1.5 – 3T (Davis et al., 1998).

For small changes in R_2^* equivalent to those responsible for BOLD signal change, the fractional change in BOLD signal can be represented as:

$$\frac{\Delta BOLD}{BOLD_0} \approx -TE\Delta R^*_{2dHb} \qquad [3.2]$$

This relationship for R_2^* can be reformulated in terms of a BOLD signal change at baseline and during activation:

$$\begin{aligned}\frac{\Delta BOLD}{BOLD_0} &\approx TE \cdot A(CBV_0[dHb]^{\beta}_{v0} - CBV[dHb]^{\beta}_{v}) \\ &\approx TE \cdot A \cdot CBV_0[dHB]^{\beta}_{v0}\left(1-\left(\frac{CBV}{CBV_0}\right)\left(\frac{[dHb]_v}{[dHb]_{v0}}\right)^{\beta}\right)\end{aligned} \qquad [3.3]$$

where the subscript 0 refers to baseline values. The maximum possible BOLD signal measured is represented by the group of terms: $TE \cdot A \cdot CBV_0[dHb]^{\beta}_{v0}$

These values reflect the attenuation of the BOLD signal due to the deoxyhaemoglobin level at baseline, and are generally referred to collectively as the calibration constant *M*. The equation can be further remodelled by expressing CBV in terms of CBF by applying the Grubb relationship (Grubb et al., 1979),

i.e.

$$\frac{CBV}{CBV_0} = \left(\frac{CBF}{CBF_0}\right)^{\alpha} \qquad [3.4]$$

This equation relates CBV and CBF in a steady state condition, where α was calculated as 0.38. This value is generally used when applying this model, however some studies suggest it may vary under certain experimental conditions (Ito et al., 2001; Kida et al., 2007). A further remodelling of equation [3.2] consists of presenting the change in deoxyhaemoglobin as a change in CBF and $CMRO_2$:

$$[dHb]_v = \frac{1}{4}\frac{CMRO_2}{CBF} \qquad [3.5]$$

The factor ¼ accounts for the fact that each molecule of dHb delivers $4O_2$

$$\therefore \quad \frac{[dHb]_v}{[dHb]_{v0}} = \left(\frac{CMRO_2}{CMRO_2|_0}\right)\left(\frac{CBF_0}{CBF}\right) \qquad [3.6]$$

This leads to the final form of the model:

$$\frac{\Delta BOLD}{BOLD_0} = M\left(1-\left(\frac{CMRO_2}{CMRO_2|_0}\right)^{\beta}\left(\frac{CBF}{CBF_0}\right)^{\alpha-\beta}\right) \qquad [3.7]$$

3.2.2 Alternative approaches to modelling the BOLD signal

The values for BOLD, CBF and calibration parameter M, in equation 3.7 are generally acquired using an ASL sequence. However, the use of an alternative fMRI technique known as *VASO* (Vascular space occupancy)(Lu et al., 2003) allows quantification of CBV without the need to apply the Grubb relationship to CBF measured values. This technique was modified further to obtain an inversion recovery sequence capable of simultaneous acquisition of CBV, CBF and BOLD signal (Yang et al., 2004). A recent study applied this imaging sequence in a study comparing estimated values of $CMRO_2$ during visual stimulation with a single compartment BOLD model, as outlined above, and with a *multi-compartment model*, whereby the equation describing BOLD signal change is separated into intravascular and extravascular components (Lin et al., 2008). They found both compartment models to be comparable, and that estimates of $CMRO_2$ change in response to visual stimulus with variable frequency, agreed well with previous studies, suggesting that the imaging sequence is potentially equivalent to the more standard ASL method, but may be beneficial in eliminating errors associated with the application of the Grubb relationship. It also suggests that the single compartment approach is sufficient for modelling the BOLD signal change.

An alternative approach to modelling the BOLD signal, known as the *balloon model* (Buxton et al., 1998b), was formulated in response to observations in animal studies

(Mandeville et al., 1998) that CBV returned to baseline more slowly than CBF, and may explain the post-stimulus undershoot, often observed in BOLD signals.

The model treats the venous compartment as a distensible balloon, where the inflow to the balloon is f and the outflow is f_{out}.

$$\frac{dq}{dt} = \frac{1}{\tau_{MTT}}\left[f(t)\frac{E(t)}{E_0} - \frac{q(t)}{v(t)} f_{out}(v,t) \right] \qquad [3.8]$$

where $q(t)$ and $v(t)$ are two dynamic variables, representing total deoxyhaemoglobin and balloon volume respectively. τ_{MTT} is the mean transit time of blood through the balloon at rest. It is a time constant and acts as a scaling factor. E and E_0 represent oxygen extraction fraction during activation and baseline conditions respectively.

The parameters: $f\frac{E}{E_0}$ is equivalent to $CMRO_2$ normalised to rest value, often denoted as m. To compensate for viscoelastic effects, such as transient lagging in blood volume, not accounted for in the steady state power law [3.4], f_{out} is treated as a function of balloon volume, and the rate of change of that volume.

$$f_{out} = v^{\frac{1}{\alpha}} + \tau\frac{dv}{dt} \qquad [3.9]$$

The model now assumes that there is initial resistance to change in CBV, followed by the standard steady state power law relationship. The period of transient behaviour is expressed as the time constant τ, which can take on values of τ_+ and τ_-, to represent the transient periods which occur during inflation and deflation respectively.

In addition to the standard balloon model, a number of alternative approaches have received attention in recent years (Buxton et al., 2004; Deneux et al., 2006; Friston et al., 2000; Jacobsen et al., 2008; Mandeville et al., 1999; Uludag, 2008), in an effort to correctly model sustained and transient behaviour of the BOLD signal, such as the

previously mentioned pre- and post-stimulus undershoot, and the less discussed overshoot at the beginning and end of an applied stimulus (Obata et al., 2004).

3.3 Calibration of the BOLD signal

The use of functional MRI as a tool for indirectly locating regions of neural activity in the brain by measuring associated changes in the local venous BOLD signal is an established technique. However, measured BOLD signal changes in fMRI are the result of a combination of factors including changes in CBF, CBV, and $CMRO_2$, and so any measured signal change has some level of ambiguity about the relative contributions of these effects. In subjects with compromised neurovascular function, which may be pathological or to a lesser extent the result of normal ageing, the measured BOLD signal may likely be altered, and is therefore potentially misleading. In such cases, it may be more informative to measure the relative changes in the physiological parameters CBF, CBV and $CMRO_2$, to gain a clearer understanding of the observed BOLD signal change, and the coupling between neural vascular responses.

To estimate the contribution of these changes to the BOLD signal measured during an activation task, the established 'BOLD calibration' technique is used (Davis et al., 1998; Hoge et al., 1999b), which involves the use of an isometabolic stimulus to induce changes in CBF in the absence of neural activation, from which a BOLD signal change can be obtained that is independent of changes in $CMRO_2$. This is typically achieved by inducing hypercapnia through the inhalation of moderate levels (~5%) of CO_2 gas. This would lead to the $CMRO_2$ terms in equation [3.7disappearing, and by performing ASL image acquisition, quantitative values for change in BOLD and CBF can be obtained, allowing the unknown calibration parameter M to be estimated.

$$\frac{\Delta BOLD}{BOLD_0} = M\left(1-\left(\frac{CBF}{CBF_0}\right)^{\alpha-\beta}\right) \qquad [3.10]$$

Given that an increase in oxygen metabolism, and subsequent rise in deoxyhaemoglobin, acts to reduce the BOLD signal, the signal measured during hypercapnia, which is

assumed to be independent of changes in oxygen metabolism, should theoretically represent the maximum BOLD signal obtainable for a given level of perfusion.
The calibration parameter M is proportional to baseline deoxyhaemoglobin content and CBV, both of which may vary according to the neuronal and vascular anatomy, specific to the sample or imaging voxel. As such, this parameter represents a localized value. By re-inserting the value obtained for M into equation [3.7], along with measured values for the change in BOLD and CBF during a neural challenge, it is then possible to obtain an estimate of the $CMRO_2$ contributions to the BOLD signal measured during the neural challenge. This must involve obtaining a measurement of M within the same region of interest, defined by the area of functional activation during the neural challenge.
The ratio of change in CBF to $CMRO_2$ is often denoted by the neurovascular coupling parameter n (Buxton et al., 2004), where:

$$n = \frac{CBF / CBF_0}{CMRO_2 / CMRO_2|_0} \qquad [3.11]$$

This parameter may be used as an index of the underlying normality of the neurovascular coupling, with most studies finding a value in the region of $n = 2 - 3$ in healthy participants, generally in visual and motor cortices (Ances et al., 2008a; Chiarelli et al., 2007a; Davis et al., 1998; Hoge et al., 1999a; Kastrup et al., 2002; Leontiev et al., 2007).

3.3.1 Alternative methods of BOLD calibration

The relative ease and minor discomfort associated with the CO_2 gas induced hypercapnia, as well as the consistency of measured data between studies, has meant that this has been the method of choice for calibrated BOLD studies. However, several studies have demonstrated the use of *acetazolamide* as a method for iso-metabolically increasing CBF (Bickler et al., 1988a; Bickler et al., 1988b; Brown et al., 2003), which in principle could be used as a substitute for CO_2 gas inhalation.

An alternative technique for inducing hypercapnic changes in CBF is using *breath hold* (Kastrup et al., 1999a; Kastrup et al., 1999b; Kastrup et al., 1998; Thomason et al., 2007). The reduction in O_2 and subsequent increase in CO_2 blood levels, leads to vasodilation in the absence of increased neural activity, thereby inducing a BOLD and CBF response that can be used to obtain a measure of the calibration parameter, and therefore calibrate the BOLD signal measured during neural activation (Kastrup et al., 1999a).

Although breath hold calibration may be advantageous in regards to implementation, in that it is non-invasive and does not require any specialized equipment, there is a potential issue regarding the reproducibility of the technique. This is based primarily on the need for subject compliance, which is non-passive and it may be difficult to monitor adherence to task.

A recent advancement in BOLD calibration methodology was the introduction of a *hyperoxia* calibration model, which involves the inhalation of oxygen rich air as the isometabolic stimulus. (Chiarelli et al., 2007b). Unlike the hypercapnia approach, which relies on the stimulated increase in CBF to generate a measurable change in BOLD signal; hyperoxia generates an increase in BOLD response by the reduction in deoxyhaemoglobin resulting from the saturation of venous blood with O_2. This method, although utilizing a different physiological effect, still generates a BOLD response which is independent of neural activity and therefore can be used to obtain a calibration factor, which is then applied to the standard deoxyhaemoglobin model.

The use of hyperoxia as a calibration method may offer a number of advantages to the hypercapnia approach. Perhaps most notably is the potential for use within patient groups who may have an intolerability to hypercapnia, but also because the BOLD response generated through CO_2 inhalation may not be an entirely isometabolic response (Kliefoth et al., 1979; Rostrup et al., 2000; Zappe et al., 2008).

The hyperoxia model, outlined by Chiarelli et al. involves a reworking of the deoxyhaemoglobin model, to allow the calibration factor M to be obtained.

This first deviation from this model is the addition of CBV and dHb correction terms to equation [3.3], to account for the small reduction in CBF that was found to occur during periods of hyperoxia.

$$\frac{\Delta BOLD}{BOLD_0} \approx TE \cdot A \cdot CBV_0 [dHB]_{v0}^{\beta} \left(1 - \left(\frac{CBV + \Delta CBV}{CBV_0}\right)\left(\frac{[dHb]_v + \Delta[dHb]_v}{[dHb]_{v0}}\right)^{\beta}\right) \quad [3.12]$$

Where the ΔCBV and ΔdHb represent the cerebral blood volume and deoxyhaemoglobin correction terms due to CBF reduction during hyperoxia. However, Chiarelli proceeds with the assumption that an isolated change in deoxyhaemoglobin concentration will not induce a change in CBV, therefore CBV = CBV_0.

By applying Grubb's relationship between steady state CBV and CBF and using Fick's principle [3.4] to express change in deoxyhaemoglobin in terms of CBF change in the absence of any change in oxygen metabolism, the final version form of the hyperoxia model is expressed as:

$$\frac{\Delta BOLD}{BOLD_0} \approx M\left(1 - \left(\frac{CBF}{CBF_0}\right)^{\alpha}\left(\frac{[dHb]_v}{[dHb]_{v0}} + \frac{CBF_0}{CBF} - 1\right)^{\beta}\right) \quad [3.13]$$

To solve for M requires ASL derived measures of BOLD and CBF, and a measure of the change in dHb. This can be estimated by measuring end tidal O_2 during the course of the hyperoxia scan, and applying a number of physiological relationships for oxygen transport in blood, as outlined by Chiarelli et al.

One possible deviation from this model, which may be advantageous in regards to removing unwanted noise from the measurements, which are inherent to perfusion weighted Arterial Spin labeling (ASL) images, is to use an assumed value of CBF reduction, which according to Bulte et al, is likely be ~7% at 100% inspired O_2 (Bulte et al., 2007) in healthy adults, over a 12 minute period, although there is some discrepancy

between studies over measured values of CBF reduction during hyperoxia (Bergofsky et al., 1966; Chiarelli et al., 2007b; Ohta, 1986; Watson et al., 2000), with a study by Watson et al. showing a larger reduction in young people. If that is in the fact case, this may be one confound for using an assumed value for CBF reduction, particularly for studies comparing quantitative neurovascular coupling measurements across different age groups.

With the choice of calibration techniques currently available, it is perhaps reasonable to question, which one is the most effective. Certainly the hypercapnia technique using CO_2 gas inhalation is the favored choice; however this technique may not always be appropriate, particularly in certain clinical populations. The use of acetazolamide, although recognized as a method for inducing iso-metabolic vasodilation, may require intravenous administration, which is invasive and sometimes not without side effects (Brown et al., 2003). This has not been established as an alternative technique to CO_2 gas inhalation for the use of BOLD calibration, but could perhaps be a viable alternative in patients with pulmonary dysfunction, who may have intolerability to CO_2 gas.

The use of breath hold, as mentioned earlier has the advantages of requiring no specialized equipment, although the effectiveness of this technique for obtaining accurate measures for change in $CMRO_2$ is still questionable. For studies where $CMRO_2$ estimation is not of particular interest, breath hold derived BOLD measurements may still be useful for normalizing measurements acquired in response to a neural challenge, which has been shown to be a useful technique for reducing group variance in fMRI studies (Handwerker et al., 2007; Thomason et al., 2007).

Hyperoxia calibration appears to be the most viable alternative to hypercapnia calibration using CO_2 gas. In addition to obtaining comparable results with this technique, Chiarelli et al. also demonstrated lower overall inter-subject and intersession variability compared to the hypercapnia method.

The application of breath hold and CO_2 gas induced hypercapnia, and O_2 gas induced hyperoxia, as BOLD calibration techniques in fMRI, is demonstrated in the experimental chapters 5 – 8 of this thesis.

3.4 Imaging functional activity

The most sensitive and most common technique for measuring BOLD signal changes in fMRI is through T_2^* weighted signal changes. The small degree of change in signal intensity, usually 2-3%, and the relative instability of the BOLD signal, require rapid imaging techniques such as echo-planar sequences, with an echo time (TE) optimised for maximum signal. Increasing the TE value leads to an increase in the phase dispersal of the hydrogen nuclei due to field inhomogeneities, and the paramagnetic effects of deoxyhaemoglobin. This results in a reduction in the measured signal.
Optimisation of the TE parameter involves choosing a value between the T_2^* time of rest and activation. This is primarily dependent on the main B_0 field strength, with typical TE values at 1.5 T ~ 70ms (Jones, 2002) and ~50 ms at 3T (Fera et al., 2004). The optimal TE selection is governed by:

$$TE_{opt} = \frac{\ln[R2^*(a)] - \ln[R2^*(b)]}{R2^*(a) - R2^*(b)} \qquad [3.14]$$

Where $R2^* = 1/T_2^*$

In reality, the range of T_2^* values will vary across the sample, and so the optimal TE value will vary on a voxel by voxel basis. A reduction in this range can be achieved by acquiring higher resolution images, leading to a higher number of voxels with equal BOLD sensitivity. This is increasingly relevant at higher field strengths, where the microscopic susceptibility effects are greater, leading to image distortion at high TE values. In practice, multislice imaging is usually acquired at a TE value lower than optimum (~35ms at 3T). This is generally a requirement of high temporal sampling, which becomes more significant with a greater numbers of slices.

3.4.1 Gradient echo vs. Spin echo

The use of a second, 180° RF pulse in Spin echo EPI, effectively eliminates T_2^* effects that result from magnetic field inhomogeneities and static tissue susceptibility gradients, whereby magnetisation vectors across the sample become out of phase with one another after the first 90° pulse, leading to destructive interference and loss of signal. The insensitivity to T_2^* effects may mean that Spin echo imaging has added benefit to gradient echo EPI in regions where T_2^* is particularly short, leading to fewer image artefacts. However, the attenuation of static dephasing effects leads to a BOLD dependency on T_2 relaxation, which results in a reduced BOLD response when compared to the equivalent gradient echo measurement. One study showed that the average gradient-echo/spin-echo ratio of activation-induced signal changes at the TE for maximal BOLD contrast for each sequence was calculated to be 1.87 +/- 0.40 (Bandettini et al., 1994).

Despite this fact, Spin Echo does offer potential benefits at higher field strengths, where insensitivity to extra-vascular dephasing proximal to larger vessels, and the sensitivity to the random dephasing of hydrogen protons nearer microvasculature, leads to an extravascular contribution to the BOLD signal which, spatially is more representative of the area of neural activity (Norris et al., 2002; Thulborn et al., 1997), but at lower field strengths would be relatively weak (Jones, 2002).

3.4.2 Spatial and temporal resolution

One of the major constraints of fMRI in making inferences about underlying neural activity is the temporal and spatial resolution of the measured response.

The ability to resolve two distinct sources of activation, is dependent on the spatial extent of the haemodynamic response, the spatial resolution of the image acquisition, and the sensitivity of the experiment, of which the most complex is the haemodynamic response (Norris, 2006).

The timescales associated with neural events, such as evoked responses and action potentials, occur in the millisecond range. The haemodynamic response associated with that activity is comparatively slow, with the standard BOLD response to a brief stimulus taking several seconds, and up to one minute to return to baseline.

Figure 3.1 shows the three typically distinct phases in the BOLD response to a brief stimulus. An initial post stimulus *fast response* is thought to occur as a result of increased $CMRO_2$ prior to an increase in CBF (Buxton et al., 2004; Devor et al., 2003; Devor et al., 2005), followed by the main CBF driven BOLD response. Some degree of uncertainty remains over the final phase of the BOLD response, which has been thought to be the result of either a delayed reduction in CBV, or a continuation of oxygen metabolism after the CBF has returned to baseline (Lu et al., 2004b).

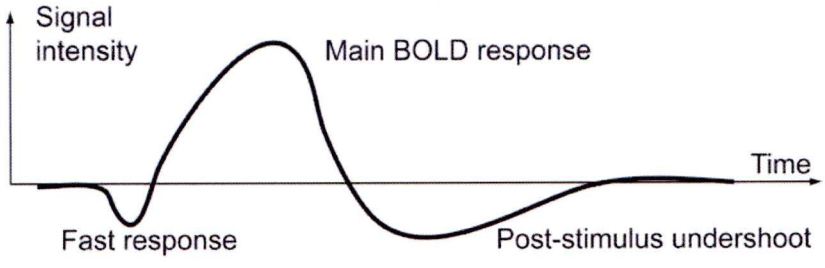

Figure 3.1 The three phases of the BOLD response. The initial fast response taking 2 – 3 seconds post stimulus. The main BOLD response taking up to 5 seconds, with the post stimulus undershoot taking up to 1 minute to return to baseline (Norris, 2006).

The temporal resolution of BOLD signal is fundamentally limited by the duration and dispersion of the haemodynamic response, whereas the spatial resolution is to some degree dependent on the acquisition protocol. Typically, the measured vascular response to neural activity extends over approximately 3mm FWHM at 3T, but can often be mislocalized due to the change in deoxyhaemoglobin content in draining veins and venules, causing an increase in the spatial extent or point spread function of the response (Parkes, 2005). Studies at higher field strengths (4 – 7T) have shown that sub-millimetre resolution is obtainable (Yacoub et al., 2003), and that the use of Spin echo rather that Gradient echo, can lead to reduced mislocalization of the response caused by out flowing large vessels, with the signal originating from the microvasculature being accentuated.

Despite the improvement in spatial resolution, and localisation that can be obtained in high field Spin echo EPI, the majority of fMRI studies are performed at 1.5 – 3T using gradient echo techniques, which benefit from significantly higher contrast to noise.

3.5 Experimental design and analysis

The design of an fMRI experiment and the subsequent analysis of the imaging data is perhaps one of the least standardised aspects of MRI application. The interaction of methodological limitations and the physiological properties being measured in an fMRI study, place some confines on the experimental paradigm. However, this can also be a source of variation between research groups. Factors such as type of scanner, type of sequence, or the stimulus paradigm itself, are all factors which have a bearing on the measured results.

In addition, the analysis of fMRI data varies considerably, dependent in part on the research question, but also on the researchers themselves, with a number of different software and analytical techniques available. Nonetheless, this section will detail the two main types of experimental paradigm; *blocked design* and *event related.* It will also introduce the commonly applied *general linear model*; a statistical technique for observing activation data that correlates to the experimental paradigm.

3.5.1 Paradigm design

The most common and most easily implemented experimental paradigm in fMRI is the *block designed* approach. This approach involves the participant's engagement during the scan with an activity such as a motor task, visual presentation or some cognitive related task, for discrete epochs typically ranging from between 16 seconds to 1 minute in length, and interspersed with discrete epochs of either contrasting conditions or rest periods.

The activation epochs will generally require a repetition of the particular stimulus throughout the duration of each of the epochs, such as the flashing checkerboard stimulus shown in Figure 3.2. The epochs themselves are repeated generally at least 3 – 4 times to allow contrast between epoch conditions. Time integrated averaging

procedures can then be applied across each epoch, for each stimulus condition and regions of activity change between one condition and another can be obtained within the respective areas within the brain.(Donaldson, 2002). Block design studies are robust, simple to execute, and well suited to studies that require steady state changes in activation, such as calibrated fMRI

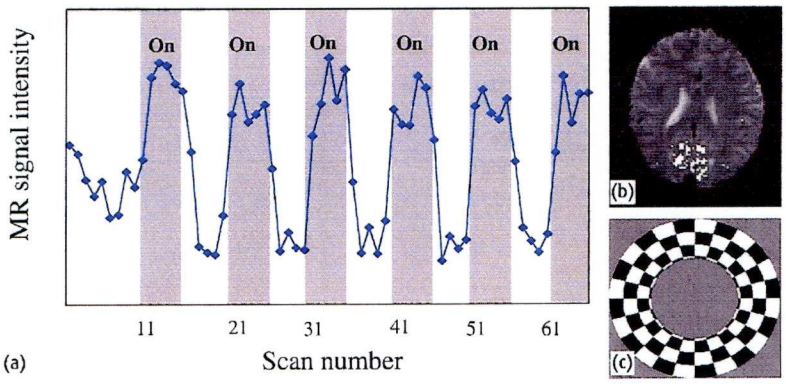

Figure 3.2 Typical Block design experiment. a) BOLD signal change is measured corresponding to application of visual stimulus shown in c), and measured in activated visual cortex b). (McRobbie et al., 2003)

studies, where the Grubb relationship is utilised for equating steady state CBV and CBF changes, that occur in response to a sufficiently long activation period. However, this approach may not be well suited to the study of neural events of a more transitory nature, such as certain cognitive tasks generate.

In such cases, it may be preferable to use an *event – related* paradigm. This technique differs from the block design approach in that individual trial events are measured, rather than a temporally integrated signal (Donaldson, 2002). Stimuli used in such experiments can occur in fairly rapid succession and for short durations (<3 sec), and generally require an image acquisition rate faster than what is necessary for block design experiments. However, given that a BOLD response can be generated from a stimulus lasting tens of milliseconds duration (Boynton et al., 1996; Rosen et al., 1998), it is possible, despite the lag and temporal blurring of the haemodynamic response, to measure corresponding BOLD signal changes in relation to the stimuli.

Early event related averaging work using visual stimuli to study the linearity of the stimulus time series, compared with the voxel response time series, showed the

amplitude of the measured BOLD response and the duration of the BOLD response, increased proportionally with the duration of the stimulus (Boynton et al., 1996; Donaldson, 2002). However, later studies have found that the relationship between the linearity and time-intensity of BOLD response and stimulus, is probably more complex (Bandettini et al., 2000) (Friston et al., 1997).

In general, event related studies are employed to study transient changes in activity that are time locked to events of interest, whereas Block design studies are more sensitive to sustained changes in activity that exist across prolonged periods of time. However, it is also possible using a linear model approach (detailed in next section) to combine both techniques in one experimental paradigm, thereby obtaining sensitivity to both transient and sustained activations, and a better understanding of cognitive processing (Figure 3.3).

3.5.2 The General Linear Model

The most popular statistical approach for obtaining activation maps in fMRI studies is through the use of the *general linear model* (GLM). After pre-processing of raw data images, which generally includes some level of temporal and spatial smoothing, and often motion correction, the GLM can be fit to the data. The model is essentially a pattern that describes when you expect to see activation in the data. If the timing of the model is derived from the timing of the stimulus application, and a good fit is obtained between the measured activation and the model, then it is most likely the result of the applied stimulus. For a brief review of GLM theory, the reader is referred to the chapter by Smith (Jezzard et al., 2001).

A *univariate* approach to fMRI data analysis is usually performed with the GLM. That is, the time series of each voxel is analyzed independently, which is also a conceptually easier way to understand how the model works. In a simple case, the model can be described by the equation:

$$\gamma(t) = \beta * x(t) + c + e(t) \qquad [3.15]$$

Where $\gamma(t)$ is the data, a 1-D vector for each time point, $x(t)$ is the model, also a vector for each time point. β is the value that the model needs to be multiplied by to fit the data,

c is a constant corresponding to the baseline intensity, or rest period in this example, and e is the error in the model fit. If a particular voxel responds strongly with the model fit x, then the model fitting will find a large value for β.

This GLM model can be expanded to include multiple waveforms or stimulus conditions by introducing multiple x and β terms, allowing analysis of different processes within the data:

$$\gamma = \beta_1 * x_1 + \beta_2 * x_2 + c + e \qquad [3.16]$$

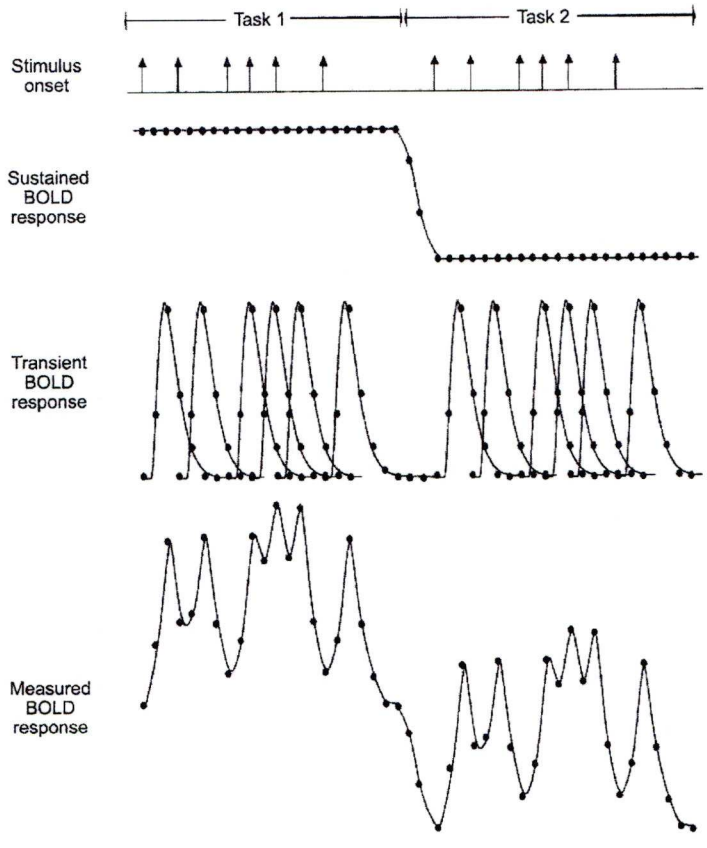

Figure 3.3 An example of a mixed event related – block design experiment. By applying the GLM with two models, correlating to both the event related and block design paradigms, both transient and sustained activation changes can be fit to two models respectively (Donaldson, 2002).

An additional step in the application of the GLM is the convolution of the stimulus function with the haemodynamic response function (HRF). In its original form, the stimulus model can be thought of as a series of square waves, describing discrete on / off

events, which do not accurately represent the physiological profile of the haemodynamic response to neural activity, which tend to be temporally and spatially blurred. The HRF therefore, changes the profile of the stimulus model to closer replicate the physiological response that is likely to occur, and therefore improve the fit of the model to the data.

After the GLM is applied to each voxel, for each model, a measure of the 'goodness of fit' is made between the time course of the measured voxel and the model. This can be used to gain a statistical measure of the significance of the fit (T) where: $T = \beta / SE$. *SE* is a measure of the standard error, or uncertainty of the measure. If the parameter estimate β is low compared to *SE*, then the T value will not be statistically significant. That is, the activation cannot be directly attributed to the applied stimulus.
Statistical certainty or probability in fMRI measurements is often expressed with the alternative *p* or *Z* statistic, both of which can be obtained from the *T* value, and which both essentially describe how significantly the measured data relates to the model.
The GLM remains the method of choice for fMRI analysis; however there is an increasing interest in a Bayesian approach to the analysis of fMRI data analysis (Friston, 2002; Jacobsen et al., 2008; Penny et al., 2003; Woolrich et al., 2006).

Chapter 4. Validation of the Q2TIPS ASL technique

In this chapter, the results of two Q2TIPS (Luh et al., 1999) ASL studies are presented, which were carried out in order to assess the accuracy of the technique, and validate its use for future fMRI-based experiments using the sequence. The first study investigates the assumption that the Q2TIPS sequence is insensitive to the transit time of labelled blood, as well as the reproducibility of resting state CBF measurements. It also assesses the effect of surrounding slices on resting state CBF estimates obtained from a single slice with the imaging volume. The second study was a test of principle for the use of Q2TIPS to simultaneously acquire BOLD and CBF time courses in an fMRI finger tapping experiment.

4.1 Establishing Q2TIPS ASL accuracy

4.1.1 Introduction

In chapter 2 it was mentioned that one of the main advantages of the Q2TIPS sequence, is the insensitivity to the arrival time of labelled blood in the imaging slices. This is a result of the saturation of the tail end of the bolus of labelled blood, which gives the labelled bolus a defined temporal width. Therefore, by knowing when the bolus begins and ends, and by accounting for the relaxation of blood, a more accurate estimate of CBF should be obtainable, independent of transit time effects. However, this requires that the condition $TI_2 > TI_1 + \delta t$ is true, which we hypothesised might not hold for more distal slices where the arrival time is longer.

The onset of EPI acquisition in the Q2TIPS sequence commences after a time TI_2, at which time it is assumed that all labelled blood has perfused into the capillary bed within the imaging volume. If this is not the case, then blood that is still flowing through the imaging volume after time TI_{1s}, may be susceptible to saturation prior to EPI readout. These issues, as well as establishing the precision of the measurements, lead to the objectives for this study:

1. To assess the assumption that Q2TIPS is insensitive to transit time by varying the distance between the label and image volume distance (LID) on a single slice perfusion value, and acquiring resting state CBF measurement in the same region of the brain.

2. To test the assumption that all blood has perfused into the capillary after TI_2 by measuring the effect of surrounding slices on an individual slice within the imaging volume.

3. To determine the precision of CBF estimates by measuring the reproducibility of the technique over the duration of the scanning period.

4.1.2 Method

Nine healthy female volunteers aged 18-30, participated in this study. Full written consent was obtained.

A Q2TIPS ASL sequence was used with an 11 slice imaging plane, TR - 3s, TE - 17ms, TI_{1stop} - 1.3s, TI_1 - 0.7s, TI_2 - 1.4s, no crusher gradient applied, slice thickness – 3.5mm, to acquire 120 resting state averages. In addition, three sets of 60 averages were acquired using a single imaging slice. In each case the labelling plane position was varied to obtain data with three different LID's, specifically 10mm, 29mm, and 50mm. A calibration scan was acquired without labelling and with TR = 10s for calculation of the equilibrium magnetization of the arterial blood (equation [2.8]).

The physiological parameters used for CBF quantification were:

T2b, T2t Transverse relaxation times of blood & tissue = 0.1s, 0.05s respectively

T1b, T1t Longitudinal relaxation times of blood & tissue = 1.5s, 1.0s

N.B- The *T1b* value of 1.5 s is an approximation. It has been shown (Parkes et al., 2002) that at 1.5T, *T1b* = 1.4s and at 4T, *T1b* = 1.8s. Therefore, at 3T a value of 1.5 s is used, which may in fact be slightly low.

4.1.3 Analysis

Averaged CBF values of whole brain were calculated from the acquired images using MATLAB, where the differences in tissue magnetization between label/control calculated using the method outlined in chapter 2 (equation [2.12]).

To evaluate the sensitivity of Q2TIPS to arrival time, the average CBF values for each subject at LID's of 10, 29, and 50mm were compared. Paired t-tests were

performed between each set of values to determine if they were significantly different.

To investigate the effect of surrounding slices on an individual slice within a multislice volume, a paired T-test was performed between average CBF values across all subjects from the 6th slice of an 11slice volume, and CBF values acquired from a single slice at an equal LID of 29mm.

To assess the reproducibility of the resting state CBF measures, the first 20, 40 and 60 images were compared with the last 20, 40 and 60 images. The standard deviation (S.D) of the difference between each set of measurements across all subjects was obtained; from which the 95% confidence interval was calculated for a single measurement, using the following relationship:

$$95\%\,C.I = 1.95 \times \frac{S.D}{\sqrt{2}} \quad \text{(Leontiev et al., 2007; Parkes et al., 2004)} \quad [4.1]$$

Where the factor of $\sqrt{2}$ accounts for the fact that the individual differences of two measurements drawn from the same probability distribution, leads to a distribution that is $\sqrt{2}$ broader than the *true* distribution. Therefore the standard deviation to the mean is divided by the equivalent factor.

Results

1) The effect of varying the LID on single slice perfusion value

Resting state CBF values were obtained at three LID's and averaged across nine subjects (Figure 4.1). A One-way ANOVA test showed no significant difference between CBF values obtained at the three LID's (Table 4.1).

The relatively small absolute difference in CBF for each LID may be the result of the biological variation that occurs over the course of the scanning session, as each estimated average value is still within the range of normal measurement (Floyd et al., 2003; Leenders et al., 1990).

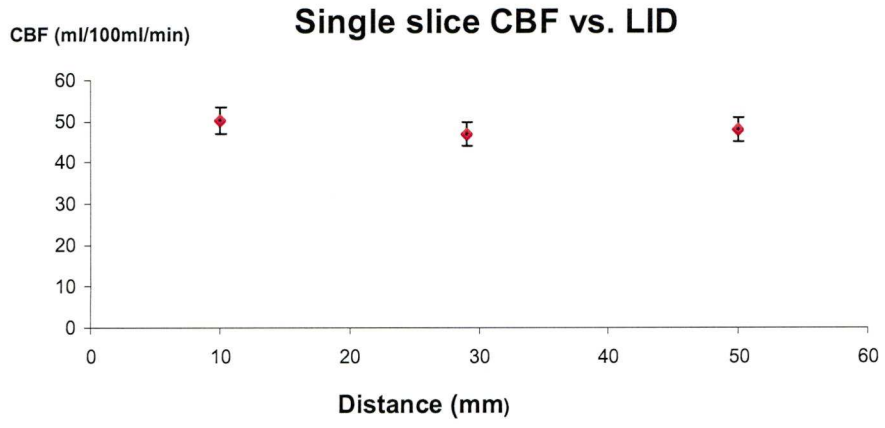

Figure 4.1 Mean values (ml blood/100ml/min tissue ± S.D) of single slice resting state CBF (grey and white matter averaged) across nine subjects, for three LID's. In each case the labelling plane was moved, and images were acquired from the same region of the brain.

Another possibility is that repositioning of the labelling plane leads to a contribution of labelled blood from different vessels. However, the lack of statistical significance between the CBF measurements at each LID suggests that any effect resulting from the contribution of different vessels is minimal, and that the sequence is in fact insensitive to transit time.

Table 4.1 Baseline CBF values for a single slice at various LID's. A One way ANOVA test revealed no significant difference between measurements acquired at each LID (p = 0.56)

	1 slice(10mm)	1 slice(29mm)	1 slice (50mm)
Ave. CBF (ml/min/100g)	50.2 ± 6.7	47.1 ± 5.9	48.2 ± 5.9
***p* value =** 0.56			

2) The effect of surrounding slices on an individual slice

Table 4.2 shows mean values for both the single slice and the 6th slice of a 11 slice volume. A paired t-Test showed no significant difference between the measurements (p = 0.74), suggesting that there is no saturation effect resulting from adjacent slices. This suggests that at the time of EPI acquisition, the labelled blood has effectively entered the capillary bed. If the blood had still been flowing through the larger arterioles, it may have been saturated prior to the EPI, which may in theory lead to saturated blood moving through the imaging volume. This result further supports that the sequence is working correctly.

Table 4.2 Shows mean resting state CBF values (± S.D) (ml/min/100g) for the 6th slice in an 11 slice volume, compared to single slice at 29mm LID, which are equivalent positions. The *p* value suggests no significant difference between the two.

	1 slice at 29mm	6th slice at 29mm
Ave. CBF	47.1 ± 5.9	46.3 ± 8.7
***p* value**	0.74	

3.) Reproducibility

The confidence intervals shown in Table 4.3 and Figure 4.2, represent CBF units (ml/100ml/min), and can be seen to decrease with increasing number of averages, reflecting improved signal to noise.

Table 4.3 As a test of reproducibility, the first 20 perfusion averages of the 11 slice imaging volume were compared to the last 20 averages. Also compared were the first 40 and 60 averages with the last 40 and 60 averages. 95% confidence interval was calculated in each case, shown here in CBF units of ml/min/100ml.

No. Averages	mean diff. ± S.D	95% C.I.
20	-0.2 ± 6.9 (-1.6 ± 15.8%)	9.45 (21.8%)
40	-0.8 ± 3.8 (-2.0 ± 8.9%)	5.2 (12.3%)
60	-0.6 ± 2.7 (-1.4 ± 6.1%)	3.7 (8.5%)

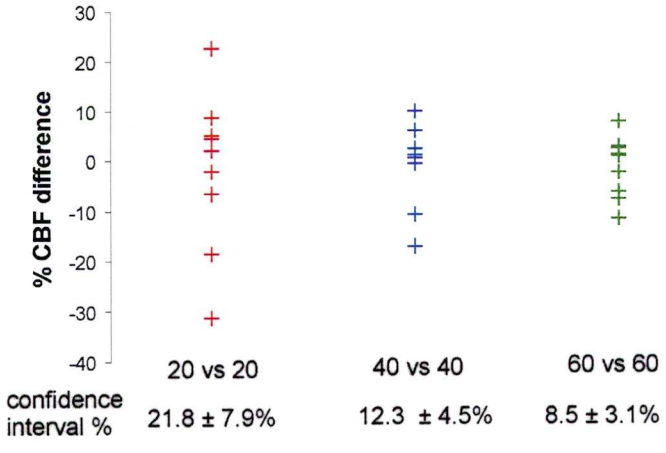

Figure 4.2 Reproducibility results for first 20, 40 and 60 averages, compared with the last 20, 40 and 60 averages during a single scan of 120 averages.

These results show that over 60 averages, which for this experiment represent a 6 minute scan time, any difference in measurement greater than 7.4 ml/100ml/min between two separate scanning sessions, should represent real biological variation. In practice, a six minute scan is slightly less than a typical baseline ASL scan (8 – 12 minutes), so with a higher number of averages, the level of precision could be improved further. Figure 4.3 shows the three 95% C.I values plotted against the number of acquired averages. The non-linear equation suggests that over the entire 120 averages, a 95% C.I closer to 5% may be obtainable.

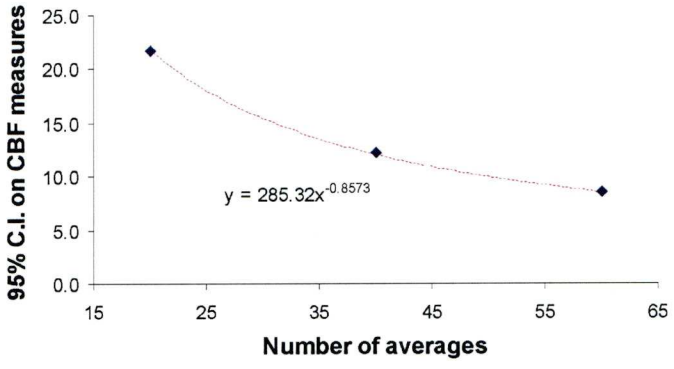

Figure 4.3 Non-linear relationship between the number of averages and the 95% C.I

4.1.4 Discussion

1. One-way ANOVA analysis showed no statistically significant difference between CBF values measured at LID's ranging from 10 – 50mm in length, suggesting that over this range the sequence is insensitive to the transit time effects of labelled blood. However, It is recognised that a reduction in SNR will tend to occur for the more distal slices (Luh et al., 1999), so in practice a LID of 10mm is more appropriate for future work using this sequence.

2. No significant effect was observed on a single slice CBF estimate due to the surrounding slices within a multi slice imaging volume. This result suggests that at the time of data read out, the labelled blood has fully perfused the capillary bed, and is not susceptible to inflowing saturated blood.

3. The results obtained from studying the reproducibility of the measured CBF values over the course of the scan duration, are informative for obtaining confidence intervals on future measurements. The results demonstrate that over the course of 60 averages, there is an 8.5% confidence interval on measured CBF values. This suggests that any measured difference in CBF greater than 8.5 % for a single subject over multiple scans with 60 averages, can be considered to be, with a 95% confidence level, of a biological nature.

This result compares quite favourably with previous PET and 1.5T MRI based CBF studies measuring reproducibility on CBF measurements made in separated scanning sessions (Carrol et al., 2002; Matthew et al., 1993; Yen et al., 2002), as well as previous ASL CBF reproducibility data (Parkes et al., 2004).
As demonstrated in Figure 4.3, the number of averages is a critical factor for determining the confidence level on a single measurement. This is also true for field strength, which also results in a higher SNR.

4.2 Simultaneous BOLD and CBF measurements of motor activity

4.2.1 Introduction

In the previous study, the accuracy of the Q2TIPS sequence for obtaining measurements of resting state, whole brain CBF estimates was tested. In this study the sensitivity of the sequence for measuring functional changes with simultaneous BOLD and CBF measurements was explored. As a precursor to calibrated fMRI work, it also provided the opportunity to explore the relationship between BOLD and CBF activation, and how it relates to brain region, as well as the stimulus type and duration of stimulus.
As such, the main objectives for this study were:

1. To obtain simultaneous measurements of BOLD and CBF during motor activation.
2. To investigate the effect of stimulus duration on BOLD and CBF activation.
3. To determine if any variation in BOLD / CBF coupling exists between left and right motor cortices.

4.2.2 Methods

Six right handed, female volunteers aged 25–55 were required to perform right or left thumb presses, comprising either 1,5 or 10 presses, interspersed with 18s rest, with a total of 15 trials for each condition.

The Q2TIPS ASL technique (Luh et al, 1999) was used on a Siemens 3T system with the following parameters: TR=2s, TE=20ms, TI_1=0.8s, TI_{1stop}=1.2s, TI_2=1.4s, 12 slices, voxel size 3.5mm^3. As with the previous experiment, a calibration scan was acquired with parameters: TI_2 = 4.0s and TR = 10s for calculation of the equilibrium magnetization of the arterial blood (equation [2.8]). The equivalent physiological parameters listed in the methods section of the previous study for the quantification of CBF, were also applied in this case.

4.2.3 Analysis

Interleaved control and labelled images were subtracted to give perfusion weighted images (equation [2.12]), and added to give BOLD images using Matlab.

The BOLD and CBF image series were pre-processed and analysed with *Brainvoyager* software. A general linear model was applied to both image series, and used to find regions of positive BOLD activation in the left (right) primary motor cortex for right (left) thumb presses, for each subject. Event related averaging was performed, and average BOLD and CBF time courses were obtained for each condition, from regions of interest of approximately 1cm^3, centred on the area of maximum activation.

To obtain a measure of absolute signal change for BOLD and CBF in response to each stimulus condition, maximum responses were subtracted from an average baseline value measured during a 4 second pre-stimulus period.

4.2.4 Results

Identifying primary motor cortices

In Figure 4.4, clearly defined contralateral BOLD activation is shown for 10 right thumb button presses for one subject. Negative BOLD is also shown in ipsilateral motor cortex; the same effect was also observed for 10 left thumb button presses. These areas of activation were well defined in all subjects. Averaged BOLD and

CBF time courses were extracted from each contralateral region of activation to acquire measures for percentage signal change.

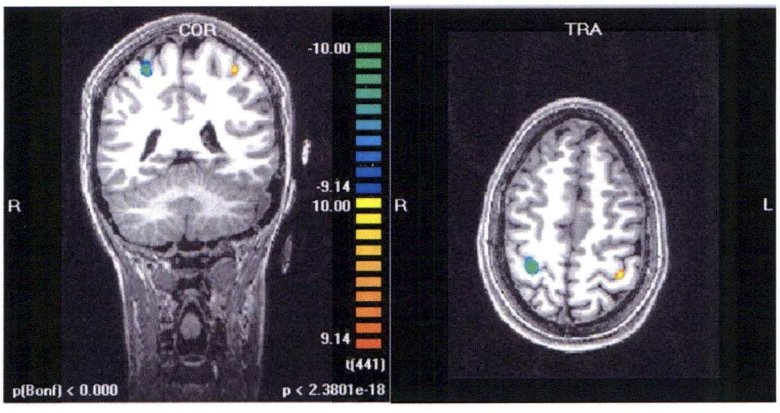

Figure 4.4 Activation maps showing ipsilateral and contralateral BOLD activation for 10 right thumb, button presses.

An average of contralateral activation (triangles) and ipsilateral activation (circles) curves for both left and right button presses are shown in Figure 4.5 for each of the button press conditions. The curves show a clear modulation of both BOLD and CBF changes in correlation with the duration of the finger tapping task. However, the equivalent measurements in the ipsilateral cortex are less defined, with only the BOLD showing a very small reduction below baseline. The ipsilateral CBF change always appears positive. In light of the results of the previous study, it is not possible to attribute this change as a biological effect, but rather a reflection of the insensitivity of the measurements to CBF changes of this magnitude, as such the apparent increasing CBF in the ipsilateral cortex is most likely driven by noise. The curves also show that none of the stimulus conditions generated a plateaued response. Therefore, it is unlikely that a stimulus of this duration would be sufficient for calibrated fMRI studies where application of the Grubb relationship for equating CBF and CBV changes requires a steady state conditions.

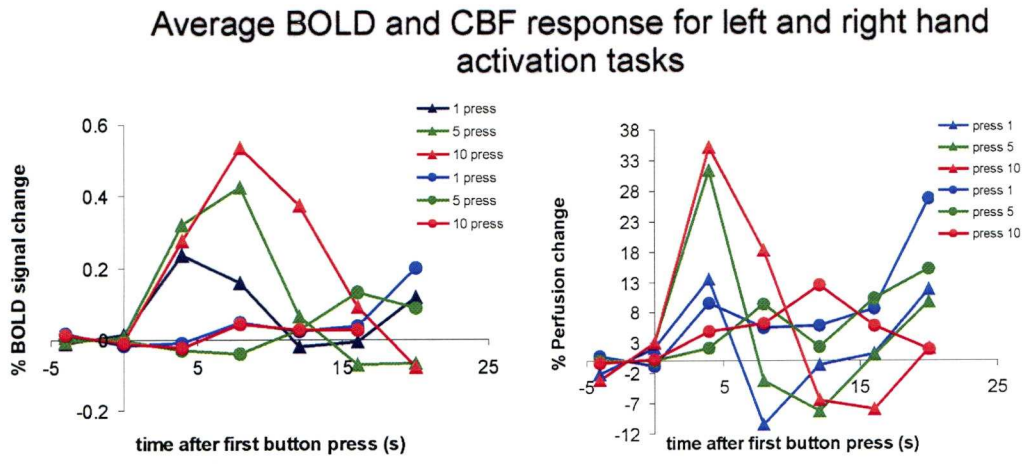

Figure 4.5 Combined BOLD and CBF averaged time courses for contralateral motor activation from one subject from both left and right thumb presses, showing graded activation in both BOLD and CBF in correlation to the number of button presses.

Table 4.4 shows a comparison between the BOLD and CBF signal change in the left and right motor cortices (values quoted as % signal change). For each subject the average maximum signal for contralateral activation over the 3 conditions is shown. A paired t-test showed no significant difference between the activation levels in left and right motor cortices. There is also no significant difference in the ratio of BOLD / CBF in the two regions.

Table 4.4 Percentage signal change for left and right contralateral BOLD and CBF for six subjects, as well as the relative change in BOLD / CBF ratio. Paired T- test's between left and right for each measured showed no significant difference.

	LEFT			Right		
Subject	**BOLD**	**CBF**	**BOLD / CBF**	**BOLD**	**CBF**	**BOLD / CBF**
1	0.65	30	0.022	0.73	41	0.018
2	0.46	28	0.016	0.36	20	0.018
3	0.45	39	0.012	0.44	41	0.011
4	0.51	38	0.013	0.26	28	0.009
5	0.41	27	0.015	0.44	29	0.015
6	0.22	17	0.013	0.29	21	0.014
average	**0.45**	**30**	**0.015**	**0.42**	**30**	**0.014**
t-test p value	**0.59**	**0.96**	**0.32**			

The ratio of BOLD and CBF measurements in left and right motor cortices are consistent across subjects and across brain hemispheres. However, this was only demonstrable in contralateral regions. The data obtained from the negative BOLD

ROI was insufficiently reliable to determine whether the coupling that was found in the contralateral region of positive BOLD activation, also applied in the ipsilateral negative BOLD region.

Relationship between BOLD and perfusion changes for graded motor activity.
By acquiring data with three levels of stimulus duration, it was possible to investigate the coupling of BOLD and CBF over the three conditions. In Figure 4.6, an apparent linear trend is observed between the BOLD and CBF changes for each of the six participants. The gradient of the linear trend line appears to reflect the underlying neurovascular coupling, where a reduced gradient would suggest a reduced BOLD response for a given CBF value. The uncertainty of the relative CBF and $CMRO_2$ contributions to the BOLD signal make it difficult to interpret the reduced coupling BOLD / CBF, which is a primary motivation for calibration of the BOLD signal.

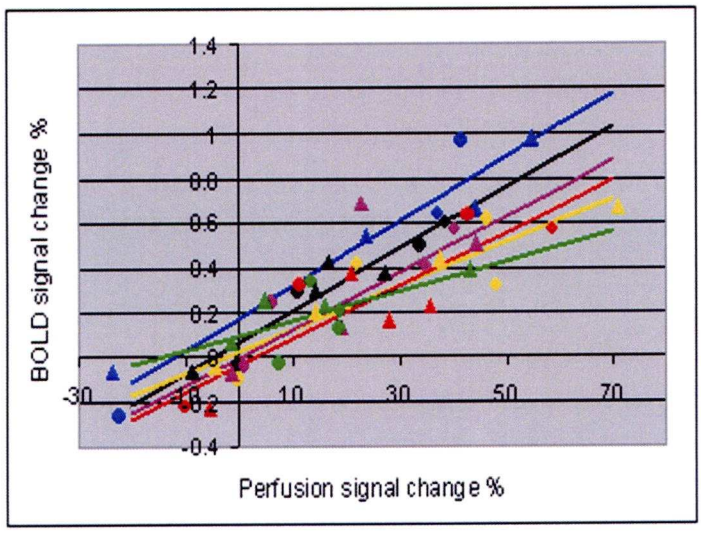

Figure 4.6 Linear relationship between BOLD and CBF change in response to motor activation. Each colour represents a different subject. Signal change in both the left (triangles) and right (circles) primary motor cortices is shown for 4 conditions: 1, 5, 10 taps with the contralateral thumb, and ten taps with the ipsilateral thumb (giving negative signal change in some cases). Linear fits are shown for data from each subject.

4.2.5 Discussion

The results from this study have demonstrated that Q2TIPS ASL is sufficiently sensitive to obtain meaningful quantitative information regarding positive BOLD and

CBF changes in response to a motor task. Data obtained from ipsilateral areas of activation was less robust, reflecting the insensitivity of the technique at particularly low levels of activation.

It was found that amplitude of the BOLD and CBF changes correlated with the duration of the stimulus, in a positive and apparently linear fashion. However, none of the three stimulus conditions was sufficient for generating steady state, plateaued responses, suggesting that this particular stimulus type is probably unsuitable for future calibrated fMRI studies involving steady state responses.

No significant difference was found between BOLD, CBF or the BOLD / CBF ratio between left and right hemispheres. The similarity of the BOLD and CBF measurements suggests some level of homogeneity in the motor cortices. The ratio of the two measures may be more insightful as a measurement of underlying neurovascular coupling, and may be consistent with other brain regions. However, as previously mentioned, further understanding of the CBF and $CMRO_2$ contributions is required before any definitive conclusions can be made about any relative change in these parameters.

For future work, a more informative approach would be the use of graded stimuli that provides steady state changes in BOLD and CBF in different brain regions, as well as the use of a calibration scan to investigate the relative CBF and $CMRO_2$ contributions to the BOLD response across a larger, healthy subject cohort. This would also enable an investigation of the task dependency of $CMRO_2$ / CBF coupling.

Chapter 5. Quantitative measures of BOLD, CBF and $CMRO_2$ using breath hold calibration – reproducibility and the effect of age

5.1 Introduction & aims

The motivation for this study arose from recognition of the ambiguity that exists in the interpretation of the BOLD signal, and the variation that exists in this measurement, even within an apparently homogenous cohort. It is well established that the response is primarily the result of a local increase in CBF, which correlates with increased $CMRO_2$ in regions of neural activation, but if we consider the variation in vascular and neuron population densities across brain regions (Cavaglia et al., 2001), and the effects of age related changes in anatomy such as atrophy and arteriosclerosis (Bangen et al., 2007; Benedetti et al., 2006; Drayer, 1988; Hesselmann et al., 2001) then it is likely that even within a healthy population, both intra- and inter-subject variation in the BOLD signal will occur. There is also evidence of gender based differences (Marcar et al., 2004; Moulton et al., 2006), as well as chronic and acute effects of lifestyle and diet (Ding et al., 2006; Iso et al., 2001; Perthen et al., 2008), which are likely to manifest as increased variability in the BOLD signal across a healthy population.

In developing a calibrated fMRI methodology that could be used for the assessment of pathological changes in oxygen metabolism or haemodynamics in the human brain, it is first necessary to recognize how these functions vary in *normal* brains. In addition, the accuracy of the measurements and the variability in the experimental methodology itself needs to be established, before any accurate assumptions about real physiological variability can be made.

This study attempts to address these issues by using breath hold as a BOLD calibration technique, to obtain quantitative measures of BOLD, CBF, and $CMRO_2$ in the visual and motor cortices, across a healthy, ageing population. In addition, repeat measurements were acquired at a later date on a subset of the experimental cohort, to test the reproducibility of the technique.

The objectives of this study were to assess:

1) The reproducibility of breath hold calibrated BOLD measurements in visual and motor cortices.
2) The accuracy of the breath hold technique, relative to the traditional CO_2 approach used in previous studies.
3) Regional variation in these measures.
4) Age or gender related differences in these measures.
5) Task dependency on the linearity of CBF / $CMRO_2$ coupling

5.2 Materials & methods

5.2.1 Subjects

Thirty two healthy, right handed, non smoking volunteers were recruited (aged 18 – 72, 15 male), with twelve of the younger volunteers (aged 18 – 32) returning for a second scanning session at a later date. Participants were asked to abstain from caffeine and alcohol on the day of the scan, and were required to have their blood pressure measured immediately prior to scanning. Healthy participants were considered to be those who were not on any cardiovascular of neurological regulatory medication, and had normal BMI, normal blood pressure, who consumed only moderate levels of alcohol and engaged in moderate levels of exercise. Ethical approval for this study was obtained from Sefton Local Research Ethics Committee, Liverpool.

5.2.2 Stimulus paradigms

Visual stimulus

The visual stimulation paradigm consisted of block designed; reversing isoluminent checkerboard, displayed via back projection, in a pseudo random fashion at one of three possible contrasts levels (1, 0.5, 0.25) for twenty second periods, interspersed with twenty second rest periods with a fixation cross. Each of the three checkerboard stimuli were displayed 6 times, with a total scan time of 12 minutes.

Motor stimulus

A graded stimulus paradigm was also used in this task, with an equivalent timing as the visual experiment. Participants used a purpose built, hand held device to perform a sustained grip with the right hand, in a psuedo random fashion, at one of three possible positions (Figure 5.1), each requiring a different degree of force (12.7N, 25.2N, 36.8N). The participants were able to rest the hand held device on their chest, and monitor the position of their sustained grip by way of a gauge connected to the device, indicating three posible positions. Participants were prompted when to apply a sustained grip with a visual cue consisting of full screen coloured projection (red, orange, green), with each colour representing a different grip position, projected on a screen at the foot of the scanner bed, which allowed the participant to fix their gaze on the grip device itself, rather than the visual projection.

Prior to commencing this scan, it was necessary to retract the scanner bed to change the direction of the mirror on the head coil to enable the participant to see their hands, as well as the front projection.

Compliance with this task was monitored throughout the scan via video capture.

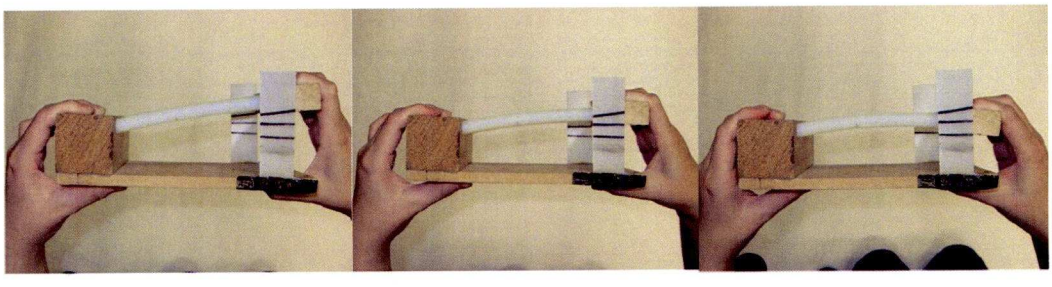

Figure 5.1 Hand held grip device, with 3 possible positions for sustained grip.

Breath hold BOLD calibration task

During this six minute scan, participants were cued via a back projection to perform breath hold on expiration for periods of twenty seconds, interspersed by fourty second periods of normal breathing. This was performed on two occasions, upon completion of both visual and motor activation scans. Participant's compliance with this task was monitored with the use of a respiratory 'bellows'.

5.2.3 Image acquisition

Prior to the visual and motor stimulus scans, a functional localizer was used to manually align 12 slices of 3.5mm slice thickness, over the respective visual and motor cortices.

Images were acquired using Siemens 3T Trio MRI scanner, during an interleaved control – label Q2TIPS (Luh et al., 1999) pulsed ASL sequence. Scanning parameters included TI_1=0.7, TI_{1stop}=1.3s, TI_2=1.4s, TE=0.017s, TR=2.5s. For CBF quantification, a calibration scan with TR=10s was also used (equation [2.8]). A whole brain structural image was acquired with MPRAGE sequence, with 1mm isotropic resolution.

5.2.4 Analysis

Image analysis

The ASL images obtained during breath hold and functional scans were first imported into Matlab, where BOLD and perfusion weighted images were generated for each data set by addition and subtraction of control and labelled images respectively, using the method outlined in chapter 2 (equation [2.12]).

Identifying the active regions of interest

The CBF and BOLD time-course data were then analyzed on an individual basis using BrainVoyager. Pre-processing consisted of spatial (FWHM 6 mm) and temporal (10 s FWHM) smoothing and linear trend removal. The BOLD and CBF images were co-registered to the structural T_1-weighted image and combined in a multi study general linear model, convolved with a haemodynamic response function. Regions of activation where the model accounted for significant variance in both of the time-courses were inspected at a threshold of $p<0.05$ (corrected for false-discovery rate). Event related averaged BOLD and CBF signal time courses for visual and sustained grip tasks, at each of the three conditions (i.e. contrast level and grip force level), were extracted in visual (V1) and primary motor cortex (M1), areas respectively, over a period of 10 volumes (50 sec). Regions of approximate volume of 1 cm^3 were chosen centered on the maximum activity for each region. The average

signal time course for both BOLD and CBF across both of these regions was recorded for both activation and breath hold stimuli.

Quantification of neural and vascular parameters

We first calculated the calibration constant M, as outlined in chapter 3 (equation [3.17]), for each region of interest using BOLD and CBF values measured during breath hold. To obtain values for the BOLD and CBF signal change during both breath hold and activation scans, we used a max – min approach using the event related averaging files. These values were combined with the calibration parameter M to obtain measures for change in $CMRO_2$ and the coupling constant n for each subject, in each region of interest. The analysis was repeated independently for the second set of visual, motor and breath hold data.

5.3 Results & discussion

5.3.1 Reproducibility

We found a clearly modulated response in group average BOLD signal change for visual and grip force stimuli on both scans 1 and 2 (Figure 5.2 & Figure 5.3), where the maximum BOLD response is associated with condition 1 (i.e. highest contrast visual stimulus, and highest force grip position) and the minimum BOLD response associated with condition 3 (i.e. lowest contrast visual stimulus, and lowest force grip position). The same effect was also observed in the CBF response to visual activation, but less so for the sustained grip task, where large variations in both magnitude of %CBF change and response timing occurred between both the grip positions, and runs. One interesting feature of the CBF response to sustained grip motor activation was an observable peak at the beginning and end of the stimulus period, which has been observed in previous studies (Obata et al., 2004).

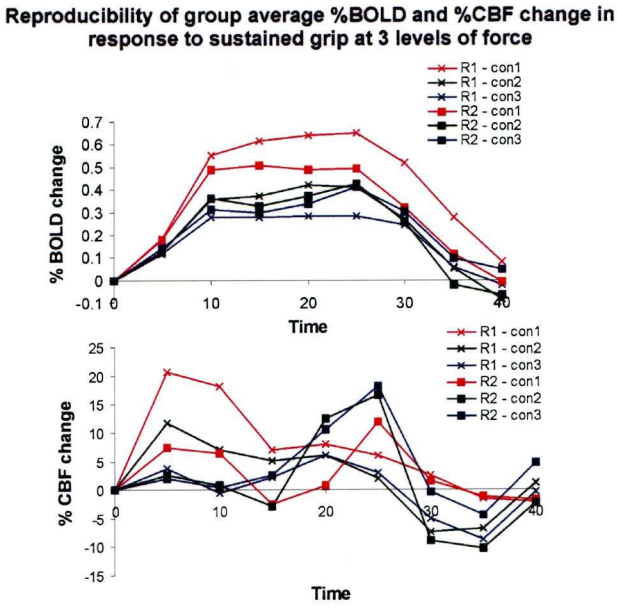

Figure 5.2 Average %BOLD and %CBF change in response to grip force for both runs 1 & 2 for 12 subjects. Condition 1 represents highest level of grip force.

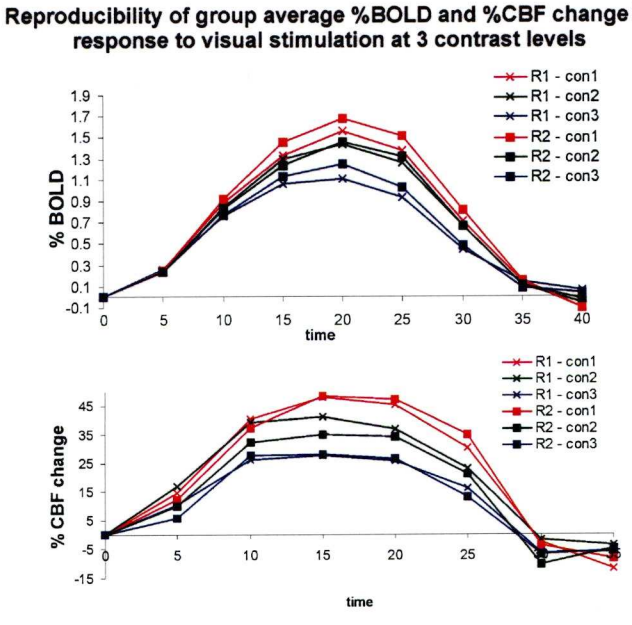

Figure 5.3 Average %BOLD and %CBF time courses in response to visual stimulus for both runs 1 & 2 for 12 subjects. Condition 1 represents highest level of visual contrast.

From visual inspection of Figure 5.2 and Figure 5.3 it is clear that despite both visual and motor BOLD responses being clearly delineated for the three levels of

activations, the CBF responses are far less defined for the motor activation compared to the visual. This suggests that further analysis involving measures of CBF change for the three levels of motor activation, may be less robust than the equivalent visual CBF values.

To evaluate the reproducibility quantitatively, we combined BOLD and CBF responses from each of the three conditions and obtained an average response. We obtained mean values across the three stimulus conditions for BOLD, CBF and the calibration parameter M for runs1 and 2 across all 12 subjects, as well as the 95% confidence interval (Equation 4.1) based on the difference between the two sets of values (Table 5.1). We found that measures of %BOLD and %CBF change obtained during breath hold, were less reproducible than the equivalent measurements obtained during both motor and visual activation (Table 5.2).

Table 5.1 BOLD and CBF values acquired during breath hold calibration in regions V1 and M1, with 95% confidence intervals obtained from individual differences between runs 1 & 2, expressed in real units.

	V1			M1		
	run1	run2	95% C. I	run1	run2	95% C. I
% BOLD	0.9 ± 0.4	1.0 ± 0.3	0.8	0.7 ± 0.6	0.7 ± 0.3	0.7
% CBF	41 ± 19	35 ± 20	29	31 ± 20	35 ± 17	42
M	3.4 ± 1.7	4.2 ± 2.1	2.8	2.8 ± 1.1	2.7 ± 1.5	2.6

Table 5.2 Reproducibility of BOLD and CBF changes during visual and motor activation. Values represent average values across three stimulus conditions. C.I values expressed in real units

	V1			M1		
	run1	run2	95% C. I	run1	run2	95% C. I
% BOLD	1.2 ± 0.4	1.3 ± 0.4	0.2	0.3 ± 0.2	0.3 ± 0.2	0.2
% CBF	54 ± 18	52 ± 25	29	21 ± 10	17 ± 9	14

The values obtained for $\Delta CMRO_2$ and the coupling parameter n, which are not shown, were found to be highly un-reproducible. This may be largely attributable to the breath hold technique itself, which is subjective and difficult to regulate consistently between the two scanning sessions, and is reflected in comparatively high 95% confidence intervals in Table 5.1, for measurements acquired during breath hold.

5.3.2 Accuracy of calibration method

When comparing our measured values of M obtained during breath hold calibration (Table 5.1), with previous BOLD calibration studies in visual and motor cortices (Table 5.3), it is clear that our values are inaccurately low. This parameter is dependent on field strength and echo time and is therefore likely to vary between studies, so it may not always be reasonable to make such a comparison. But in this case, our results are clearly lower than all the previously documented studies shown in Table 5.3, despite variations in field strength and echo time. This inaccuracy, combined with a low level of reproducibility of BOLD and CBF measures during breath hold, is the underlying cause of poorly reproducible estimates of $\Delta CMRO_2$ and n.

Table 5.3 Previous literature values for calibrated BOLD in the visual and motor cortices

Study (B_0, TE_{ASL}, TE_{BOLD})	**Region**	**M**	**$\Delta CMRO_2$**	**n**
Chiarelli (hyperox) (3T, 23ms)	visual	7.5		
	motor	6.3		
Leontiev (3T, 9.4ms, 30ms)	visual	11.1	27	2.6
Davis (1.5T, 45ms, 70ms)	visual	7.9	16	
Hoge (1.5T, 20ms, 50ms)	Visual	22		2
Hyder (PET)*	sensory cortex		16	2.9
Kastrup (1.5T, 5.3ms, 40ms)	Motor	9		3.3
Uludag (3T, 26ms)	Visual	25		2.2
Stefanovich (1.5T, 22ms, 50ms)	Visual	7.6		4.5
	motor	7.2		3.2
Chiarelli (hypercap) (3T, 23ms, 32ms)	visual	4.3		4.2
	Motor			2.9
Restom (3T, 2.8ms, 24ms)	MTL	9.2		1.8
Ances (3T, 9.4ms, 30ms)	Visual	5.7	37	2.2
	LN	5.8	20	1.6

To demonstrate the effect of inaccurate values of M on the BOLD calibration process, BOLD and CBF values from run 1 of both visual and motor tasks were averaged across 12 subjects and the three stimulus conditions, to give:

Vis 1 - $\Delta BOLD = 1.2\%$, $\Delta CBF = 55\%$ and M1 – $\Delta BOLD = 0.32\%$, $\Delta CBF = 21\%$.

These values were then substituted into the BOLD calibration model (equation [3.7]) to obtain values for the change in $CMRO_2$ over of a range of M values (Figure 5.4a),

as well as the neurovascular coupling parameter n (Figure 5.4b). From the simulated values in Figure 5.4, it can be seen that underestimation of M leads to underestimated values for $\Delta CMRO_2$, which results in grossly inflated values n as $CMRO_2 \rightarrow 0$. Previous calibration studies listed in table 3 show that normal coupling between ΔCBF and $\Delta CMRO_2$ is in the range of $n = 2 - 3$. Based on the simulated values presented in Figure 5.4b, which use BOLD and CBF values averaged across 12 subjects and three stimulus conditions, this range of coupling corresponds to values in M ranging from approximately 5 -10 in the visual cortex, and 3 – 5 in the motor cortex. Comparing our real measured values for the calibration parameter M during breath hold, we found average values in the same subjects of 3.4 ± 1.7 in the visual cortex, and 2.8 ± 1.1 in the motor cortex, both of which fall below the normal range for M values found in the simulated data, required to give accurate values for $CBF/CMRO_2$ coupling for a normal population.

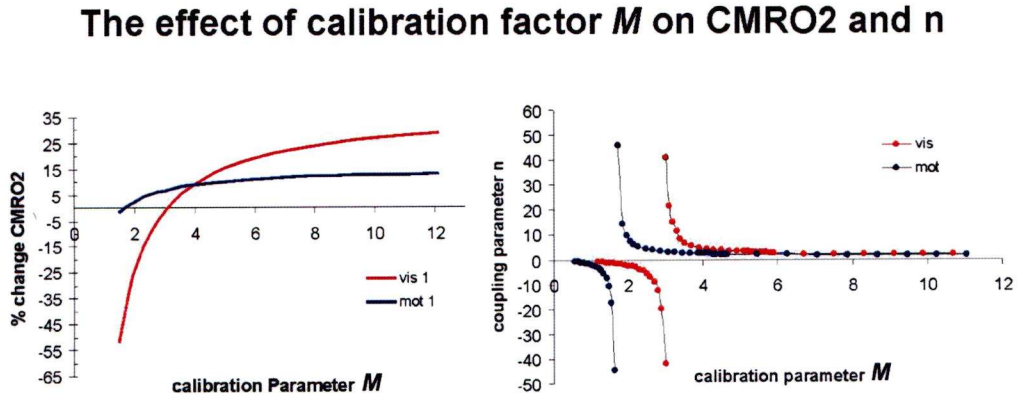

Figure 5.4 a) Simulation of $CMRO_2$ dependency over a range of M values for motor and visual activation. b) An underestimation of the calibration parameter M leads to underestimation of $\Delta CMRO_2$, resulting in an inflated coupling value ($n \rightarrow \infty$, as $\Delta CMRO_2 \rightarrow 0$).

The general inaccuracy that we observed in this experiment can be attributed largely to the insufficiently high $\Delta BOLD$ / ΔCBF ratio measured on an individual basis during breath hold calibration. This resulted, on average in an underestimation of the calibration factor M, and therefore inaccurate values for $\Delta CMRO_2$ during both functional tasks.

This may be the result of a mixed hypercapnic / hypoxic effect during breath hold, which leads to a comparatively smaller BOLD response than expected for pure hypercapnia. In standard hypercapnia calibration involving inhalation of a of 5% CO_2, 21% O_2, 74% N_2 gas mixture, the introduction of 5% CO_2 gas, which is usually only present in trace quantities in normal air, is compensated for by a reduction in nitrogen concentration, leaving the oxygen concentration equivalent to that of standard atmosphere.

Therefore, when CBF increases in response to the increased arterial tension of CO_2 ($PaCO_2$), the inflowing blood to the brain remains sufficiently oxygenated. During the period of breath hold however, arterial oxygen tension (PaO_2) begins to decrease exponentially after approximately 10 seconds (Sasse et al., 1996), resulting in hypoxemia.

To test the effect that the breath hold paradigm has on venous dHb concentration, the breath hold procedure was repeated on two subjects external to the MRI scanner.

Method:

The equivalent paradigm as the breath hold calibration scan was used, with six, 20 second breath hold on expiration periods, interspersed with 40 second periods of normal breathing. In this case the subjects end tidal O_2 was measured using a nasal cannula, and oxygen analyzer.

The end tidal values measured on the first expiration immediately after the breath hold periods, were averaged (min.end tidal % - Table 5.4) and compared to an average of the three lowest end tidal values, measured during the last 20 seconds of each period of normal breathing (ave. end tidal %). An average reduction of 1.3 % in end tidal O_2 was measured immediately following a 20 second breath hold period.

Table 5.4 End tidal O_2 values for two volunteers measured via nasal cannula using an oxygen analyzer.

	min. end tidal %	STDEV	ave. end tidal %	STDEV
Subject 1	14.52	0.30	15.75	0.03
Subject 2	14.64	0.27	15.98	0.03
mean	14.58	0.3	15.87	0.03
diff %	**1.29**			

By applying the measured change in end tidal O_2 to standard physiological equations for oxygen transport in blood (Chiarelli et al., 2007b), with an assumed value for oxygen extraction fraction of 0.4, an estimated increase of approximately 1.3 % venous dHb concentration was calculated over the breath hold period (Table 5.5).

Table 5.5 Mean values across two subjects for measured change in dHb/dHb_0 during breath hold, based on end tidal O_2 measures. Where F_iO_2 represents the fraction of inspired oxygen, S_aO_2 and C_aO_2 is the arterial oxygen saturation and concentration, and C_vO_2 and S_vO_2 is the venous oxygen concentration and saturation.

FiO2 %	SaO2	CaO2	CvO2	SvO2	CHANGE dHb
21	0.987	20.212	12.127	0.603	1.013
B.H	0.983	20.108	12.023	0.598	~1.3%

According to the deoxyhaemoglobin model as shown in equation [3.3], an increase in dHb during the breath hold period will result in a reduced BOLD response, and therefore an underestimation of the parameter *M*. However, a change of dHb of 1.3 % is unlikely to fully account for the general inaccuracy observed in our measures.

An alternative hypothesis, proposed in a recent study (Donahue et al., 2008) where the BOLD response measured during breath hold, was significantly lower than the BOLD response measured during visual activation, is that a larger increase in CBV occurs during breath hold, with no significant change in CBF, which Donahue et al. observed in CBV weighted time courses during both scans.

They suggest that because no significant difference in CBF was measured between the two tasks, that CBV changes may be occurring in vasculature that is not spatially related with CBF change during the visual task. If this hypothesis is true, i.e. if the Grubb parameter $\alpha > 0.4$, then this relationship is not accounted for in the current deoxyhaemoglobin calibration model, and the BOLD and CBF relationship measured during breath hold, would lead to underestimated values for the calibration parameter *M*. It may also have implications for BOLD calibration using CO_2 gas inhalation.

5.3.3 Regional variation in measurements

We found the graded BOLD and CBF response to visual and motor activity to be preserved when averaging across all 32 subjects, and found consistently higher values for both measurements in the visual cortex (Figure 5.5 & Figure 5.6).

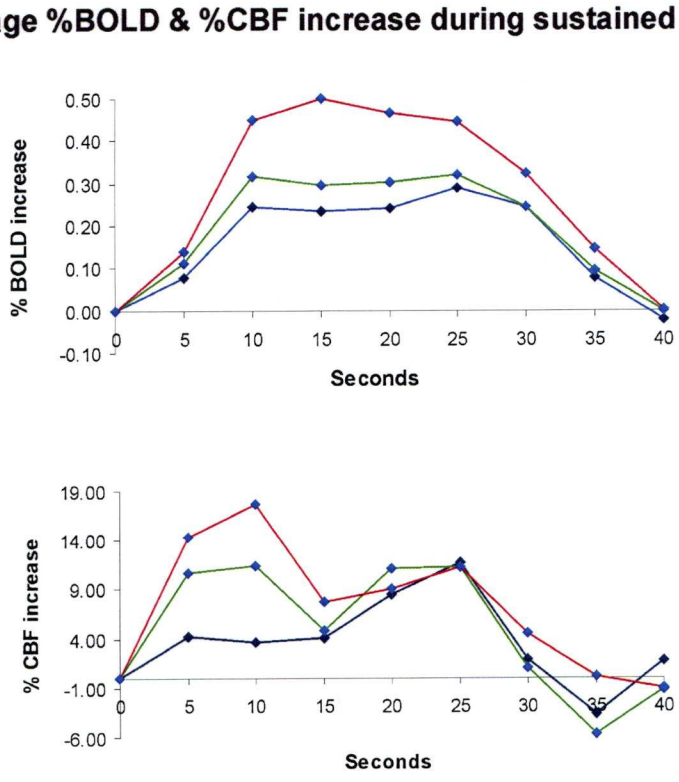

Figure 5.5 Average %BOLD and %CBF change in response to graded sustained grip across 28 subjects. Four out of original 32 participants excluded based on unusable data or abnormalities. Grip force levels presented, from highest to lowest in red, green and blue curves respectively.

This result is supported by previous work showing higher BOLD and CBF responses to visual activation (Chiarelli et al., 2007b) as well as modulated response to visual contrast level (Hoge et al., 1999a). The higher BOLD and CBF values obtained during breath hold, as well as those measured during visual and motor activation tasks, suggest that the differences between these two regions may not be task specific, and that in general there may be a tendency to observe higher BOLD and CBF response in the visual cortex. However, the observed delineation between stimulus

activation levels shows that the absolute values of these changes is task dependent and can be modulated by stimulus intensity.

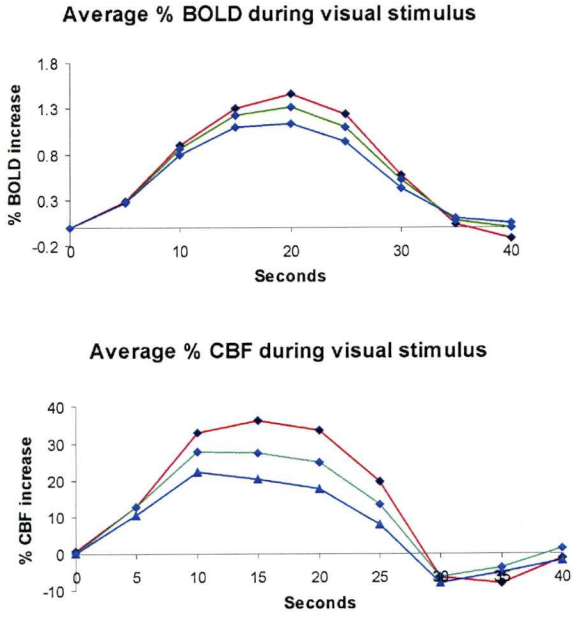

Figure 5.6 Average %BOLD and %CBF change in response to graded contrast visual stimulus across 30 subject, with contrast levels of 1, 0.5, 0.25 shown in red, green and blue curves respectively.

Table 5.6 Average responses for three stimulus conditions over all subjects. Values represent average of absolute signal change values used for the calibration model, rather than an average of the BOLD and CBF time courses as shown in **Figure 5.5** & **Figure 5.6**.

	MOT		VIS	
	BOLD	CBF	BOLD	CBF
con1	0.80 ± 0.20	28 ± 14	1.49 ± 0.48	47 ± 24
con2	0.32 ± 0.15	28 ± 13	1.35 ± 0.42	43 ± 23
con3	0.27 ± 0.14	23 ± 9	1.17 ± 0.32	33 ± 17

The variation in BOLD and CBF changes measured during breath hold in motor and visual cortices is also reflected in the measured M values (Table 5.1). Although it has been established that values obtained in this study for the parameter M are inaccurate, the apparent difference between the values for the two regions may be real. Previous work by Chiarelli et al. and Stefanovic et al. observed similar results, with the value for M being slightly less in the motor cortex, albeit with higher overall values for M in both regions.

If we assume that the BOLD signals measured during calibration are independent of neural activity, or with no-significant change in deoxyhaemoglobin levels, we might conclude that small differences in baseline oxygen extraction fraction (E_0) or baseline blood volume (V_0) exist between these two regions, which would account for the variation observed in the calibration parameter M in motor and visual cortices. However, it is perhaps more likely that the effects of variation in V_0 across the brain would be the larger contributing factor to the variation in M, due to the variations in vasculature, rather than the baseline oxygen extraction fraction, which is thought to be fairly uniform across the brain, suggesting the brain extracts a similar amount of oxygen for maintaining normal neuronal function (An et al., 2002).

5.3.4 Simulated $CMRO_2$ change

The coupling between CBF and $CMRO_2$ has previously been reported to be linear over a normal physiological range of CBF change (Hoge et al., 1999a). In this work neurovascular coupling was investigated over a range of values, in both visual and motor cortices.

In the absence of useable BOLD calibration values, we used the previously determined 'optimal' M values for both motor ($M = 4$) and visual ($M = 7$) data, along with the BOLD and CBF values obtained during the respective activation tasks, and the deoxyhaemoglobin dilution model, to obtain simulated values for $\%\Delta CMRO_2$ in response to ΔCBF (Figure 5.7b).

The CBF/$CMRO_2$ coupling was found to be linear over the range of measured values. By assuming that any increase in $CMRO_2$ above baseline is coupled with an increase in CBF, allows extrapolation to the origin of the graph, with the line of best fit taking an asymptotic form. This suggests that the neurovascular coupling parameter n; the gradient of the curve in Figure 5.7b may be, to a small extent task dependent with a progressively larger change in CBF relative to $CMRO_2$, and therefore n with increasing activation levels.

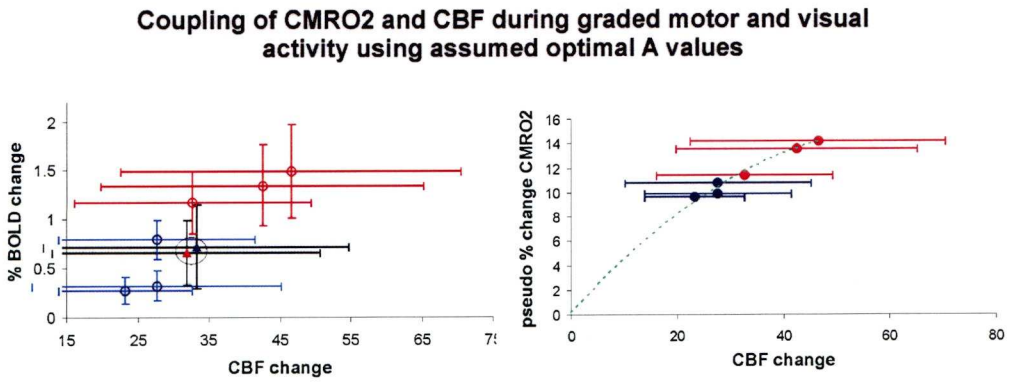

Figure 5.7a) Relationship between BOLD and CBF change during visual (red) and motor (blue) activation. Values shown are averages across all subjects (30 for visual, 28 motor) ± 1 S.D. Also shown are values obtained during breath hold calibration (circled) in motor and visual cortices. b) Using optimized M values of 4 and 7 for motor and visual data respectively, we obtained graded $CMRO_2$ response to three levels of motor and visual activation.

5.3.5 Age & gender effects

We examined the relationship between BOLD and CBF change with age and found no significant correlation with either measurements obtained during visual, or motor activation (Figure 5.8). Recent work has shown a reduction in baseline CBF and an increase in CBF change with age in the medial temporal lobe, in response to a memory encoding task (Bangen et al., 2007), with no significant change in BOLD, as well as a recent study using a visual stimulus, which found significantly reduced baseline CBF and BOLD response, but no change in CBF response (Ances et al., 2008b). Despite some apparent variations in reported results, it is generally accepted that a reduction in baseline CBF occurs with age, on the order of ~ 0.5 % per year (Parkes et al., 2004). However, this effect may be region specific, and may be larger in regions other than primary sensory areas.

We also tested for any gender specific age related effects in the measures, but found no significant effect. However, we did find in both ROI's, the average BOLD signal in men was higher than women, and the CBF response was lower. However a two sampled t-test showed no significant difference between the values (Motor BOLD: p =0.38, CBF: p = 0.30, VIS BOLD: p =0.51, CBF: p = 0.09) (see Table 5.7).

Table 5.7 Differences in average BOLD and CBF responses for men and women.

	Visual		Motor	
	ΔBOLD	ΔCBF	ΔBOLD	ΔCBF
male	1.40 ± 0.45	34.7 ± 15.3	0.33 ± 0.11	17.3 ± 8.8
female	1.29 ± 0.34	46.9 ± 21.6	0.29 ± 0.15	21.4 ± 10.8

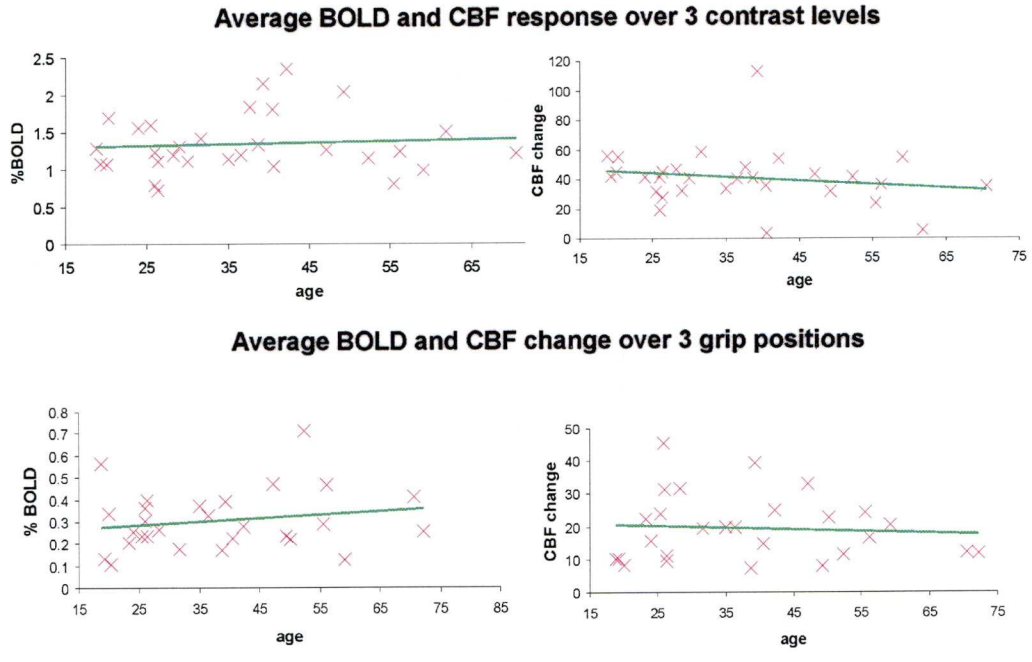

Figure 5.8 BOLD and CBF responses for 32 subjects, averaged across three conditions for visual and motor stimulus. Linear correlation test showed no significant age effect of either BOLD or CBF change. No significant change with age in any of the measurements.

5.4 Summary

We tested the use of Breath hold calibration on the premise that, if it was found to be an adequate BOLD calibration technique, it would be far more advantageous to CO_2 calibration, both in terms of practicality and cost, but also far less invasive and generally more comfortable for the subject. However, we found that the BOLD and CBF measurements obtained in the visual and motor cortices during the breath hold scan, suffered from poor reproducibility, when compared to the equivalent measurements obtained in those regions during activation tasks. This resulted in poor reproducibility for the BOLD calibration parameter *M*. We attribute this largely to

the breath hold technique itself, which was subjective and difficult to control. In addition to poor reproducibility during breath hold, we found that on average the values measured for the parameter M were underestimated in both visual and motor cortices. Application of the measured M values yielded a significant number of physiologically implausible values for $\Delta CMRO_2$ and the coupling parameter n during activation tasks.

We hypothesize that this inaccuracy is the result of a mixed hypercapnia / hypoxemia effect, occurring in the blood during the breath hold period, which may lead to increased dHb concentrations, and reduced BOLD signal measurement. This would lead to an underestimation of the calibration parameter M in both ROI's.

We found regional variation in measured BOLD and CBF in our ROI's, with consistently higher values measured in the visual cortex. This may be due in part to the tasks themselves, but may also reflect underlying baseline dHb and CBV levels. This view would be supported by previous literature showing lower values for the calibration factor in the motor cortex.

By applying assumed values of M in the calibration model, we showed a quasi linear response between CBF and $CMRO_2$ change in both regions. However, the coupling between these parameters appears to become progressively smaller with increased neural activity, leading to an asymptotic relationship at higher levels of CBF. This suggests that to a small degree, the coupling between these parameters is task dependent.

We examined the effect of age on measured BOLD and CBF change, and found no significant correlation in these parameters in either region of interest. This is contrary to a number of previous studies, which show a definite reduction in baseline CBF with age. However, it is generally recognized that larger and therefore more measureable reductions in CBF with age occur in cognitive regions such as frontal cortex (Jarnum et al., 2008; Parkes et al., 2004), rather than primary sensory regions. This is supported by the fact that general cognitive decline is one of the first signs of ageing.

We also found no gender specific correlation with age in either BOLD or CBF measures, however we did find a trend toward significant difference in CBF response to neural activation between men and women.

5.4.1 Implications for future work

The results suggest that the use of breath hold as a calibration technique is inferior in terms of both reproducibility and accuracy, to more traditional calibration techniques such as CO_2 gas inhalation.

BOLD and CBF responses appear consistently higher in the visual cortex and may be preferable and more easily achievable than motor tasks, particularly for developing calibration methodology.

The coupling between CBF and $CMRO_2$ change is essentially linear, but is to a small degree task dependent, whereby activation tasks generating large CBF changes likely to give smaller values of n.

The inclusion of a mixed male / female cohort may not be a confound or a significant source of variability for calibrated fMRI studies, however the effect of age on BOLD and CBF measures still needs to be addressed, particularly in relation to baseline CBF and primary sensory versus cognitive regional differences.

Chapter 6. Quantitative fMRI during visual activation: comparison of hypercapnia and hyperoxia calibration techniques and the effects of age

6.1 Introduction & aims

This chapter details experimental work comparing hypercapnia and hyperoxia calibration techniques during a visual stimulation task. In Chapter 3 the physiological basis for the two calibration techniques was described, along with the relevant models for estimating $CMRO_2$ contributions to the BOLD signal measured during a neural challenge.

However, at the time of commencing this study, no direct comparison between these two techniques had been made within the same cohort of people. Therefore, some uncertainty existed as to whether the value for M calculated using the two models, was in fact equivalent.

The hyperoxia model in particular involves a number of assumptions and additional calculations to quantify the physiological transport of oxygen in the blood, via measurement of end tidal O_2, the accuracy of which may be compromised by factors such as age or disease. Additionally, the hyperoxia model accounts for small CBF reductions likely to occur during the hyperoxia period, which may be below the sensitivity level of our acquisition capabilities. In which case, the inclusion of measured CBF data could potentially reduce the signal to noise of the measurements, and so from a methodological perspective a source of variability may exist between the two calibration techniques.

In this study, we aimed to assess the equivalence of the parameter M derived using both models, by performing hyperoxia and hypercapnia BOLD calibration scans within the same scanning session, across a female cohort with an age range spanning almost sixty years. These values were then used to calibrate BOLD signal measurements obtained during a visual stimulus, to obtain estimates of percentage change in $CMRO_2$.

Additional factors we aimed to address in this study were the feasibility of using fixed, rather than measured CBF changes during hyperoxia calibration, by comparing hypercapnia derived values with the equivalent hyperoxia derived values at three fixed CBF reduction levels (0%, 5%, and 10%), as well as resting state CBF in the visual cortex.

6.2 Materials & methods

6.2.1 Subjects

Approval for this study was obtained from the Human Brain Research Centre Ethics Committee at the Kyoto University Graduate School of Medicine, and all volunteers provided signed informed consent prior to their participation. A cohort of 29 healthy, non-smoking, female subjects aged 18 – 76 participated in the study. It was decided that to avoid an uneven gender distribution within the cohort due to the difficulties in recruiting male volunteers over this age range, we would focus the study only on female volunteers.

6.2.2 Visual stimulus Paradigm

For the visual activation scan we used a high contrast, square, reversing checkerboard presentation, which was displayed via front projection onto a purpose built Perspex screen, fitted to the top of the receiver head coil. The experiment consisted of an 8 minute, block designed presentation with 30 second periods of visual stimulation, interspersed with 30 seconds of blank screen. To maintain subject alertness, a small cross, which periodically changed to red, blue or green, was positioned at the centre of the screen during both on and off periods. Volunteers were asked to fixate on the cross at the centre of the screen throughout the duration of the task, and to respond to the periodic colour changes by pressing one of three corresponding buttons on a hand held button box.

6.2.3 Hyperoxia and Hypercapnia Paradigms

The hyperoxia and hypercapnia calibration scan paradigms were equivalent, however in order to prevent contamination of data resulting from residual physiological effects of O_2 or CO_2 inhalation, the time between the two scans was maximized by performing the calibration scans at the beginning and end of each scanning session respectively. Gas was supplied at 30L/min through a closed face mask for two periods of 3 minutes, interspersed with 5 minutes rest (Figure 6.1). Gas mixtures of 100% O_2 and 5%CO_2 21% O_2 74% N_2, were used for hyperoxia and hypercapnia scans respectively. End tidal O_2 and CO_2 were sampled via nasal cannula throughout

the scanning session using *Biopac systems Inc.* gas analyzing hardware, and recorded with *Acqknowledge* software. To prevent unwanted changes in baseline end tidal values due to build up of exhaled CO_2, and to minimize volunteer discomfort, atmospheric air was pumped through an auxiliary tube connected to the face mask, during the 5 minute rest period.

As an added safety requirement, the scanner fan was set to maximum to prevent any build up of high concentration O_2 levels within the magnet bore.

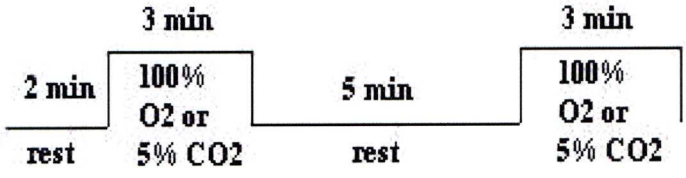

Figure 6.1 Schematic representation of hyperoxia and hypercapnia paradigm. The timing was equivalent for both scans where hyperoxia consisted of normal air during rest and 100% O_2 (30l /min) showing during 'on' periods. Whereas, the hypercapnia scan consisted of normal air during rest, and 5% CO_2 21% O_2 74 % N_2 mixture during 'on' periods.

6.2.4 Image acquisition

MRI measurements were performed using a 3 Tesla Trio whole-body scanner (Siemens, Erlangen, Germany). An 8-channel RF coil was used for signal collection and the body coil for signal transmission. Images were acquired using a PICORE Q2TIPS Arterial Spin Labeling sequence (Luh et al., 1999) in order to collect simultaneous BOLD and CBF signal. Acquisition parameters were: TR 2.13 s, TI_1 0.7 s, TI_{1stop} 1.3s, TI_2 1.4 s, TE 25ms. Crusher gradients with b=5 mms^{-1} were used in order to remove signal from the larger vessels. Twelve slices of 3.5 mm thickness and 0.35mm gap were collected, covering visual cortices (Figure 6.2). The pulse sequence included prospective motion correction (PACE (Thesen et al., 2000)). At the end of each functional run an M_0 calibration image was also collected for use in producing quantitative CBF maps (chapter 2, equation [2.18]). The Q2TIPS sequence with parameters as above was used with the labelling switched off and a TR of 10 s. A 3D MPRAGE (Mugler et al., 1990) sequence with 1mm isotropic resolution was used for the anatomical scan.

Figure 6.2 Imaging volume used for BOLD and CBF measurement during hyperoxia, hypercapnia and visual activation scans, with slices positioned to cover the visual cortex.

6.3 Data analysis

6.3.1 Calculating CBF

The ASL data from all functional runs (hyperoxia, hypercapnia and visual task) was first processed in Matlab in order to extract BOLD and CBF time-courses. Pairs of control and label images were subtracted to produce perfusion-weighted images or averaged to produce BOLD images. The perfusion-weighted images were converted into quantitative CBF maps through the use of a model that assumes a single blood compartment model, i.e. assuming that the labelled water does not cross the capillary wall or leave the voxel during the inversion time (Parkes et al., 2002). The equilibrium magnetization of arterial blood was estimated from the average signal of the calibration image, assuming a whole-brain value of 0.9 for the brain:blood partition coefficient (Roberts et al., 1994).

Correcting for the different T2* relaxation times of blood and tissue (Buxton et al., 1998a), perfusion maps were produced using the model outlined in Chapter 2, equation [2.12]. With physiological parameters: $T1_b = 1.6$ s is the T1 of blood (Lu et al., 2004a), $T2_b^* = 100$ ms and $T2_t^* = 50$ ms are the approximate T2* of blood and

tissue respectively. Previous work in this thesis applied a T_{1b} value of 1.5s, however it was decided based on previous studies that a value of 1.6s may be more accurate.

6.3.2 Identifying the active regions of interest

Analysis of BOLD and perfusion weighted images, was performed with Brainvoyager QX software. Spatial smoothing (6mm FWHM) and temporal smoothing (10sec FWHM) was performed on all images. To locate regions of interest (ROI's) within the visual cortex, perfusion weighted images acquired during the visual activation task were used in a single study general linear model, convolved with a haemodynamic response function. In each case, the statistical threshold was set at a FDR value of $q = 0.05$ and a cubic voxel cluster ($1cm^3$) was selected within the visual activation map to define the ROI. The position of the ROI within the visual activation map was determined by visual inspection of sagittal, coronal and axial projections, with the cubic cluster placed centrally within the area of activation in each projection (Figure 6.3a). From within the ROI, numerical time courses were extracted for BOLD and CBF changes in response to the visual activation task, as well as for hypercapnia and hyperoxia calibration scans.

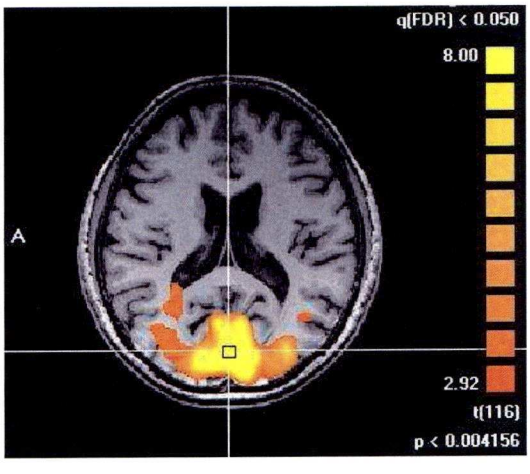

a

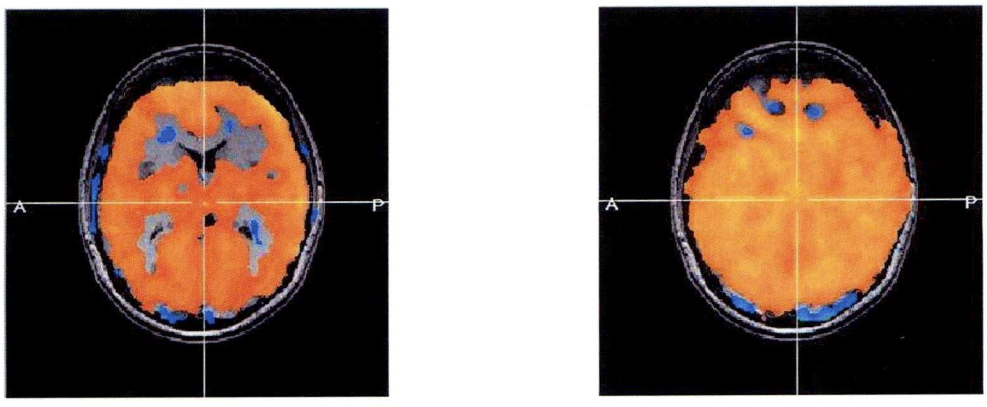

b c

Figure 6.3 Activation maps for a single subject for: a) perfusion activation during visual activation, showing ROI used for extracting BOLD and CBF data. ROI's were inspected at a false detection rate q (FDR) <0.05, p<0.004, using CBF time course data. b) Hypercapnia BOLD activation map, c) Hyperoxia BOLD activation. Hyperoxia appears to generate a more homogenous BOLD response across the brain, when compared to the hypercapnia BOLD response.

6.3.3 BOLD calibration process

6.3.3.1 Hypercapnia

Calculation of the calibration constant M involves implementation of equation [3.17], where measured values of change in BOLD and CBF in response to CO_2 inhalation are used, together with an assumed constant $CMRO_2$. Average values were extracted for four, 1 minute time-periods: two rest periods of 1 minute prior to hypercapnia, and the last minute of each hypercapnia period. The BOLD and CBF signal change was found by averaging over the last minute of each hypercapnia period, and comparing it to the last minute of rest occurring prior to each respective period of hypercapnia.(see Figure 6.1). This allowed the calculation of two values of M, i.e. one for each on/off period, from which a mean value of M over both periods was also calculated.

6.3.3.2 Hyperoxia

The process for calculating BOLD and CBF changes during hyperoxia was equivalent to that used during hypercapnia. The main difference between the two calibration techniques from a practical perspective lies in the inclusion of end tidal O_2 values in the hyperoxia calibration process, which are used to estimate changes in

the deoxyhaemoglobin content of venous blood, as outlined in equation [3.13]. We used Matlab to extract end tidal values over the same periods as the BOLD and CBF values, from which averaged values for change in dHb in venous blood could be inferred.

In order to investigate the effects of CBF reduction on the hyperoxia calibration process, and to avoid the inclusion of low SNR CBF measurements into the model, we performed calculations of the calibration parameter M using three *fixed* values for CBF change, namely 0%, 5% and 10%. Chiarelli et al. showed that a reduction of up to 10% may occur during hyperoxia periods, although factors such as O_2 concentration, flow rate, and duration of the hyperoxia period are likely causes of variability in this value. Another potential source of variability is age, where younger people may have a greater CBF reduction compared to older people, as noted by Watson et al. Therefore the fixed values chosen for testing the sensitivity of the model to CBF reductions are thought to be typical of reductions that may occur during the hyperoxia period, but which would normally be below the sensitivity of our measurement capability.

6.3.3.3 Calculation of $\Delta CMRO_2$ and the coupling parameter n

Changes in BOLD and CBF in response to the visual activation task were obtained using event related averaged responses over 15 volumes (~64sec), with a baseline period defined as the mean of the first 3 volumes (~8.5sec) prior to onset of the stimulus. We then subtracted the mean baseline value from the maximum signal change to obtain values for ΔBOLD and ΔCBF. These values, together with the respective values for the calibration parameter M determined using both calibration methods, were used with equation [3.7] to estimate values for $\Delta CMRO_2$ (m) and the neurovascular coupling constant n within the ROI.

6.3.3.4 Resting state CBF

To measure resting state CBF within our region of interest, we took an average of CBF values measured during the initial two minute rest period of both hypercapnia and hyperoxia scans, as well as the final minute of the rest period between periods of gas inhalation.

6.4 Results and Discussion

6.4.1 Measuring change in BOLD and perfusion during calibration

Figure 6.4 shows the BOLD and CBF time courses during hypercapnia (a) and hyperoxia (b). BOLD signal was significantly increased for both gas challenges. While we found significant changes in CBF during hypercapnia, we saw no significant change during hyperoxia. This suggests that inclusion of measured CBF data in the hyperoxia calibration model may not be beneficial due to the level of noise introduced, relative to the expected reduction in perfusion signal.

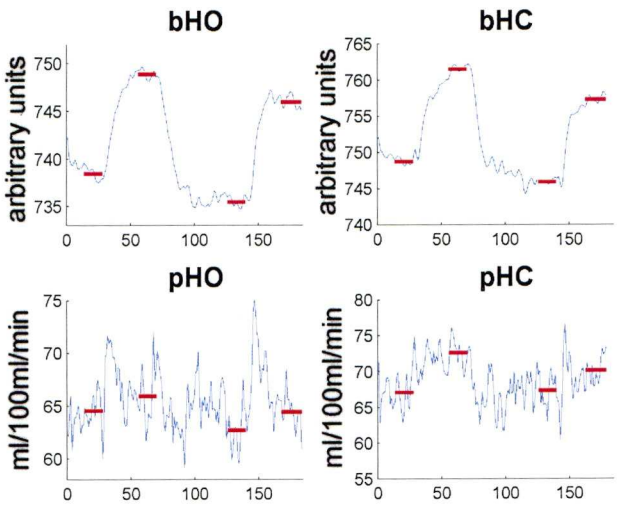

Figure 6.4 Average BOLD (b) and perfusion (p) time courses across all subjects for hyperoxia (HO) and hypercapnia (HC). The periods used within the time course to obtain numerical values for the calibration models are shown in red, where the x-axis is represented in volumes of TR = 4.26secs.)

However, the time course shown in Figure 6.4 for the CBF measure obtained during hyperoxia (pHO), does not account for $T1_b$ correction (Bulte et al., 2007), and so the values are most likely not accurate. However, the overriding noise that exists in these measurements suggests that on an individual basis, the current ASL acquisition protocol, is not sufficiently sensitive enough to measure the small hyperoxia induced reductions in blood flow, and therefore supports the use of an assumed value for CBF reduction in the hyperoxia calibration model.

Figure 6.5 shows the measured end tidal responses for O_2 during hyperoxia and CO_2 during hypercapnia, used to generate the responses shown in Figure 6.4.

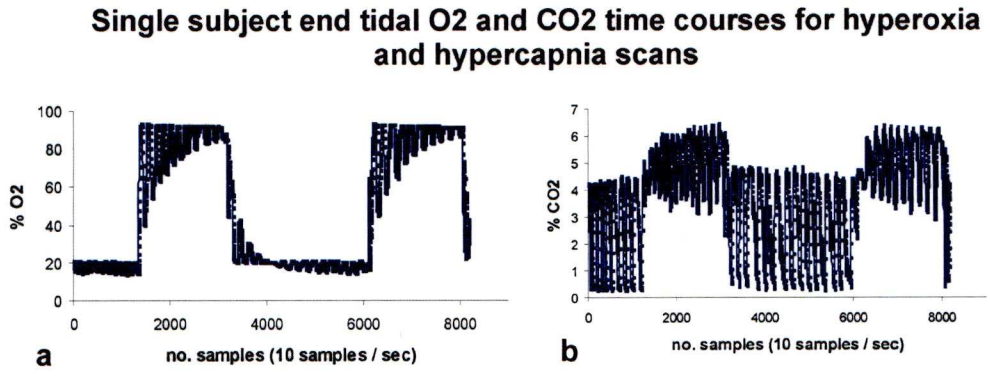

Figure 6.5 Measured end tidal responses for a single subject for a) O_2 during hyperoxia, and b) CO_2 during hypercapnia calibration scans.

6.4.2 Comparison of calibration factor *M*

We compared values for *M* obtained via hypercapnia calibration (M_HC), with those obtained via hyperoxia calibration, at three assumed levels of CBF reduction (M_HO 0%, M_HO 5%, M_HO 10%). Figure 6.6 shows both sets of values for 23 of the original 29 subjects, plotted against a line of parity between the two models (shown in red). Subject data sets were rejected from analysis on the basis that only those subjects with estimated $\Delta CMRO_2 \geq 5\%$ during the visual activation task using all calibration models, that is, hypercapnia and hyperoxia with three assumed values for CBF reduction, were deemed significant and therefore included. This lead to 6 of the original 29 subjects being rejected.

From visual inspection it can be seen that in Figure 6.6b) M_HC vs. M_HO 5% data points fit closest to the line of parity with a paired student T-test between the two data sets giving a value $p = 0.42$, showing no significant difference between the values. A linear correlation test gave a value of $r^2 = 0.17$. This is in contrast to Figure 6.6a), where it can be seen that M_HO 0% values are significantly lower than M_HC ($p = 0.004$), and Figure 6.6c) where M_HO 10% values are significantly higher than M_HC values ($p = 0.007$). Therefore, we suggest that the use of 5% reduction may be a suitable approximation for real physiological change during this hyperoxia paradigm.

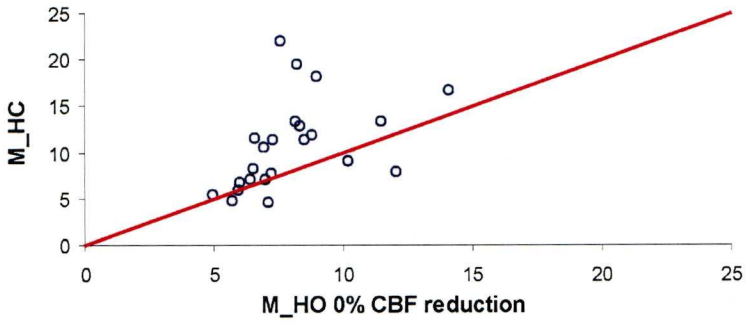

a

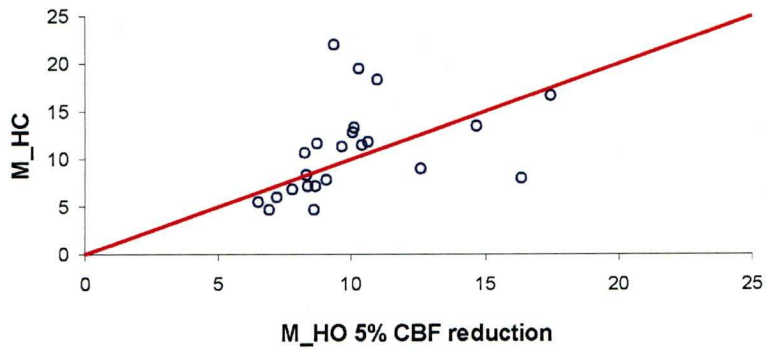

b

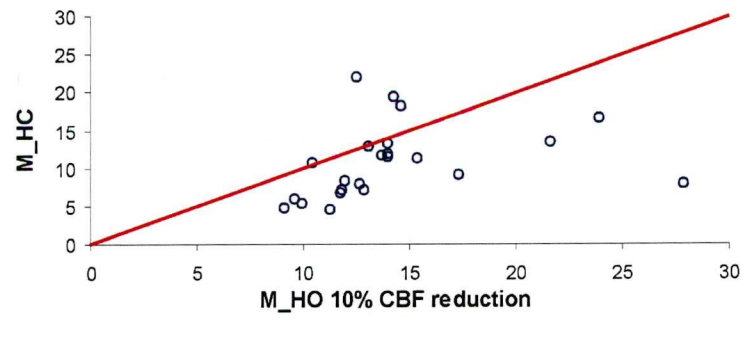

c

Figure 6.6 Comparison between the BOLD calibration factor *M*, obtained via hypercapnia calibration, versus hyperoxia calibration with three assumed values of CBF reduction. Paired T-tests showed highest agreement between (b) M_HC vs. M_HO 5% (p=0.42), and a correlation value of $r^2 = 0.17$. Whereas (a) M_HC values were significantly higher than M_HO 0% (p=0.004), and (c) M_HC values were significantly less than M_HO 10% (p=0.007). Red line represents equality between models.

6.4.3 Visual activation results

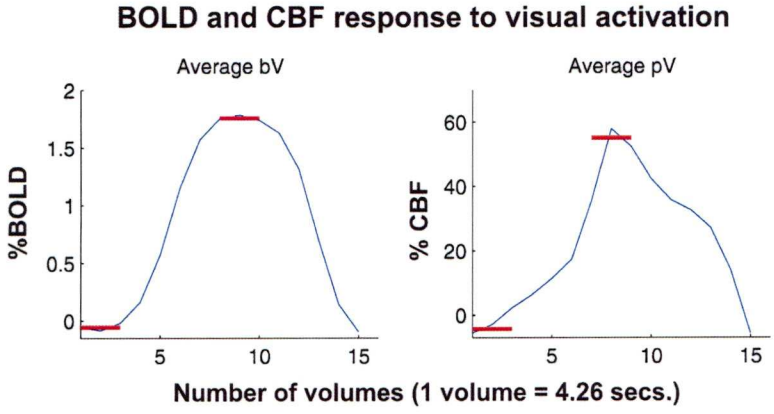

Figure 6.7 Average %BOLD and %CBF changes for 29 subjects during visual activation. Red bars indicate periods used for obtaining signal change values.

BOLD and CBF data was averaged across 15 time points using Brainvoyager QX. Determination of m and the neurovascular coupling parameter n requires measures of signal change for both these parameters. To achieve this, mean values were extracted for each subject's data across data points corresponding to baseline and peak values (Figure 6.7, shown in red). The mean values across all subjects for % change in BOLD and CBF in response to visual activation were 1.9 ± 0.5 % and 62 ± 19 % respectively.

6.4.4 Neurovascular coupling parameters

Table 6.1 Average values across all subjects ± 1S.D for M, % $CMRO_2$ change (m), and neurovascular coupling parameter n.

	M	**m**	**n**
Hypercapnia	9.6 ± 3.9	23 ± 12	4.2 ± 3.4
Hyperoxia 0% CBF reduction	7.7 ± 2.1	20 ± 10	4.2 ± 2.3
Hyperoxia 5% CBF reduction	9.6 ± 2.6	26 ± 9	2.9 ± 0.8
Hyperoxia 10% CBF reduction	13.4 ± 3.7	32 ± 9	2.2 ± 0.35

It can be seen from Table 6.1 that the average values for M that hypercapnia derived values compare most favorably with hyperoxia using an assumed 5% CBF reduction. The sensitivity of the hyperoxia model to the value of CBF reduction is demonstrated

in the progressively larger estimates of m and smaller values of n, with an increase in the assumed value for CBF reduction. Figure 6.8 demonstrates the effect of varying the CBF reduction from 0 to 10%, on the calibration parameter M.

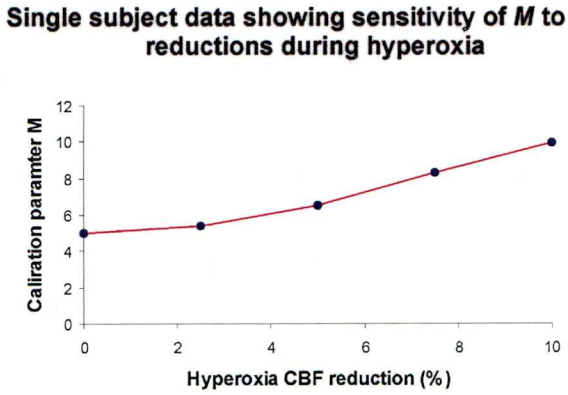

Figure 6.8 Sensitivity of M on the CBF reduction during hyperoxia. It can be seen that a difference in CBF reduction from 0 to 10% leads to a doubling of M.

There is an approximate 2-3 fold increase in CBF compared to $CMRO_2$ in response to visual cortex activation (Figure 6.9), which is reflected in the measured n values. Similar relationships between these parameters have also been observed in previous studies (Davis et al., 1998; Hoge et al., 1999b; Kastrup et al., 2002; Leontiev et al., 2007), which suggests that the value for n of 3.7, derived with the 0% CBF reduction model is too high, and therefore the assumption that no reduction in CBF is occurring during the hyperoxia paradigm, may be inaccurate.

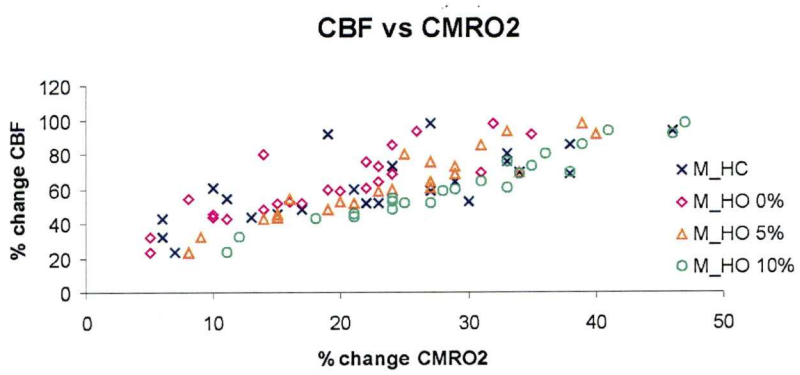

Figure 6.9 Relationship between % change in CBF in response to visual activation and the associated estimate of % change in $CMRO_2$ above baseline, derived using hypercapnia calibration constant (M_HC) and the hyperoxia calibration constant (M_HO) with three levels of CBF reduction.

6.4.5 Age effects

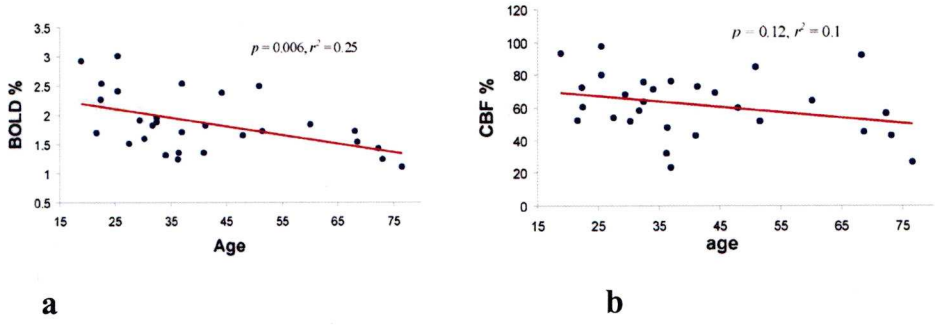

a b

Figure 6.10 Measured values of % change in a) BOLD and b) CBF across 29 subjects during visual activation.

Regression analysis showed a significant correlation between %BOLD signal measured during visual activation and age, ($p = 0.006$, $r^2 = 0.25$) with a reduction of around 0.7% per year (Figure 6.10), and a non-significant trend towards reduced %CBF with age ($p = 0.12$, $r^2 = 0.1$) of 0.5% per year. However, we found no correlation with age in resting state CBF taken from rest periods of both hyperoxia and hypercapnia scans.

We also observed a significant reduction with age in the hypercapnia derived values for calibration factor M_HC ($p = 0.025$, r^2=0.22) (Figure 6.11a), and a trend toward reduced $\%\Delta CMRO_2$ (m_HC) ($p = 0.09$, $r^2 = 0.13$) (Figure 6.9b). A reduction in the parameter M would be consistent with previous studies that have observed reduced BOLD signal amplitude with age in the visual cortex (Hesselmann et al., 2001; Huettel et al., 2001; Ross et al., 1997) and reduced spatial extent of activation (Buckner et al., 2000). The trend toward reduced $\%\Delta CMRO_2$ implies a reduction in neural activity with age, but previous studies have also shown reduced baseline $CMRO_2$ level with age (Takada et al., 1992; Yamaguchi et al., 1986) which would imply that a reduction of $CMRO_2$ occurs in the visual cortex that is greater than that observed in the resting state, therefore leading to a $\%\Delta CMRO_2$ value that decreases with age.

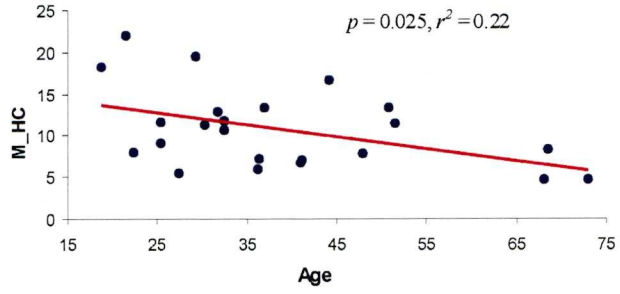

a

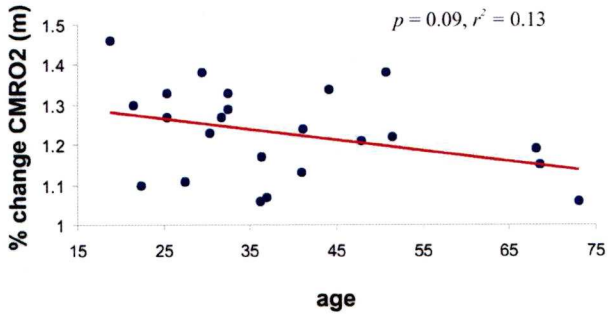

b

Figure 6.11 Hypercapnia derived values a) M_HC, and b) m_HC for 23 subjects.

If we consider the calibration factor M, which according to Davis' model, is proportional to baseline deoxyhaemoglobin content in the form of E_0V_0, and according to our hypercapnia calibrated value, has a significant reduction with age. With no measured reduction in resting state CBF with age, we would expect baseline blood volume V_0 to remain unchanged, which would suggest that a reduction in the baseline oxygen extraction E_0 is the cause of the trend toward reduced M.

As mentioned, we also observed a trend toward reduced $\%\Delta CMRO_2$ in response to our visual stimulus, which might suggest that the stimulus is not *as* stimulating in older people, causing fewer neurons to activate, or alternatively there is a reduction in population density of neurons in the visual cortex with age. Which raises the question that if the latter case is true, would this not be reflected in a reduced baseline CBF, where it might be reasonable to assume that a reduced demand would result in a reduced supply? It is interesting to note also that no significant age related decline was observed in the neurovascular coupling parameter n, which implies that

the reduction in CBF change with age, measured during visual activation, is roughly proportional to the reduction in % $\Delta CMRO_2$.

No age related reductions were observed in values for M or m derived via hyperoxia calibration, which may be attributed to some extent to the use of a fixed value of CBF reduction rather than a measured value, which is reflected in the lower variability of the hyperoxia derived values shown in Table 6.1. It may be reasonable to assume that a natural variability in these measurements might occur across the subject age range used for this study, which may be vascular in origin and therefore more likely to manifest in hypercapnia derived values, which depend on measured values of BOLD and CBF change in response to inhalation of CO_2 gas, rather than the saturation of arterial haemoglobin and arterial plasma with O_2, as is the case during hyperoxia.

There is evidence that the level of CBF reduction during hyperoxia is age dependent (Watson et al., 2000). Therefore, it may be that by using an assumed value for CBF reduction in our model, we are compromising sensitivity to individual vascular differences, which may exist across an age range, in favour of less variability due to reduced noise.

In Figure 6.8, the sensitivity of the hyperoxia model to CBF change was shown in respect to the effect of M, whereby a reduced CBF reduction leads to a reduced M value. To emphasize this point further and to demonstrate how the hyperoxia derived value for M might be affected by age if we could obtain sensitive enough measures of CBF, and if we did observe a reduced CBF reduction in the older participants compared with the young, we divided the subjects into three age groups and used three levels of assumed reduction; 0%, 5%, 10% for the old, middle and young groups respectively. This gave a significant reduction with age in the parameter M ($p = 0.003$, $r^2 = 0.36$) (Figure 6.12). We then reversed the order so the eldest group had the largest CBF reduction. In this case, there was a non-significant increase in the abovementioned calculated values with age, suggesting that there may in fact be age related reductions in CBF during hyperoxia, which are to some degree masked with the use of an assumed value for CBF reduction.

This would also be supported by the fact that we observed an age related reduction in the parameter *M* when using hypercapnia calibration.

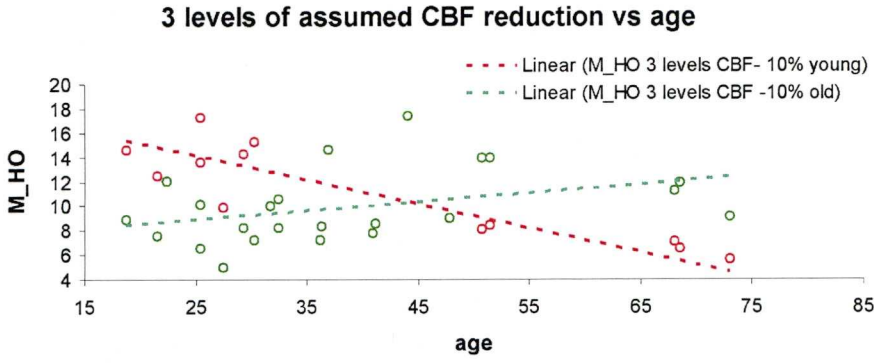

Figure 6.12 Simulated age effect using hypercapnia calibration. The data points in the graph are representative of three age groups as mentioned. The CBF reduction values for the middle aged group were the same for each condition, that is, where the old aged group was given a 10% reduction and when the young aged group was given a 10% reduction, meaning some of the data points are common to both conditions but are also shown in green.

Although the values of 0% 5% and 10% are arbitrary, and by simply dividing the cohort into three age groups and applying one of these CBF reduction values to each group is statistically not that meaningful, they are representative of values of CBF reduction, which according to literature are within the realms of normal for the level of hyperoxia to which our subjects were exposed.

Despite minimal evidence supporting the observation that CBF reduction during hyperoxia is greater in younger people, if you consider the effects associated with atherosclerosis and reduced vessel wall elasticity and dilatory ability, frequently reported with ageing, it seems likely that such physiological changes may also lead to a reduced ability for vessel constriction. Figure 6.12 demonstrates the potential for masking age related effects associated with the calibration parameter *M*, by using a fixed value for CBF reduction.

It was found that averaged values obtained using hyperoxia calibration with a fixed 5% reduction in CBF agreed most closely with averaged hypercapnia data, albeit with less variance. If we consider the hypercapnia technique as representing something of a *gold standard* in calibrated fMRI, then this suggests that real CBF reductions in our subjects during hyperoxia, ranged above and below the 5% estimate,

and while it appears to be a fair estimate of average CBF reduction, applying it across a large cohort age range may be masking natural physiological variance.
It may therefore be the case that the application of hyperoxia calibration with a fixed value for CBF reduction, for the study of age related changes, specifically vascular in origin, may be inferior to hypercapnia calibration. However, for a relatively age matched cohort, the use of hyperoxia with a fixed value for CBF reduction may be preferable, due to the absence of variability resulting from the inclusion of ASL acquired CBF data. It also suggests, given the age range of our cohort (18 – 76) that a 5% reduction might be a suitable estimate for middle aged adults.

6.4.6 Resting state CBF

To investigate any age related decline in baseline CBF in the ROI within the visual cortex, perfusion weighted images obtained during periods of normoxia in hypercapnia and hyperoxia scans were used. However, no significant reduction was observed across the age range of the cohort. A recent publication (Ances et al., 2008b) did measure a significant reduction in baseline CBF in the visual cortex, although previous literature using ASL to investigate age related reductions in baseline CBF, have shown significant reductions of around 0.5% per year in the frontal cortex (Jarnum et al., 2008; Parkes et al., 2004), with no-significant CBF reduction observed in the visual cortex, which supports our results.

6.5 Summary

No significant change in CBF was observed in response to O_2 gas induced hyperoxia. Instead, three levels of fixed CBF reduction were used in the hyperoxia calibration model, to obtain values for the calibration constant M, which were used to obtain estimates of $\%\Delta CMRO_2$, and the neurovascular coupling parameter n, in response to a flashing checkerboard visual stimulus.
These values were then compared with the equivalent values derived using the CO_2 induced hypercapnia calibration approach.
It was found that across the age range of our cohort, measurements obtained through the use of the hyperoxia model with a fixed 5% value for CBF reduction, agreed most favorably with the equivalent hypercapnia derived measurements.

Hyperoxia calibration provided quantitative values with less variance across our subject cohort, but also did not elicit any age related decline in the parameters M or m, unlike the hypercapnia calibration derived values, which gave a significant age related reduction in M and a trend toward a reduced value of m during neural activation.

No age related decline in resting state CBF was measured from the ROI within in the visual cortex.

Chapter 7. Quantitative fMRI using Hyperoxia Calibration: Reproducibility during a cognitive Stroop task

7.1 Introduction & aims

In the previous chapter the use of hyperoxia calibration was demonstrated as a potential alternative to the more established hypercapnia calibration technique, for the study of oxygenation and blood flow changes in response to stimulus of the visual cortex. In this work we extend the application of the hyperoxia calibration technique by acquiring reproducibility of fMRI measurements: %ΔBOLD, %ΔCBF, %ΔCMRO, the calibration parameter *M*, the neurovascular coupling parameter *n*, and resting state CBF during a cognitive Stroop task (Langenecker et al., 2004; Milham et al., 2002; Zysset et al., 2001) with button response. This technique is known to provoke activation in primary motor area (M1), supplementary motor area (SMA), left and right parietal lobes (LPL, RPL), and left and right medial frontal gyrus (LMFG, RMFG) brain regions. The activation of multiple frontal regions in response to a cognitive Stroop task is thought to be the result of inhibitory control of overlearned words, requiring recruitment of additional brain regions to aid with task performance. Previous studies have shown that this so called 'Stroop interference effect' is more pronounced in older people, who show higher BOLD activation in frontal areas, thought to be a result of increased activation in those regions.

Therefore, the motivations for this study were to validate the methodology, for application in future studies investigating neurovascular changes associated with cognitive decline in normal ageing and cerebral small vessel disease, as well as obtain quantitative measures in a young cohort.

7.2 Materials and Methods

Approval for this study was obtained from the University of Liverpool Ethics Committee and all volunteers provided signed informed consent prior to their participation. 10 subjects (4 male, 6 female; age range 19 – 36) participated in the study. Subjects took part in a single scanning session consisting of a hyperoxia calibration scan (13 minutes), a cognitive stroop task (8 minutes) a structural scan (7 minutes) and then a repeat of both the hyperoxia scan and stroop task, giving a total imaging time of approximately 50 minutes.

7.2.1 Stimulus Paradigm

A colour-word Stroop task was used, similar to that described in (Zysset et al., 2001), programmed in *Presentation* software (http://www.neurobs.com/). Subjects had to decide if the meaning of a word presented in white font at the bottom of the screen matched the font colour of the top word (Figure 7.1). They were asked to respond as quickly and accurately as possible with a press of the index or middle finger of the right hand as to whether the words matched or not. There were 20 self-paced stimuli in each block, with a minimum time of 1.5s between stimuli, giving a total block length of approximately 30 s. Following each response a fixation cross was displayed before the presentation of the next stimulus. Eight active blocks of 30 s were interspersed with 30 s fixation cross on a black screen, giving a run time of 8 minutes.

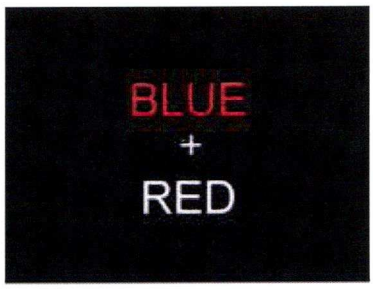

Figure 7.1 Stimulus Paradigm – the Stroop task. Subjects had to decide if the meaning of the bottom word matched the font colour of the top word. The incongruent stroop task was used, in which the meaning of the top word was always incongruent with the ink colour.

7.2.2 Hyperoxia Paradigm

For the BOLD calibration scan, oxygen was delivered via an open mask (100% O_2 at 15l/min) interspersed with breathing normal air through the holes in the mask. The protocol consisted of 2 minutes normoxia, 3 minutes of hyperoxia, 5 minutes normoxia and 3 minutes of hyperoxia. The gas composition inside the subject's nose was continuously sampled via a nasal cannula.

The cannula was connected to a vacuum pump and oxygen analyser supplied by Applied Electrochemistry Inc, Pittsburgh USA (S-3A/I O_2 sensor and *Flowcontrol* R-2 vacuum pump). End tidal O_2 sampled and recorded at intervals of 1 ms using Powerlab software (ADInstruments, Colorado Springs, USA). End tidal CO_2 was also monitored during the experiment in case of possible CO_2 build up during periods of normoxia.

7.2.3 Image acquisition

MRI measurements were performed using a 3 Tesla Trio whole-body scanner (Siemens, Erlangen, Germany). An 8-channel RF coil was used for signal collection and the body coil for signal transmission. Images were acquired using a PICORE Q2TIPS Arterial Spin Labeling sequence (Luh et al., 1999) in order to collect simultaneous BOLD and CBF signal. Acquisition parameters were: TR 2.13 s, TI_1 0.7 s, TI_2 1.4 s, TE 25 ms. Crusher gradients with b=5 mms^{-1} were used in order to remove signal from the larger vessels.

Twelve slices of 3.5 mm thickness and 0.35 mm gap were collected, covering frontal, motor and parietal cortices as shown in Figure 7.2. The pulse sequence included prospective motion correction (PACE (Thesen et al., 2000)). Two 'dummy' scans were discarded at the start of each functional run in order to avoid T1 relaxation effects. At the end of each functional run an M_0 calibration image was also collected for use in producing quantitative CBF maps (see Chapter 2, equation [2.8]). The Q2TIPS sequence with parameters as above was used with the labelling switched off and a TR of 10 s.

A 3D MPRAGE (Mugler et al., 1990) sequence with 1mm isotropic resolution was used for the anatomical scan.

Figure 7.2 Slice coverage during Stroop and hyperoxia scans. Limited coverage of the ASL sequence restricted our acquisition to cover frontal, motor and parietal regions.

7.2.4 fMRI data analysis

7.2.4.1 Calculating CBF

The ASL data from all 4 functional runs (2 stroop and 2 hyperoxia) was first processed in Matlab in order to extract BOLD and CBF time-courses. Pairs of control and labelled images were subtracted to produce a time-course of perfusion-weighted images, and also averaged to produce a time-course of BOLD images. The perfusion-weighted images were converted into quantitative CBF maps through the use of a model that assumes a single blood compartment model, i.e. assuming that the labelled water does not cross the capillary wall or leave the voxel during the inversion time (Parkes et al., 2002). The equilibrium magnetization of arterial blood was estimated from the average signal of the M_0 calibration image, assuming a whole-brain value of 0.9 for the brain:blood partition coefficient (λ) (Roberts et al., 1996). Correcting for the different T2* relaxation times of blood and tissue (Buxton et al., 1998a), perfusion maps were produced using the method outlined in chapter 2, equation [2.12].

7.2.4.2 Identifying the active regions of interest

The CBF and BOLD time-course data were then analyzed on an individual basis using BrainVoyager. Pre-processing consisted of spatial (FWHM 6 mm) and temporal (10 s FWHM) smoothing and linear trend removal. The BOLD and CBF images were co-registered to the structural T_1-weighted image and were then transformed into Talairach space. Activated regions of interest were found on each individual for each stroop run using incongruent conditions only, where the meaning and font-colour of the top word did not match.

The general linear model consisted of the block design (taken from the timings in the individual *Presentation* log files) convolved with a haemodynamic response function. Both the CBF and BOLD data was modeled simultaneously and regions where the model accounted for significant variance in both of the time-courses were inspected at false-detection threshold of $p<0.05$. BOLD and CBF signal time courses for the stroop and hyperoxia runs were recorded in 6 regions of interest: left and right middle frontal

gyrus (MFG), primary motor cortex (M1), left and right parietal lobule (PL), and supplementary motor area (SMA). Regions of approximate volume of 1 cm^3 were chosen centered on the maximum activity for each region.

The average signal time course for both BOLD and CBF in each of these regions was recorded for both the stroop and hyperoxia stimuli. All analysis was repeated independently for the second set of stroop and hyperoxia data.

For the stroop task, following averaging over the 8 activation blocks, the maximum percentage change in BOLD and CBF was recorded.

7.2.4.3 Quantification of neural and vascular parameters

First, the calibration constant M was calculated for each region of interest. The respiratory data was analyzed in Matlab in order to extract the end-tidal oxygen values. Average values were extracted for 4 time-periods: two rest periods of 1 minute prior to hyperoxia, and the last minute of each hyperoxia period. The BOLD signal percentage change was found averaged over the last minute of each hyperoxia period compared to one minute prior to hyperoxia. (Chiarelli et al., 2007b) demonstrated that for simplification of analysis, it is sufficient to use an assumed value of CBF change in response to hyperoxia rather than measured values, which are inherently noisy, and need to be corrected for changes in the T_1 of arterial blood that occur in response to high levels of hyperoxia. For each period of hyperoxia the calibration constant M was found using the Chiarelli and Bulte model (Chapter 3, equation [3.13]), and the mean value of M from both periods was used.

The percentage change in BOLD and CBF in each region was calculated by averaging the time-courses over the 8 activation blocks and finding the maximum signal change. Values for change in $CMRO_2$ (m) and the coupling constant n were then calculated using the model described in (Buxton et al., 2004) in each region of interest:

These values were calculated for each subject individually in each region of interest, and the analysis was repeated independently for the second set of stroop and hyperoxia data.

7.3 Results and Discussion

7.3.1 Behavioral Data

All participants performed the stroop task correctly with mean accuracy of 97% and standard deviation of 4%. Mean reaction time was 1021 ms with a standard deviation of 175 ms. No significant difference was measured in either accuracy or reaction time across the two runs.

7.3.2 Activated regions

We found consistent activation of regions for the stroop task across the two runs for each subject, but less consistency across subjects with some subjects showing activation in only a few regions. Figure 7.3 shows a typical activation map from one subject for one functional stroop run.

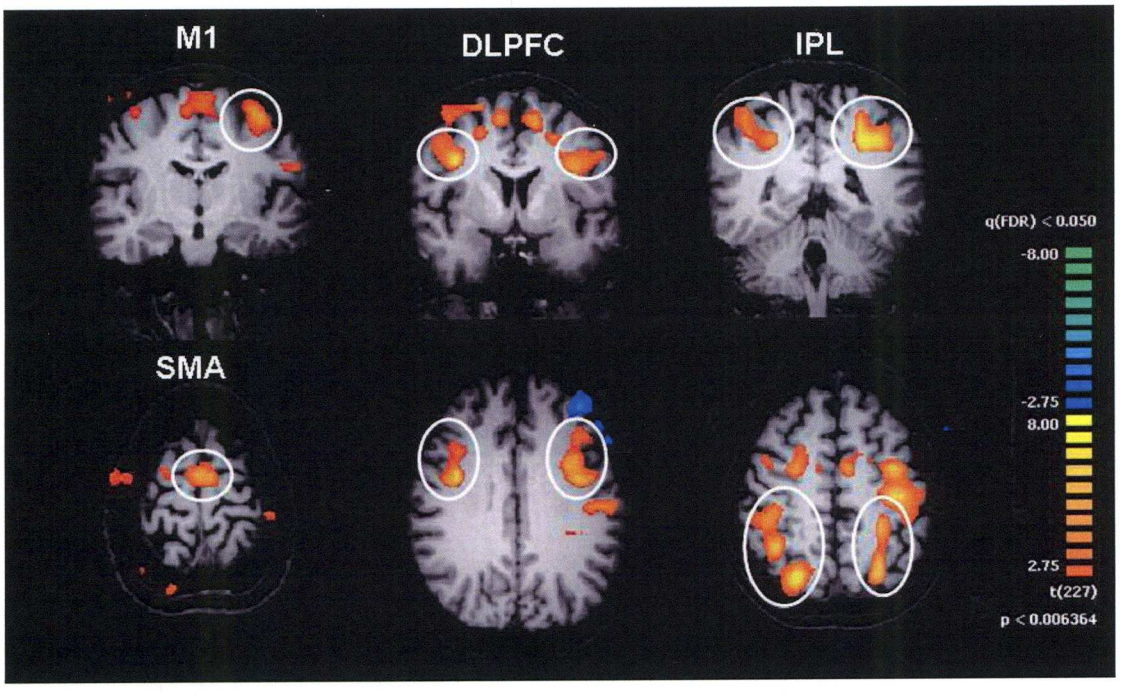

Figure 7.3 Activated regions for a single run in a single subject at a statistical threshold of $p<0.05$ corrected for false detection rate. The white circles indicate the regions of activation from which data was recorded.

Group analysis over all subjects revealed the central Talaraich coordinates for ROI identification for the 6 regions to be: M1 (-35 -23 54); SMA (-3 -5 53); Left Parietal

Lobule (-24 -61 45); Right Parietal Lobule (-31 -57 45); Left MFG (-47 0 37) and Right MFG (46 0 38), as confirmed with the Talairach daemon (www.talairach.org). Previous work using the stroop task found similar regions of activation (Zysset et al., 2001), with the exception of the primary motor cortex, which we obtained through button box presses, in response to the task. This allowed us to compare quantitatively, fMRI measures in cognitive and non-cognitive related brain regions.

Previous work has focused on the differential activity between the congruent and incongruent stroop task (Langenecker et al., 2004; Zysset et al., 2001). In this application we instead chose only to use the incongruent case with respect to fixation in order to produce robust activation over a large number of regions in the brain.

7.3.3 Signal time-course

The signal time-course for BOLD and CBF averaged across all regions and all subjects for both stroop and hyperoxia runs is shown in Figure 7.4. It can be seen that both the amplitude and the shape of the signal time-course for the stroop task (a & b) are similar across the two runs, shown in red and blue.

Interestingly, the shape of the BOLD signal and CBF time-courses appear quite different. The BOLD signal shows a later and slower onset than the CBF signal but clearly reaches a plateau unlike the CBF response. CBF appears to respond more strongly to the onset and offset of activity with a clear peak in the response to the stimulus onset and a smaller peak corresponding to the offset. The shorter lag time and faster rise time of the CBF response in comparison to the BOLD response has been previously reported (Huppert et al., 2006; Liu et al., 2000; Yang et al., 2000; Yang et al., 2004), and is thought to reflect the arterial origin of the ASL signal in comparison to the venous origin of the BOLD signal with added delay and dispersion. Previous studies in the visual cortex do not report an increased CBF response to onset and offset as we see in our data. Previous visual studies at our centre using the same ASL technique do not produce such a response shape (Figure 7.5), which suggests that this may be a feature in our CBF response to the cognitive stimulus. However, there is also a possible BOLD contamination effect occurring during the ASL 'label-control' subtraction, during the dynamic phase of the signal change. The changing BOLD response leads to variation in

the static tissue measurement between the label and control images, and may lead to inaccuracies of CBF measurement during the dynamic phase, that is during the onset and offset of signal change.

The BOLD response measured during hyperoxia (Figure 7.4c) is less consistent than the response to the cognitive task (Figure 7.4a) over the two runs. This partly reflects the known drift in BOLD baseline measures. In addition, due to the open mask system the exact concentration of oxygen delivered on each run is not controlled, causing differences in the BOLD response between the two runs.

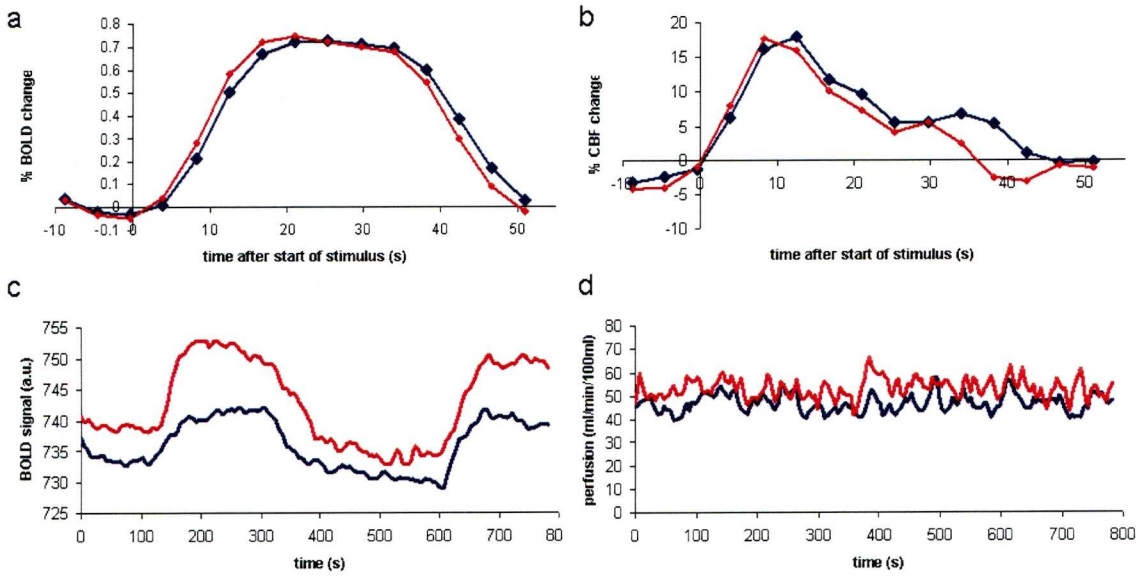

Figure 7.4 Average signal time-courses over the two runs. The figure shows the signal change for both BOLD and perfusion averaged across all regions and all subjects for run 1 (red) and run 2 (blue). (a) shows the BOLD signal during the stroop task, (b) shows the CBF signal during the stroop task, (c) shows the BOLD signal during hyperoxia and (d) shows the perfusion signal during hyperoxia.

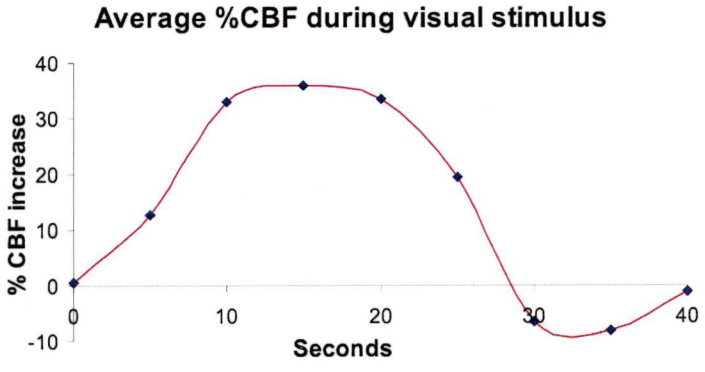

Figure 7.5 Example of average CBF response across 30 subjects from previous study using reversing checkerboard stimulus.

No significant reduction was found in CBF during hyperoxia (Figure 7.4d), which conflicts with previous findings using alternative measurement techniques (Brown et al., 1985; Leahy et al., 1980; Watson et al., 2000).However, CBF calculation in this study does not correct for the increase in T_1 of blood that occurs during hyperoxia which, if used in the kinetic model to calculate change in CBF, would give a reduction of around 7% in CBF for 100% inspired oxygen (Bulte et al., 2007).

Therefore, by not accounting for the T_{1b} changes during hyperoxia, our measured values for CBF during hyperoxia are most likely overestimated. This factor, combined with the inherently low signal to noise of our measured CBF data suggests that the use of an assumed CBF reduction of ~5% is a reasonable compromise, at least for an age matched cohort. There is evidence that CBF reduction changes with age (Watson et al., 2000), hence the application of an assumed CBF value rather than a measured one may not be ideal over a large cohort age range.

As no significant change in CBF was measured during hyperoxia, the data acquired over the 13 minute scan was used as a measure of 'resting state' in each region.

7.3.4 Reproducibility

Approximately 8% of all data was discarded due to very low values for ΔCMRO2 (those of less than 3% increase; sometimes negative values were found). This leads to inaccurate values for the neurovascular coupling parameter 'n' due to the discontinuity of n at ΔCMRO2=0. The source of these errors appears to be low values of M in

comparison to relatively large values of ΔBOLD during the stroop task. This may occur for regions of interest close to the ventricles or the edge of the brain where M may be particularly susceptible to movement artefacts.

In addition, not all subjects showed significant activation in all regions on both runs, leaving a total of 37 regions from which to calculate the reproducibility of each parameter. The percentage differences between measurements acquired on different scans were calculated for each region according to:

$$\Delta = 100 * \frac{x_1 - x_2}{x_{avg}}. \qquad [7.1]$$

Figure 7.6 shows a 'Bland-Altman' plot of these percentage differences. The coefficient of variation for each parameter is also given, which is equal to the standard deviation of the differences (retaining the sign) divided by the square root of 2 (Leontiev et al., 2007).

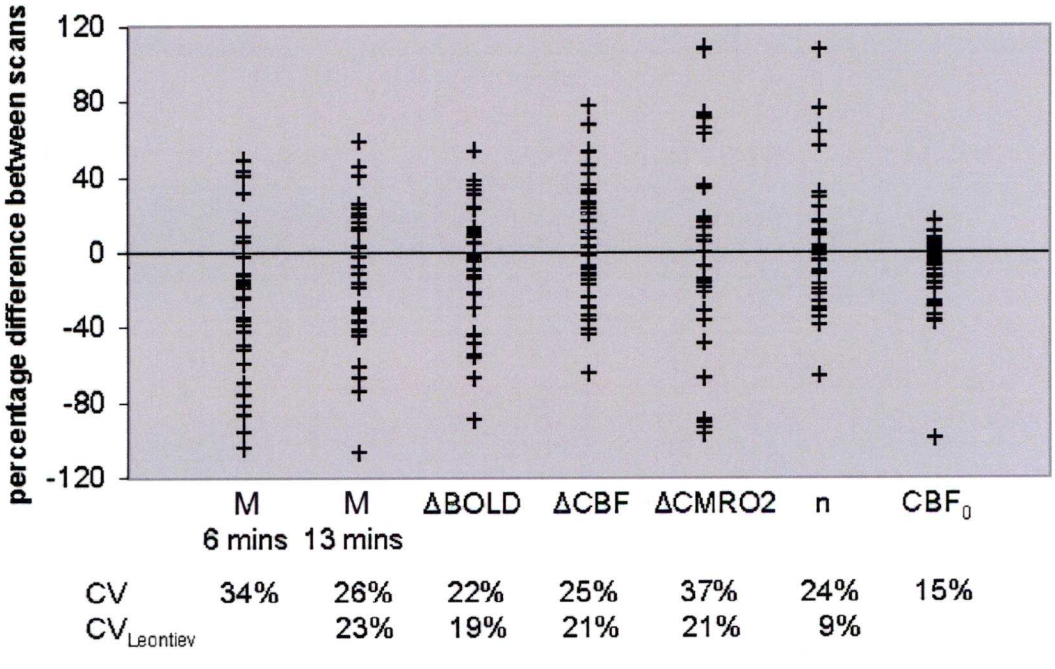

Figure 7.6 Reproducibility of Neurovascular Coupling Parameters. The figure shows percentage difference between measurements from the two scans, for each subject in each region, and the coefficient of variation (standard deviation between these differences divided by the square root of 2). 'M 6 mins' refers to the value of M calculated from only 6 minutes of the hyperoxia data (i,e, the first period of 3 mins off and 3 mins on). 'M 13 mins' is the value for M calculated from the full hyperoxia scan. $CV_{Leontiev}$ refers to the equivalent values reported in (Leontiev et al., 2007) for a hypercapnic calibration using a V1 localizer.

Table 7.1. Neurovascular coupling measurements

Region	M	ΔCBF	ΔBOLD	$\Delta CMRO_2$	n	Resting CBF
M1	8.4 ± 2.0	32.2 ± 12.6	0.58 ± 0.16	16.8 ± 7.6	2.02 ± 0.35	49.5 ± 11.0
SMA	9.5 ± 2.9	34.1 ± 5.5	0.89 ± 0.25	15.6 ± 4.0	2.41 ± 0.61	43.5 ± 7.9
LPL	9.9 ± 6.4	44.7 ± 11.9	1.04 ± 0.41	20.4 ± 6.5	2.35 ± 0.46	59.2 ± 19.6
RPL	10.2 ± 4.9	36.2 ± 6.5	0.95 ± 0.24	16.5 ± 3.8	2.34 ± 0.56	58.8 ± 20.9
LMFG	6.8 ± 3.1	34.3 ± 6.4	0.80 ± 0.23	12.9 ± 3.0	2.94 ± 0.74	42.6 ± 6.9
RMFG	7.2 ± 3.6	34.3 ± 7.5	0.78 ± 0.25	14.2 ± 5.2	2.83 ± 1.44	47.7 ± 12.6
Average	**8.7**	**36.0**	**0.84**	**16.1**	**2.48**	**50.2**

The coefficients of variation of the measurements using hyperoxia calibration are similar to those found during hypercapnia calibration (Leontiev et al., 2007), with the exception of $CMRO_2$ and 'n', as shown in Figure 7.6. Leontiev and Buxton reported improved reproducibility on use of a CBF localizer; however this was not possible for our data due to the poor activation seen in cognitive areas using the CBF data alone.

The absolute values of BOLD and CBF change we report are approximately half that in the previous study (0.84% and 36% respectively, compared to 1.9% and 73%), which is likely due to the use of a cognitive rather than a visual task. Reproducibility for a visual task using hyperoxia calibration would likely be improved compared to our results.

For comparisons of values across different brain regions, measurements were averaged over both runs in order to improve the precision. Table 7.1 shows the mean and standard deviation (across subjects) of the measured parameters. An average value for M of 8.7% is similar to previous studies (Table 7.2). However as M depends on the particular scanning parameters used, values would not necessarily be expected to be in close agreement. We find an average increase in oxygen metabolism of 16% and neurovascular coupling parameter of 2.5, which are again in good agreement with literature values (Table 7.2).

Differences in neurovascular coupling across the brain

Table 7.2 Neurovascular coupling measurements in previous studies (mean values). * Average of the 16 PET values given in this paper

Study (B_0, TE_{ASL}, TE_{BOLD})	Region	M	$\Delta CMRO_2$	n
Chiarelli (hyperox) (3T, 23ms)	visual	7.5		
	motor	6.3		
Leontiev (3T, 9.4ms, 30ms)	visual	11.1	27	2.6
Davis (1.5T, 45ms, 70ms)	visual	7.9	16	
Hoge (1.5T, 20ms, 50ms)	Visual	22		2
Hyder (PET)*	sensory cortex		16	2.9
Kastrup (1.5T, 5.3ms, 40ms)	Motor	9		3.3
Uludag (3T, 26ms)	Visual	25		2.2
Stefanovich (1.5T, 22ms, 50ms)	Visual	7.6		4.5
	motor	7.2		3.2
Chiarelli (hypercap) (3T, 23ms, 32ms)	visual	4.3		4.2
	Motor			2.9
Restom (3T, 2.8ms, 24ms)	MTL	9.2		1.8
Ances (3T, 9.4ms, 30ms)	Visual	5.7	37	2.2
	LN	5.8	20	1.6
Current study (3T, 25ms)	Motor cortex	8.4	17	2.0
	MFG	7.0	14	2.9

Table 7.3 Significance of comparisons between the motor cortex and other regions. Bonferroni correction for multiple tests for each measured parameter gave a significance value of $p = 0.016$, showing p values for difference in BOLD values in red remain significant.

Region	M	ΔCBF	ΔBOLD	$\Delta CMRO_2$	n	Resting CBF
SMA	0.95	0.58	0.24	0.27	0.78	0.17
PL	0.29	0.11	0.003	0.58	0.03	0.09
MFG	0.06	0.59	0.02	0.11	0.04	0.28

Previous work has shown regional variations in coupling parameters, with higher values of both M and n in the motor cortex compared to the visual cortex ((Hoge et al., 1999a; Kastrup et al., 2002; Stefanovic et al., 2004; Uludag et al., 2004). Furthermore, a recent study has shown reduced coupling 'n' in the medial temporal lobe compared to the motor cortex (Restom et al., 2008). From inspection of the data in Table 7.1 it can be seen that both BOLD and n appear lower in primary motor cortex compared to other regions, whereas other parameters such as M do not. This was tested formally. First, in

associated with the Stroop task due to the interference effect, is normally achieved with contrasting congruent and incongruent conditions. It was decided for this study based on pilot work that contrast of resting state vs. incongruent conditions gave a more measurable effect, suggesting that the subtlety of signal difference between congruent and incongruent conditions may be beyond the sensitivity for our ASL sequence.
The successful activation of the relevant frontal cortex ROI's, suggests this methodology may be a useful technique for studying neurovascular changes and cognitive decline in normal aged and diseased populations.

Chapter 8. Applications of hyperoxia calibrated fMRI

In this chapter, results are presented for two studies exploring the use of hyperoxia calibrated fMRI, as a novel imaging technique for assessing neurovascular changes associated with: (i) normal ageing and (ii) cerebral small vessel disease (cSVD).

8.1 Calibrated fMRI reveals altered neurovascular coupling with age during a cognitive Stroop task

8.1.1 Introduction

In this study hyperoxia calibrated fMRI was used to assess the differences in neurovascular coupling between a young, and a healthy old group during a cognitive stroop task. Previous work using the Stroop task has shown increased BOLD response with increasing age in the frontal cortex (Langenecker et al., 2004; Milham et al., 2002; Zysset et al., 2007), attributed to an increase in neural processing in this region. However, it is not clear whether it is the neuronal or vascular response that drives these differences. The use of calibrated fMRI allows quantitative measures of the relevant changes in $CMRO_2$ and CBF, which contribute to the measured BOLD response, and therefore offers more insight into the underlying neurovascular relationship.

8.1.2 Methods

10 young (age range 19-36, 4 male) and 13 older (age range 55–76, 2 male) volunteers took part in the experiment which was approved by the University research ethics committee. Participants were carefully screened according to the following criteria: not taking medication for cardiovascular disease; No history of migraines, stroke, hypertension, diabetes or any neurological disease, and no use of tobacco products.

Stroop Task: A color-word Stroop task was used, as described in Chapter 7. Subjects had to decide if the meaning of a word presented in white ink at the bottom of the screen matched the ink color of the top word and respond with a choice of two buttons with the right hand. Stimuli were self-paced with a minimum time of 1.5 seconds (young) or 2 seconds (old) between stimuli. 8 active blocks of 30 s were interspersed with 30 s fixation cross, giving a run time of 8 minutes.

Hyperoxia calibration task: 100% oxygen was delivered via an open mask (2 sessions of 3 minutes) at 15l /min interspersed with 3 minutes of normoxia, with an additional 2 minutes normoxia at the beginning. End tidal O_2 content was continuously sampled from the subject's nose via nasal cannula at intervals of 1ms, and measured with an oxygen analyzer.

8.1.3 MRI methods

All scanning was performed on a 3 T Siemens Trio system. Images were acquired using a Q2TIPS Arterial Spin Labeling sequence (Luh et al., 1999). Acquisition parameters were: TR 2.13 s, TI_1 0.7 s, TI_2 1.4 s, TE 25 ms and crusher gradients with b=5 mms^{-1}. An imaging volume consisting of 12 slices of 3.5 mm thickness was positioned to cover frontal, motor and parietal cortices. A 1mm isotropic structural MPRAGE image was also collected for co-registration purposes.

8.1.4 Analysis

Analysis was performed using BrainVoyager QX software. Label and control images were added (BOLD) or subtracted (CBF) in Matlab to produce BOLD and CBF time courses which were co-registered to the T_1-weighted image and transformed into Talairach space. BOLD and CBF time courses were combined in a multi study GLM, where regions of interest were found on an individual basis when the stroop activity accounted for significant variance in both the BOLD and CBF time-courses at a threshold of $p<0.05$ (corrected for FDR). Data was recorded from 8 regions of interest: primary motor (M1), supplementary motor area SMA, left and right parietal lobe (PL), middle frontal gyrus (MFG) and frontal cortex (FC), from regions of approximately 1cm^3 centered over the areas of maximum activation .

In each ROI individual signal time courses were recorded for BOLD and CBF for both the stroop and hyperoxia stimuli.

The calibration constant M was calculated using the Chiarelli and Bulte hyperoxia model, equation [3.13] (Chiarelli et al., 2007b), with $\alpha = 0.38$, $\beta = 1.5$, baseline oxygen extraction fraction (OEF) of 0.4 and an assumed reduction in CBF of 5% during hyperoxia. The parameters ΔBOLD, ΔCBF and ΔCMRO2 were calculated using the

deoxyhaemoglobin dilution model, equation [3.7] (Buxton et al., 2004; Hoge et al., 1999b) Regional and global differences between the groups were tested.

8.1.5 Results and Discussion

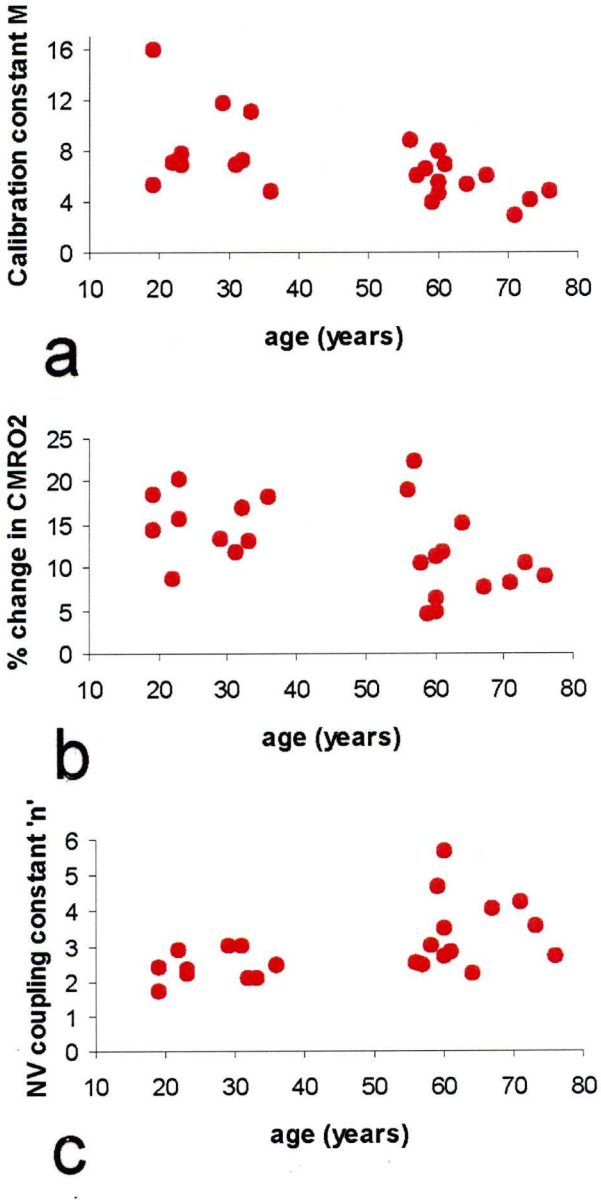

Figure 8.1 Relationships between age and a) the BOLD calibration constant *M*. b) change in $CMRO_2$, c) the neurovascular coupling parameter *n*. measured in response to the Stroop task. Values represent averages across all measured ROI's. Linear regression and T-test on the two age groups gave equivalent significance for age effect on the measurements.

The BOLD response to hyperoxia was reduced in the older group compared to the younger group. Two sample t_tests showed significant reduction in the calibration constant M in the older group (p = 0.014) as shown in Figure 8.1a, where each point shows the average value for an individual over all regions. In addition we find a reduction in ΔCMRO2 with increasing age (p = 0.038) as shown in Figure 8.1b. Despite an overall reduction in BOLD and M with age, when averaging across all ROI's, there was no correlation with age and ΔCBF, and hence the neurovascular coupling parameter n=ΔCBF/ ΔCMRO2 was significantly higher in the older group (p = 0.009) (Figure 8.1c).

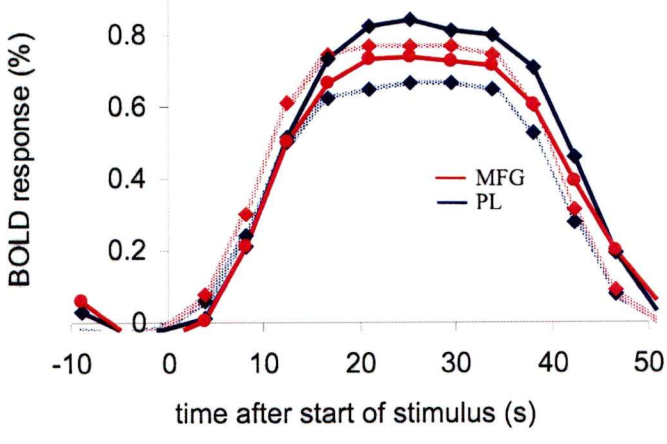

Figure 8.2 Average BOLD response curves for old (dotted line) and young (solid line) groups for MFG and PL activation in response to the stroop task.

The reduction in M may be the result of a reduction in cerebral blood volume that is known to occur with increasing age (Wenz et al., 1996). In our application of the hyperoxia calibration model, a fixed value for CBF reduction is used. However, there is evidence that CBF reduction may be smaller with increasing age (Watson et al., 2000). This could lead to an *overestimated* value for M with increased age, and hence the age-related reduction observed in this study may be underestimated.

The older group (Figure 8.2) show reduced BOLD response in PL and increased BOLD in MFG compared to the younger group, in agreement with previous studies (Langenecker et al., 2004; Milham et al., 2002).This observation has previously been interpreted as regional recruitment to aid in task perfomance in elderly subjects, as

reflected by the increased BOLD signal. But this hypothesis would imply that metabolic activtiy would be increased in those regions associated with higher BOLD activity. However, the measured coupling parameter n is increased in both of these regions in the older group, corresponding with a measured reduction in %ΔCMRO2 with no significant %CBF reduction. A reduction in ΔCMRO2 would be consistent with *reduced* neural activity, which could be attributed to age related brain atrophy (Benedetti et al., 2006), for which the frontal cortices are particularly susceptible (Raz et al., 2005). However, one might expect such volume reductions to manifest in reduced cerebral blood flow changes; however this was not the case.

These results demonstrates the care needed in interpretation of differences in the BOLD response between groups where the neurovascular coupling and resting blood volume may be altered, such as in two groups of different ages or in comparisons of a clinical and control group. It also highlights the added benefit that calibrated fMRI offers in terms of interpreting the underlying physiological changes that give rise to the measured BOLD resposne.

8.2 Hyperoxia calibrated fMRI of cerebral small vessel disease during a cognitive Stroop task

8.2.1 Introduction

Cerebral small-vessel disease (cSVD) or cerebral microangiopathy, is a condition with highest prevalence in elderly people, and is a common risk factor associated with the development of subcortical ischemic *vascular dementia* (VaD) (Schroeter et al., 2007), which is the second most common dementia type after Alzheimer's disease, making up 9%-39% of all dementia cases, and as much as 50% in Japanese populations (O'Sullivan et al., 2005a; Schroeter et al., 2007). Progression of cSVD will in time, manifest as *vascular cognitive impairment* (VCI), a relatively new term, as yet without consensus defining criteria, but which encompasses vascular dementia and other cognitive impairment resulting from vascular disease (Bowler, 2004; Schmidtke et al., 2005), and is associated with stroke and death from stroke. VaD is an important sub-

group of dementia, which is becoming more prevalent with an ageing population, but which has the potential to be prevented.

The most commonly recognised feature of VCI associated with cSVD is executive dysfunction (Nitkunan et al., 2008; O'Sullivan et al., 2005b) Attention and the speed of information processing are also impaired, whilst memory is relatively spared (Markus, 2007; Schmidt et al., 2006) Executive function is a faculty associated with higher cognitive processes, such as planning, attentional set shifting, the selection of appropriate responses and working memory (O'Sullivan et al., 2005b).

These cognitive processes have been shown to be mediated by the frontal cortices, and more specifically in the dorsolateral prefrontal cortex (Schmidt et al., 2006). They are generally attributed to be the result of either arteriolar occlusion and *lacunes* (3 to 15mm cerebrospinal fluid (CSF) filled cavities in the basal ganglia or white matter) (Wardlaw, 2008) or widespread incomplete infarction of white matter due to critical stenosis of medullary arterioles and hypoperfusion (Binswanger's disease), which probably manifest as executive dysfunction from ischemic interruption of parallel circuits from the prefrontal cortex to the basal ganglia and corresponding thalamocortical connections (Roman et al., 2002).

The white matter changes (leukoaraiosis) often associated with cSVD, are typically the pathology of interest in regards to MRI based investigations, where most investigations of the disease have focused on Diffusion tensor MRI or T_2 weighted structural images, to detect pathological changes in diffusivity in white matter (Nitkunan et al., 2008; O'Sullivan et al., 2004; O'Sullivan et al., 2001). However, fMRI has also been used in conjunction with hyperventilation to measure cerebrovascular reactivity, a measure of vessel wall compliance, which has shown to be reduced in grey matter in cSVD patients, with the most pronounced impairment in frontal cortices (Hund-Georgiadis et al., 2003). This issue was explored further using near infrared spectroscopy during a cognitive Stroop task, which found a reduced haemodynamic response in lateral prefrontal cortex in cSVD patients (Schroeter et al., 2007). This apparent uncoupling of the neurovascular activity has obvious implications for exploration of this phenomenon through the use of calibrated fMRI, where functional metabolic activity in the brain is compromised, and the standard fMRI blood oxygen level dependent signal (BOLD) is difficult to interpret.

Recent related applications of this technique using *hypercapnia* calibration, include the exploration of age related neurovascular changes and cognitive decline (Restom et al., 2007; Restom et al., 2008).

Application of calibrated fMRI in the study of cSVD and VCI requires careful consideration of inclusion and exclusion criteria when recruiting possible participants. One hypothesis suggests that cSVD leads to lacunar infarcts (LI's) that cause particular syndromes (Gerraty et al., 2002), which suggests that LI's may be important markers of cSVD (Norrving, 2003). However, this is not true in all cases, where it is thought that up to a third of patients presenting with a lacunar syndrome, are the result of an embolism or other causes such as dissection of arterioles (Fisher, 1982; Gerraty et al., 2002; Norrving, 2008).

Both pathologically and radiologically, LI's and leukoaraiosis are seen in patients with vascular dementia (Markus, 2007; Schmidt et al., 2006), with 93% of those with vascular dementia having discrete lacunae (Bowler, 2004). A further study found that 83% of Lacunar stroke patients with LI's and leukoaraiosis had cognitive impairment. Therefore, in regards to recruitment of people with cSVD, the most clinically relevant cohort is Lacunar stroke patients, whereby a meticulous case definition with particular attention to radiological confirmation of a clinically relevant lacunar infarct, and exclusion of other stroke aetiologies would be expected to improve the likelihood that cSVD is the cause.

The use of calibrated fMRI in the study of cSVD is a new and potentially useful technique for the assessment of haemodynamic and metabolic changes that may accompany executive dysfunction and VCI. While the bulk of other MRI modalities focus on structural changes such as atrophy and white matter lesions, as well as diffusion weighted images to assess leukoaraiosis or white matter re-organization, calibrated fMRI performed during an executive function task such as the *Stroop* task (Zysset et al., 2001) allows the possibility to assess grey matter function, particularly frontal lobe regions, previously implicated in VCI and reduced executive function.

In this section of the chapter, preliminary results are presented for an ongoing study using hyperoxia calibrated fMRI to assess neurovascular function in patients with suspected cSVD. This forms part of a larger study whereby a number of different MRI scans are performed, in an effort to establish novel imaging techniques, useful for the assessment and diagnosis of cSVD.

8.2.2 Method

6 patients with symptomatic cSVD (defined by history of lacunar stroke and exclusion of alternative stroke aetiology) (mean age 62, 4_{male}/ 2_{female}) and 15 healthy aged matched control subjects (mean age 62, 4_{male} / 11_{female}) were scanned (Siemens 3T), using an 8-channel RF coil. A Q2TIPS Arterial Spin Labeling sequence (Luh et al., 1999) was used to collect simultaneous BOLD and CBF signal: TR 2.13s, TI_2 1.4s, TE 25ms, 12 slices of 3.5mm covering frontal and motor cortices, during a Stroop task (Zysset et al., 2001), as well as a calibration scan. During the Stroop task, subjects had to decide if the meaning of a word presented at the bottom of the screen matched the ink color of the top word and respond with a choice of two buttons with the right hand. Stimuli were self-paced with a minimum time of 2 seconds between stimuli. 8 active blocks of 30 seconds were interspersed with 30 seconds fixation cross, giving a run time of 8 minutes. For the calibration scan, 100% oxygen was delivered via an open mask at 15l / min for two periods of 3 minutes interspersed with 3 minutes normoxia, with an additional 2 minutes normoxia at the beginning. End-tidal oxygen was continuously sampled via nasal cannula.

We also collected standard diagnostic scans including FLAIR images, T2-weighted images, Susceptibility Weighted Images, and angiography of the carotids and circle of Willis.

8.2.3 Analysis

ASL data analysis and ROI selection was performed on a group basis in Talairach space using BrainVoyager. BOLD and CBF time-courses were extracted for the Stroop task and hyperoxia scans in 8 regions of interest (ROIs): (Middle Frontal Gyrus (L&R), Motor-Cortex, Parietal-Lobe (L&R), MFG (L&R) and SMA), where the stroop activity

accounted for significant variance in both the BOLD and CBF time-courses at a threshold of $p<0.05$ (corrected for FDR). A voxel cluster of $1\,cm^3$ covering the area of highest activation, was selected within each of the specific ROI's. Values for ΔBOLD, ΔCBF, calibration constant *M*, $\Delta CMRO_2$ and coupling parameter 'n' ($=\Delta CBF/\Delta CMRO_2$) were calculated for each ROI using the hyperoxia model (equation [3.13]) (Chiarelli et al., 2007b) with $\alpha = 0.38$, $\beta = 1.5$, baseline oxygen extraction fraction (OEF) of 0.4 and an assumed reduction in CBF of 5% during hyperoxia.

8.2.4 Results & discussion

cSVD patients were less accurate (80 ± 16 % correct responses) and had a slower response time (2.0 ± 0.8 sec.) to the stroop task in comparison to the controls (accuracy: 97 ± 2.9 % correct responses, response time 1.1 ± 0.2 sec.), in agreement with previous work (Zysset et al., 2007). Single tailed t-Tests gave *p* values of 0.02, and 0.05 for the showing significant difference in response time and accuracy respectively, between the two groups.

The BOLD response to the Stroop task was higher in the frontal cortices for the cSVD group (Figure 8.3 top), which corresponded with reduced values of $\Delta CMRO_2$ in those regions. This agrees with previous work showing reduced glucose metabolism in frontal regions (Reed et al., 2001). A Reduced BOLD signal was observed in the patient group in primary motor cortex, compared to the control group, in agreement with previous work (Pineiro et al., 2002), and higher average values for the calibration parameter *M* were measured in *all* ROI's for the cSVD patients compared to the controls (Figure 8.3 middle).

It was expected that *M* would be lower in the patient group due to expected reduction in baseline blood volume, mirroring baseline reductions in CBF which have been observed in cSVD (Sabri et al., 1999). However this discrepancy may be in part attributable to the use of an assumed 5% CBF reduction in the hyperoxia calibration model. Previous studies have suggested that this value is age dependent, and that hyperoxic induced changes in CBF become reduced with age (Watson et al., 2000). This effect may be exaggerated in cSVD cases, where arteriopathy may impede vessel wall elasticity, resulting in smaller CBF reductions during hyperoxia, and therefore an

overestimation of the value for M in our model. It should also be noted that M varies proportionally with baseline OEF, which may potentially be higher in this particular patient group (Nakane et al., 1998).

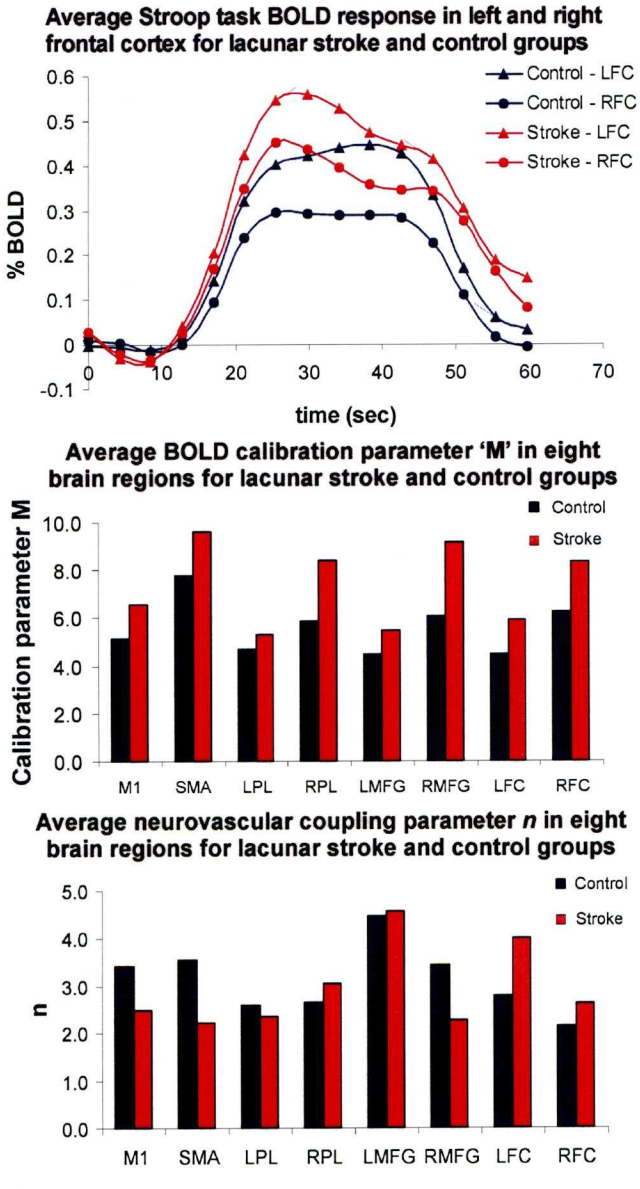

Figure 8.3 Average responses for control group and cSVD group for: (top) BOLD signal change in left and right frontal cortex, showing larger response in both regions for the patient group, (middle) calibration parameter M for eight regions of interest, consistently higher in the patient group in all regions (bottom) neurovascular coupling parameter n for the 8 ROI's.

We found evidence for regional variation in the neurovascular coupling parameter n (bottom right), with average values across all regions of 2.95 ± 0.88 for stroke patients, and 3.13 ± 0.74 for the control group.

8.2.5 Summary

In this work we have presented preliminary data for an ongoing study investigating cognitive performance in patients with symptomatic cSVD using hyperoxia calibrated fMRI. We aim to recruit a sufficient number of subjects to fully evaluate the use of this methodology, as well as FLAIR images, T2-weighted images, Susceptibility Weighted Images, and angiography of the carotids and circle of Willis, as potential imaging techniques for establishing sensitive markers of cSVD.

Chapter 9. Summary & Future work

9.1 Summary of experimental work

This thesis has focussed on the development of calibrated fMRI methodology, with applications in the study of neurovascular changes associated with normal ageing and disease. From the first experimental work in chapter 4, where the use of Q2TIPS for simultaneous BOLD and CBF measurement was tested, to the most recent application of hyperoxia calibrated fMRI in cSVD patients; the experimental work in this thesis represents a progression of ideas and techniques, from paradigm design and stimulus type, to calibration and data analysis.

In Chapter 4 the accuracy of the Q2TIPS sequence, as well as the insensitivity to transit time effects were tested. Also tested was the use of the sequence for obtaining simultaneous BOLD and CBF time courses during a finger tapping exercise, in which it was found that a linear relationship exists between BOLD and CBF change, demonstrated by increasing the number of finger taps. The results from these two studies raised a couple of issues: a) the duration of stimulus required for improved assessment of relative BOLD and CBF changes for primary sensory stimulation in a block design experiment, should be sufficient to generate steady state responses. This was not the case in this study, although a graded response was observed in response to the three finger tap conditions. The steady state requirement is also necessary for the application of the Grubb relationship for equating CBV and CBF changes, which would be necessary for any advancement on this work in the region of BOLD calibration, to quantify the $CMRO_2$ contributions to the BOLD signal change. b) is the observed BOLD / CBF linearity and graded response region specific? And how is it affected by age?

In Chapter 5 these issues were explored further, as was the potential for breath hold induced hypercapnia as a calibration technique. It was observed that a graded linearity could also be observed in the visual cortices, and that the measured BOLD and CBF changes were generally greater in this region when compared with the measurements obtained from the graded motor grip task. This observation was no doubt influenced by the tasks themselves, but may also be the neurovascular properties associated with those regions, which is also supported by the fact that the

average BOLD and CBF changes measured during breath hold, were also larger in the visual cortex.

The use of breath hold as a calibration method was tested, and found to be generally not reliable. The reproducibility was lower than the more established hypercapnia techniques, and provided generally inaccurate measurements for the calibration parameter *M*, which resulted in inaccurate estimates of $CMRO_2$ changes during the functional tasks. As a result, no meaningful examination of $CMRO_2$ / CBF coupling could be made. However, the BOLD / CBF relationship was examined in relation to age, but no significant age effect was observed in either the motor or visual cortices. This was particularly surprising as a reduction in baseline CBF is known to occur with increasing age, but it was not observed in this study, suggesting that neurovascular properties of primary sensory areas may be more immune to age related decline. The absence of any significant age related decline in visual cortex measurements, correlates with previous work looking at reductions in brain volume with age, which showed no significant reduction in volume in the visual cortex area V1 (Raz et al., 2005). This study showed that breath hold, although easier and more implementable than other calibration methods, is not as reproducible or accurate. The inability to measure age related reductions in the visual or motor cortices, suggests that age related changes may be more detectible in areas relating to cognition rather than primary sensory stimulation. It may also suggest that the stimuli or paradigm used were not sufficient to elicit these measurable age related differences.

The experimental work outlined in Chapter 6, was borne out of the recognition that breath hold, as a potential candidate for future calibrated fMRI studies with clinical application, would not be sufficient. The recently introduced hyperoxia model had obvious appeal as a possible alternative technique, which may also be more suited to clinical application. However, a direct comparison between the hyperoxia and hypercapnia techniques had not been made within the same cohort, which became the basis for this study. In this study it was demonstrated that the hyperoxia model is a viable alternative to the hypercapnia calibration method. However, this was true only when using an assumed value for CBF reduction, for which an assumed value of 5% gave the most comparable results to hypercapnia. The use of an assumed value may be critical for age related studies, where we found no measureable age related

differences in the calibration parameter M or change in $CMRO_2$ when using hyperoxia with an assumed value, unlike hypercapnia, which gave a significant reduction in M, and a trend toward reduced $CMRO_2$ with age.

Significant age related reductions in the BOLD signal were measured during visual activation, unlike the previous experiment. In this case, the stimulus was also a flashing checkerboard but only one visual contrast was used, which was presented for longer stimulus blocks. Whether the change in stimulus type and duration, was the key to eliciting a measured age related reduction in the BOLD signal in this study, or whether the cohort themselves, whom were all Japanese and all female was the critical difference, remains uncertain.

After establishing the potential for hyperoxia calibration as an alternative to the hypercapnia method, the reproducibility needed to be assessed, as well as the application in brain regions other than primary sensory areas. In Chapter 7, these issues were addressed by using hyperoxia calibrated fMRI during a cognitive Stroop task, which is known to activate, among other areas, the frontal cortex, which is recognised as susceptible to age related atrophy and CBF reduction (Parkes et al., 2004; Raz et al., 2005). This technique also allows a comparison to be made between cognitive performance, determined by the accuracy and speed with which the participants performed the Stroop task, and the corresponding fMRI measurements.

A comparable level of reproducibility was measured across an average of the various regions activated by the Stroop task, compared to Leontiev et al. hypercapnia reproducibility experiment, with the exception of $CMRO_2$ and n values which did not compare as favourably. We attributed this difference in part to our inability to use a CBF localiser for ROI selection, due to the low level activation changes that occurred in CBF during the Stroop task, as well as the BOLD measurements themselves, which were considerably smaller than those measured by Leontiev et al. in the visual cortex, and would therefore have a direct effect on the reproducibility due to the reduced SNR.

This study did however demonstrate the potential for hyperoxia calibration for application in fMRI studies of cognitive processing or impairment.

In Chapter 8 two studies were documented, which are based on the hyperoxia / Stroop methodology outlined in Chapter 7. The first of which focused on age related

neurovascular differences in healthy adults, in regions associated with cognition, in which significant age related reduction was observed in both the calibration constant M, as well as the change in $CMRO_2$. The observation that the parameter M reduces with age, may be a reflection of the direct proportionality with baseline blood volume, which is known to decrease with age, particularly in frontal cortex regions, which are activated during the Stroop task. Previous studies have shown increased BOLD activation in frontal gyrus regions in older subjects during the Stroop task (Langenecker et al., 2004; Zysset et al., 2007), in agreement with our results. This has previously been attributed to the increased need for compensatory strategies in older people to inhibit over learned words, resulting in a greater recruitment of neurones in frontal gyrus regions. However, in addition to observing higher BOLD activation in these regions, we observed a reduction in $CMRO_2$, with no significant change in the CBF response to the stimulus, which may explain the source of the BOLD signal increase. However, this also suggests that the reduction in metabolic activity is a result of reduced neural activation in those regions, which appears contradictory with the previously mentioned studies. The results also suggest that the coupling between in ΔCBF and $\Delta CMRO_2$ is changing in these regions with age, as reflected in the parameter n, which we found increased with age.

The second study utilised hyperoxia calibrated fMRI during a stroop task, as well as several other MRI techniques, to investigate their use as novel imaging techniques in the assessment of cSVD. This study is ongoing, and will require a sufficient number of cSVD patients before any conclusions can be made, but the preliminary data suggests there may be some obvious differences between the patient and age matched control group, particularly in the frontal cortices. This area of research, along with many age related disorders, may be increasingly relevant in an ageing population, and will hopefully prove informative in understanding the nature of cSVD, and its relationship with cognitive decline, dementia and stroke.

9.2 The future

Calibrated fMRI has the potential to be applied clinically in a number of applications associated with neurodegenerative diseases. In our most recent work, we have demonstrated the potential for hyperoxia calibrated fMRI in the assessment of cSVD,

which may be informative in understanding the disease progression and how it manifests as cognitive impairment. Application of calibrated fMRI may also be applicable to other forms of dementia such as Alzheimer's disease, or mixed dementia where obtaining quantitative measures of the underlying neurovascular changes may be particularly useful for disease prognosis.

In regards to the question: hyperoxia or hypercapnia, which one is the best? It seems this may depend on the application, and availability of necessary equipment etc. The main limitation of the hyperoxia methodology that we implemented, was the inability to accurately measure small changes in CBF that occur during prolonged periods of hyperoxia. This meant that an estimated value was applied to everyone, which may have obscured some underlying variability, due vascular reactivity and vessel wall compliance, and may not have been as effective as hypercapnia calibration for exploring age related effects. Therefore an obvious improvement to this methodology would be to focus on improving the quantification of small CBF changes that occur during hyperoxia. This may be better achieved through non ASL MRI methods, such as phase contrast angiography (McRobbie et al., 2003), allowing CBF quantification through the measurement of blood velocity. However this would not be simultaneously acquired with BOLD signal change, and would only provide measures of global change in CBF. Therefore attention should probably be directed at trying to optimise the sensitivity of the ASL sequence itself to the small CBF changes, as well as exploring improved quantification and analysis procedures.

One aspect in favour of the hyperoxia approach is that the general consensus of the volunteers who participated in the hyperoxia / hypercapnia comparison study, found that the inhalation of the O_2 gas was more tolerable than the CO_2 gas mixture. Therefore, in terms of volunteer or patient comfort, the hyperoxia approach may be more suitable, but the overwhelming support and development of hypercapnia calibration methodology over the last decade, has demonstrated the viability of the technique, to the extent that it has become something of a gold standard in calibrated fMRI. An increasing investigation into the use of the hyperoxia method, including perhaps some validation of the accuracy of the technique for estimating $CMRO_2$, through a combined MRI, PET or SPECT study, may see this method become the method of choice for future calibrated fMRI work.

References

Alsop, D.C., Detre, J.A., 1996. Reduced transit-time sensitivity in noninvasive magnetic resonance imaging of human cerebral blood flow. J Cereb Blood Flow Metab 16, 1236-1249.

An, H., Lin, W., 2002. Cerebral oxygen extraction fraction and cerebral venous blood volume measurements using MRI: effects of magnetic field variation. Magn Reson Med 47, 958-966.

Ances, B.M., Leontiev, O., Perthen, J.E., Liang, C., Lansing, A.E., Buxton, R.B., 2008a. Regional differences in the coupling of cerebral blood flow and oxygen metabolism changes in response to activation: implications for BOLD-fMRI. Neuroimage 39, 1510-1521.

Ances, B.M., Liang, C.L., Leontiev, O., Perthen, J.E., Fleisher, A.S., Lansing, A.E., Buxton, R.B., 2008b. Effects of aging on cerebral blood flow, oxygen metabolism, and blood oxygenation level dependent responses to visual stimulation. Hum Brain Mapp.

Attwell, D., Iadecola, C., 2002. The neural basis of functional brain imaging signals. Trends Neurosci 25, 621-625.

Bandettini, P.A., Cox, R.W., 2000. Event-related fMRI contrast when using constant interstimulus interval: theory and experiment. Magn Reson Med 43, 540-548.

Bandettini, P.A., Wong, E.C., Hinks, R.S., Tikofsky, R.S., Hyde, J.S., 1992. Time course EPI of human brain function during task activation. Magn Reson Med 25, 390-397.

Bandettini, P.A., Wong, E.C., Jesmanowicz, A., Hinks, R.S., Hyde, J.S., 1994. Spin-echo and gradient-echo EPI of human brain activation using BOLD contrast: a comparative study at 1.5 T. NMR Biomed 7, 12-20.

Bangen, K.J., Restom, K., Liu, T.T., Jak, A.J., Wierenga, C.E., Salmon, D.P., Bondi, M.W., 2007. Differential age effects on cerebral blood flow and BOLD response to encoding: Associations with cognition and stroke risk. Neurobiol Aging.

Belliveau, J.W., Kennedy, D.N., Jr., McKinstry, R.C., Buchbinder, B.R., Weisskoff, R.M., Cohen, M.S., Vevea, J.M., Brady, T.J., Rosen, B.R., 1991. Functional mapping of the human visual cortex by magnetic resonance imaging. Science 254, 716-719.

Benedetti, B., Charil, A., Rovaris, M., Judica, E., Valsasina, P., Sormani, M.P., Filippi, M., 2006. Influence of aging on brain gray and white matter changes assessed by conventional, MT, and DT MRI. Neurology 66, 535-539.

Bergofsky, E.H., Bertun, P., 1966. Response of regional circulations to hyperoxia. J Appl Physiol 21, 567-572.

Bickler, P.E., Litt, L., Banville, D.L., Severinghaus, J.W., 1988a. Effects of acetazolamide on cerebral acid-base balance. J Appl Physiol 65, 422-427.

Bickler, P.E., Litt, L., Severinghaus, J.W., 1988b. Effects of acetazolamide on cerebrocortical NADH and blood volume. J Appl Physiol 65, 428-433.

Bowler, J.V., 2004. Vascular cognitive impairment. Stroke 35, 386-388.

Boxerman, J.L., Bandettini, P.A., Kwong, K.K., Baker, J.R., Davis, T.L., Rosen, B.R., Weisskoff, R.M., 1995. The intravascular contribution to fMRI signal change: Monte Carlo modeling and diffusion-weighted studies in vivo. Magn Reson Med 34, 4-10.

Boynton, G.M., Engel, S.A., Glover, G.H., Heeger, D.J., 1996. Linear systems analysis of functional magnetic resonance imaging in human V1. J Neurosci 16, 4207-4221.

Brown, G.G., Eyler Zorrilla, L.T., Georgy, B., Kindermann, S.S., Wong, E.C., Buxton, R.B., 2003. BOLD and perfusion response to finger-thumb apposition after acetazolamide administration: differential relationship to global perfusion. J Cereb Blood Flow Metab 23, 829-837.

Brown, M.M., Wade, J.P., Marshall, J., 1985. Fundamental importance of arterial oxygen content in the regulation of cerebral blood flow in man. Brain 108 (Pt 1), 81-93.

Buckner, R.L., Snyder, A.Z., Sanders, A.L., Raichle, M.E., Morris, J.C., 2000. Functional brain imaging of young, nondemented, and demented older adults. J Cogn Neurosci 12 Suppl 2, 24-34.

Bulte, D.P., Chiarelli, P.A., Wise, R.G., Jezzard, P., 2007. Cerebral perfusion response to hyperoxia. J Cereb Blood Flow Metab 27, 69-75.

Buxton, R.B., Frank, L.R., 1997. A model for the coupling between cerebral blood flow and oxygen metabolism during neural stimulation. J Cereb Blood Flow Metab 17, 64-72.

Buxton, R.B., Frank, L.R., Wong, E.C., Siewert, B., Warach, S., Edelman, R.R., 1998a. A general kinetic model for quantitative perfusion imaging with arterial spin labeling. Magn Reson Med 40, 383-396.

Buxton, R.B., Uludag, K., Dubowitz, D.J., Liu, T.T., 2004. Modeling the hemodynamic response to brain activation. Neuroimage 23 Suppl 1, S220-233.

Buxton, R.B., Wong, E.C., Frank, L.R., 1998b. Dynamics of blood flow and oxygenation changes during brain activation: the balloon model. Magn Reson Med 39, 855-864.

Carrol, T.J., Teneggi., V., Jobin., M., Squassante., L., Treyer., V., Hany., T.F., Burger., C., Wang., L., Bye., A., Schulthess., G.K.v., Buck., A., 2002. Absolute Quantification of Cerebral Blood Flow With Magnetic Resonance, Reproducibility of the Method, and comparison With H215O Positron Emission Tomography. Journal of Cerebral Blood Flow & Metabolism 22, 1149 -1156.

Cavaglia, M., Dombrowski, S.M., Drazba, J., Vasanji, A., Bokesch, P.M., Janigro, D., 2001. Regional variation in brain capillary density and vascular response to ischemia. Brain Res 910, 81-93.

Chalela, J.A., Alsop, D.C., Gonzalez-Atavales, J.B., Maldjian, J.A., Kasner, S.E., Detre, J.A., 2000. Magnetic resonance perfusion imaging in acute ischemic stroke using continuous arterial spin labeling. Stroke 31, 680-687.

Chiarelli, P.A., Bulte, D.P., Gallichan, D., Piechnik, S.K., Wise, R., Jezzard, P., 2007a. Flow-metabolism coupling in human visual, motor, and supplementary motor areas assessed by magnetic resonance imaging. Magn Reson Med 57, 538-547.

Chiarelli, P.A., Bulte, D.P., Wise, R., Gallichan, D., Jezzard, P., 2007b. A calibration method for quantitative BOLD fMRI based on hyperoxia. Neuroimage 37, 808-820.

Crossman, A.R., Neary, D., 1998. Neuroanatomy - an illustrated colour text.

Davis, T.L., Kwong, K.K., Weisskoff, R.M., Rosen, B.R., 1998. Calibrated functional MRI: mapping the dynamics of oxidative metabolism. Proc Natl Acad Sci U S A 95, 1834-1839.

Deneux, T., Faugeras, O., 2006. Using nonlinear models in fMRI data analysis: model selection and activation detection. Neuroimage 32, 1669-1689.

Detre, J.A., 2001. MR perfusion imaging of hyperacute stroke. AJNR Am J Neuroradiol 22, 806-807.

Detre, J.A., Alsop, D.C., Vives, L.R., Maccotta, L., Teener, J.W., Raps, E.C., 1998. Noninvasive MRI evaluation of cerebral blood flow in cerebrovascular disease. Neurology 50, 633-641.

Detre, J.A., Floyd, T.F., 2001. Functional MRI and its applications to the clinical neurosciences. Neuroscientist 7, 64-79.

Detre, J.A., Leigh, J.S., Williams, D.S., Koretsky, A.P., 1992. Perfusion imaging. Magn Reson Med 23, 37-45.

Devor, A., Dunn, A.K., Andermann, M.L., Ulbert, I., Boas, D.A., Dale, A.M., 2003. Coupling of total hemoglobin concentration, oxygenation, and neural activity in rat somatosensory cortex. Neuron 39, 353-359.

Devor, A., Ulbert, I., Dunn, A.K., Narayanan, S.N., Jones, S.R., Andermann, M.L., Boas, D.A., Dale, A.M., 2005. Coupling of the cortical hemodynamic response to cortical and thalamic neuronal activity. Proc Natl Acad Sci U S A 102, 3822-3827.

Ding, E.L., Hutfless, S.M., Ding, X., Girotra, S., 2006. Chocolate and prevention of cardiovascular disease: a systematic review. Nutr Metab (Lond) 3, 2.

Donahue, M.J., Stevens, R.D., de Boorder, M., Pekar, J.J., Hendrikse, J., van Zijl, P.C., 2008. Hemodynamic changes after visual stimulation and breath holding provide evidence for an uncoupling of cerebral blood flow and volume from oxygen metabolism. J Cereb Blood Flow Metab.

Donaldson, D., 2002. Effective paradigm design.

Drayer, B.P., 1988. Imaging of the aging brain. Part I. Normal findings. Radiology 166, 785-796.

Dreier, J.P., Korner, K., Gorner, A., Lindauer, U., Weih, M., Villringer, A., Dirnagl, U., 1995. Nitric oxide modulates the CBF response to increased extracellular potassium. J Cereb Blood Flow Metab 15, 914-919.

Edelman, R.R., Siewert, B., Darby, D.G., Thangaraj, V., Nobre, A.C., Mesulam, M.M., Warach, S., 1994. Qualitative mapping of cerebral blood flow and functional localization with echo-planar MR imaging and signal targeting with alternating radio frequency. Radiology 192, 513-520.

Fera, F., Yongbi, M.N., van Gelderen, P., Frank, J.A., Mattay, V.S., Duyn, J.H., 2004. EPI-BOLD fMRI of human motor cortex at 1.5 T and 3.0 T: sensitivity dependence on echo time and acquisition bandwidth. J Magn Reson Imaging 19, 19-26.

Fisher, C.M., 1982. Lacunar strokes and infarcts: a review. Neurology 32, 871-876.

Floyd, T.F., Ratcliffe, S.J., Wang, J., Resch, B., Detre, J.A., 2003. Precision of the CASL-perfusion MRI technique for the measurement of cerebral blood flow in whole brain and vascular territories. J Magn Reson Imaging 18, 649-655.

Fox, P.T., Raichle, M.E., 1986. Focal physiological uncoupling of cerebral blood flow and oxidative metabolism during somatosensory stimulation in human subjects. Proc Natl Acad Sci U S A 83, 1140-1144.

Friston, K.J., 2002. Bayesian estimation of dynamical systems: an application to fMRI. Neuroimage 16, 513-530.

Friston, K.J., Buechel, C., Fink, G.R., Morris, J., Rolls, E., Dolan, R.J., 1997. Psychophysiological and modulatory interactions in neuroimaging. Neuroimage 6, 218-229.

Friston, K.J., Mechelli, A., Turner, R., Price, C.J., 2000. Nonlinear responses in fMRI: the Balloon model, Volterra kernels, and other hemodynamics. Neuroimage 12, 466-477.

Gerraty, R.P., Parsons, M.W., Barber, P.A., Darby, D.G., Desmond, P.M., Tress, B.M., Davis, S.M., 2002. Examining the lacunar hypothesis with diffusion and perfusion magnetic resonance imaging. Stroke 33, 2019-2024.

Gjedde, A., Marrett, S., Vafaee, M., 2002. Oxidative and nonoxidative metabolism of excited neurons and astrocytes. J Cereb Blood Flow Metab 22, 1-14.

Grubb, R.L., Jr., Ratcheson, R.A., Raichle, M.E., Kliefoth, A.B., Gado, M.H., 1979. Regional cerebral blood flow and oxygen utilization in superficial temporal-middle cerebral artery anastomosis patients: an exploratory definition of clinical problems. J Neurosurg 50, 733-741.

Haacke, E.M., Brown, R.W., Thompson, M.R., Venkatesan, R., 1999. Magnetic Resonance Imaging - physical principples and sequnce design.

Handwerker, D.A., Gazzaley, A., Inglis, B.A., D'Esposito, M., 2007. Reducing vascular variability of fMRI data across aging populations using a breathholding task. Hum Brain Mapp 28, 846-859.

Hesselmann, V., Zaro Weber, O., Wedekind, C., Krings, T., Schulte, O., Kugel, H., Krug, B., Klug, N., Lackner, K.J., 2001. Age related signal decrease in functional magnetic resonance imaging during motor stimulation in humans. Neurosci Lett 308, 141-144.

Hoge, R.D., Atkinson, J., Gill, B., Crelier, G.R., Marrett, S., Pike, G.B., 1999a. Investigation of BOLD signal dependence on cerebral blood flow and oxygen consumption: the deoxyhemoglobin dilution model. Magn Reson Med 42, 849-863.

Hoge, R.D., Atkinson, J., Gill, B., Crelier, G.R., Marrett, S., Pike, G.B., 1999b. Linear coupling between cerebral blood flow and oxygen consumption in activated human cortex. Proc Natl Acad Sci U S A 96, 9403-9408.

Huettel, S.A., Singerman, J.D., McCarthy, G., 2001. The effects of aging upon the hemodynamic response measured by functional MRI. Neuroimage 13, 161-175.

Hund-Georgiadis, M., Zysset, S., Naganawa, S., Norris, D.G., Von Cramon, D.Y., 2003. Determination of cerebrovascular reactivity by means of FMRI signal changes in cerebral microangiopathy: a correlation with morphological abnormalities. Cerebrovasc Dis 16, 158-165.

Huppert, T.J., Hoge, R.D., Diamond, S.G., Franceschini, M.A., Boas, D.A., 2006. A temporal comparison of BOLD, ASL, and NIRS hemodynamic responses to motor stimuli in adult humans. Neuroimage 29, 368-382.

Iadecola, C., Kraig, R.P., 1991. Focal elevations in neocortical interstitial K+ produced by stimulation of the fastigial nucleus in rat. Brain Res 563, 273-277.

Iso, H., Rexrode, K.M., Stampfer, M.J., Manson, J.E., Colditz, G.A., Speizer, F.E., Hennekens, C.H., Willett, W.C., 2001. Intake of fish and omega-3 fatty acids and risk of stroke in women. Jama 285, 304-312.

Ito, H., Takahashi, K., Hatazawa, J., Kim, S.G., Kanno, I., 2001. Changes in human regional cerebral blood flow and cerebral blood volume during visual stimulation measured by positron emission tomography. J Cereb Blood Flow Metab 21, 608-612.

Jacobsen, D.J., Hansen, L.K., Madsen, K.H., 2008. Bayesian model comparison in nonlinear BOLD fMRI hemodynamics. Neural Comput 20, 738-755.

Jarnum, H., Steffensen, E., Frund, T., Taagehoj Jensen, F., Wilberg Simonsen, C., Larsson, E.M., 2008. Age dependence and reproducibilty of cerebral perfusion assedssed by 3D pseudocontinuous arterial spin labelling.

Jezzard, P., Matthews, P.M., Smith, S.M., 2001. Functional MRI - an introduction to methods.

Jones, R.A., 2002. Ultra fast fMRI. Functional fMRI - an introduction to methods, 93 - 108.

Kastrup, A., Kruger, G., Glover, G.H., Moseley, M.E., 1999a. Assessment of cerebral oxidative metabolism with breath holding and fMRI. Magn Reson Med 42, 608-611.

Kastrup, A., Kruger, G., Neumann-Haefelin, T., Glover, G.H., Moseley, M.E., 2002. Changes of cerebral blood flow, oxygenation, and oxidative metabolism during graded motor activation. Neuroimage 15, 74-82.

Kastrup, A., Li, T.Q., Glover, G.H., Moseley, M.E., 1999b. Cerebral blood flow-related signal changes during breath-holding. AJNR Am J Neuroradiol 20, 1233-1238.

Kastrup, A., Li, T.Q., Takahashi, A., Glover, G.H., Moseley, M.E., 1998. Functional magnetic resonance imaging of regional cerebral blood oxygenation changes during breath holding. Stroke 29, 2641-2645.

Kida, I., Rothman, D.L., Hyder, F., 2007. Dynamics of changes in blood flow, volume, and oxygenation: implications for dynamic functional magnetic resonance imaging calibration. J Cereb Blood Flow Metab 27, 690-696.

Kim, S.G., 1995. Quantification of relative cerebral blood flow change by flow-sensitive alternating inversion recovery (FAIR) technique: application to functional mapping. Magn Reson Med 34, 293-301.

Kliefoth, A.B., Grubb, R.L., Jr., Raichle, M.E., 1979. Depression of cerebral oxygen utilization by hypercapnia in the rhesus monkey. J Neurochem 32, 661-663.

Kuperman, V., 2000. Magnetic Resonance Imaging - Physical principles and applications.

Kwong, K.K., Belliveau, J.W., Chesler, D.A., Goldberg, I.E., Weisskoff, R.M., Poncelet, B.P., Kennedy, D.N., Hoppel, B.E., Cohen, M.S., Turner, R., et al., 1992. Dynamic magnetic resonance imaging of human brain activity during primary sensory stimulation. Proc Natl Acad Sci U S A 89, 5675-5679.

Kwong, K.K., Chesler, D.A., Weisskoff, R.M., Donahue, K.M., Davis, T.L., Ostergaard, L., Campbell, T.A., Rosen, B.R., 1995. MR perfusion studies with T1-weighted echo planar imaging. Magn Reson Med 34, 878-887.

Langenecker, S.A., Nielson, K.A., Rao, S.M., 2004. fMRI of healthy older adults during Stroop interference. Neuroimage 21, 192-200.

Lauterbur, P.C., 1973. Image formation by induced local interactions. Examples employing nuclear magnetic resonance. 1973. Clin Orthop Relat Res, 3-6.

Leahy, F.A., Cates, D., MacCallum, M., Rigatto, H., 1980. Effect of CO2 and 100% O2 on cerebral blood flow in preterm infants. J Appl Physiol 48, 468-472.

Leenders, K.L., Perani, D., Lammertsma, A.A., Heather, J.D., Buckingham, P., Healy, M.J., Gibbs, J.M., Wise, R.J., Hatazawa, J., Herold, S., et al., 1990. Cerebral blood flow, blood volume and oxygen utilization. Normal values and effect of age. Brain 113 (Pt 1), 27-47.

Leontiev, O., Buxton, R.B., 2007. Reproducibility of BOLD, perfusion, and CMRO2 measurements with calibrated-BOLD fMRI. Neuroimage 35, 175-184.

Lin, A.L., Fox, P.T., Yang, Y., Lu, H., Tan, L.H., Gao, J.H., 2008. Evaluation of MRI models in the measurement of CMRO2 and its relationship with CBF. Magn Reson Med 60, 380-389.

Liu, H.L., Pu, Y., Nickerson, L.D., Liu, Y., Fox, P.T., Gao, J.H., 2000. Comparison of the temporal response in perfusion and BOLD-based event-related functional MRI. Magn Reson Med 43, 768-772.

Liu, T.T., Wong, E.C., 2005. A signal processing model for arterial spin labeling functional MRI. Neuroimage 24, 207-215.

Logothetis, N.K., 2007. The ins and outs of fMRI signals. Nat Neurosci 10, 1230-1232.

Logothetis, N.K., 2008. What we can do and what we cannot do with fMRI. Nature 453, 869-878.

Logothetis, N.K., Pauls, J., Augath, M., Trinath, T., Oeltermann, A., 2001. Neurophysiological investigation of the basis of the fMRI signal. Nature 412, 150-157.

Lu, H., Clingman, C., Golay, X., van Zijl, P.C., 2004a. Determining the longitudinal relaxation time (T1) of blood at 3.0 Tesla. Magn Reson Med 52, 679-682.

Lu, H., Golay, X., Pekar, J.J., Van Zijl, P.C., 2003. Functional magnetic resonance imaging based on changes in vascular space occupancy. Magn Reson Med 50, 263-274.

Lu, H., Golay, X., Pekar, J.J., Van Zijl, P.C., 2004b. Sustained poststimulus elevation in cerebral oxygen utilization after vascular recovery. J Cereb Blood Flow Metab 24, 764-770.

Luh, W.M., Wong, E.C., Bandettini, P.A., Hyde, J.S., 1999. QUIPSS II with thin-slice TI1 periodic saturation: a method for improving accuracy of quantitative perfusion imaging using pulsed arterial spin labeling. Magn Reson Med 41, 1246-1254.

Maccotta, L., Detre, J.A., Alsop, D.C., 1997. The efficiency of adiabatic inversion for perfusion imaging by arterial spin labeling. NMR Biomed 10, 216-221.

Malonek, D., Dirnagl, U., Lindauer, U., Yamada, K., Kanno, I., Grinvald, A., 1997. Vascular imprints of neuronal activity: relationships between the dynamics of cortical blood flow, oxygenation, and volume changes following sensory stimulation. Proc Natl Acad Sci U S A 94, 14826-14831.

Mandeville, J.B., Marota, J.J., Ayata, C., Zaharchuk, G., Moskowitz, M.A., Rosen, B.R., Weisskoff, R.M., 1999. Evidence of a cerebrovascular postarteriole windkessel with delayed compliance. J Cereb Blood Flow Metab 19, 679-689.

Mandeville, J.B., Marota, J.J., Kosofsky, B.E., Keltner, J.R., Weissleder, R., Rosen, B.R., Weisskoff, R.M., 1998. Dynamic functional imaging of relative cerebral blood volume during rat forepaw stimulation. Magn Reson Med 39, 615-624.

Mansfield, P., Grannell, P.K., 1973. NMR 'diffraction' in solids? J. Phys. C:Solid State Phys. 6.

Marcar, V.L., Straessle, A., Girard, F., Loenneker, T., Martin, E., 2004. When more means less: a paradox BOLD response in human visual cortex. Magn Reson Imaging 22, 441-450.

Markus, H.S., 2007. Mild cognitive impairment after lacunar infarction: voxel-based morphometry and neuropsychological assessment. Cerebrovasc Dis 23, 323-324.

Martin, J.H., 2003. Neuroanatomy - text and atlas. McGrawHill.

Matthew, E., Andreason, P., Carson, R., Herscovitch, P., Pettigrew, K., Cohen, R., King, C., Johanson, C., Paul, S., 1993. Reproducibility of resting cerebral blood flow measurements with H215O positron emission tomography in humans. J Cereb Blood Flow Metab 13, 748–754

Matthews, P.M., 2001. An introduction to functional magnetic resonance imaging of the brain. Oxford University Press, USA.

McRobbie, D.W., Moore, E.A., Graves, M.J., Prince, M.R., 2003. MRI - From Picture to Proton.

Milham, M.P., Erickson, K.I., Banich, M.T., Kramer, A.F., Webb, A., Wszalek, T., Cohen, N.J., 2002. Attentional control in the aging brain: insights from an fMRI study of the stroop task. Brain Cogn 49, 277-296.

Moulton, E.A., Keaser, M.L., Gullapalli, R.P., Maitra, R., Greenspan, J.D., 2006. Sex differences in the cerebral BOLD signal response to painful heat stimuli. Am J Physiol Regul Integr Comp Physiol 291, R257-267.

Mugler, J.P., 3rd, Brookeman, J.R., 1990. Three-dimensional magnetization-prepared rapid gradient-echo imaging (3D MP RAGE). Magn Reson Med 15, 152-157.

Nakane, H., Ibayashi, S., Fujii, K., Sadoshima, S., Irie, K., Kitazono, T., Fujishima, M., 1998. Cerebral blood flow and metabolism in patients with silent brain infarction: occult misery perfusion in the cerebral cortex. J Neurol Neurosurg Psychiatry 65, 317-321.

Nitkunan, A., Barrick, T.R., Charlton, R.A., Clark, C.A., Markus, H.S., 2008. Multimodal MRI in cerebral small vessel disease: its relationship with cognition and sensitivity to change over time. Stroke 39, 1999-2005.

Norris, D.G., 2006. Principles of magnetic resonance assessment of brain function. J Magn Reson Imaging 23, 794-807.

Norris, D.G., Zysset, S., Mildner, T., Wiggins, C.J., 2002. An investigation of the value of spin-echo-based fMRI using a Stroop color-word matching task and EPI at 3 T. Neuroimage 15, 719-726.

Norrving, B., 2003. Long-term prognosis after lacunar infarction. Lancet Neurol 2, 238-245.

Norrving, B., 2008. Lacunar infarcts: no black holes in the brain are benign. Pract Neurol 8, 222-228.

O'Sullivan, M., Barrick, T.R., Morris, R.G., Clark, C.A., Markus, H.S., 2005a. Damage within a network of white matter regions underlies executive dysfunction in CADASIL. Neurology 65, 1584-1590.

O'Sullivan, M., Morris, R.G., Huckstep, B., Jones, D.K., Williams, S.C., Markus, H.S., 2004. Diffusion tensor MRI correlates with executive dysfunction in patients with ischaemic leukoaraiosis. J Neurol Neurosurg Psychiatry 75, 441-447.

O'Sullivan, M., Morris, R.G., Markus, H.S., 2005b. Brief cognitive assessment for patients with cerebral small vessel disease. J Neurol Neurosurg Psychiatry 76, 1140-1145.

O'Sullivan, M., Summers, P.E., Jones, D.K., Jarosz, J.M., Williams, S.C., Markus, H.S., 2001. Normal-appearing white matter in ischemic leukoaraiosis: a diffusion tensor MRI study. Neurology 57, 2307-2310.

Obata, T., Liu, T.T., Miller, K.L., Luh, W.M., Wong, E.C., Frank, L.R., Buxton, R.B., 2004. Discrepancies between BOLD and flow dynamics in primary and supplementary motor areas: application of the balloon model to the interpretation of BOLD transients. Neuroimage 21, 144-153.

Ogawa, S., Lee, T.M., Kay, A.R., Tank, D.W., 1990. Brain magnetic resonance imaging with contrast dependent on blood oxygenation. Proc Natl Acad Sci U S A 87, 9868-9872.

Ogawa, S., Menon, R.S., Tank, D.W., Kim, S.G., Merkle, H., Ellermann, J.M., Ugurbil, K., 1993. Functional brain mapping by blood oxygenation level-dependent contrast magnetic resonance imaging. A comparison of signal characteristics with a biophysical model. Biophys J 64, 803-812.

Ohta, H., 1986. The effect of hyperoxemia on cerebral blood flow in normal humans. No To Shinkei 38, 949-959.

Parkes, L.M., 2005. Quantification of cerebral perfusion using arterial spin labeling: two-compartment models. J Magn Reson Imaging 22, 732-736.

Parkes, L.M., Rashid, W., Chard, D.T., Tofts, P.S., 2004. Normal cerebral perfusion measurements using arterial spin labeling: reproducibility, stability, and age and gender effects. Magn Reson Med 51, 736-743.

Parkes, L.M., Tofts, P.S., 2002. Improved accuracy of human cerebral blood perfusion measurements using arterial spin labeling: accounting for capillary water permeability. Magn Reson Med 48, 27-41.

Penny, W., Kiebel, S., Friston, K., 2003. Variational Bayesian inference for fMRI time series. Neuroimage 19, 727-741.

Perthen, J.E., Lansing, A.E., Liau, J., Liu, T.T., Buxton, R.B., 2008. Caffeine-induced uncoupling of cerebral blood flow and oxygen metabolism: a calibrated BOLD fMRI study. Neuroimage 40, 237-247.

Pineiro, R., Pendlebury, S., Johansen-Berg, H., Matthews, P.M., 2002. Altered hemodynamic responses in patients after subcortical stroke measured by functional MRI. Stroke 33, 103-109.

Rabi, I.I., Zacharius, J.R., Millman, S., Kusch, P., 1938. A new method of measuring nuclear magnetic moments. Physical review, 53:318.

Rashid, W., Parkes, L.M., Ingle, G.T., Chard, D.T., Toosy, A.T., Altmann, D.R., Symms, M.R., Tofts, P.S., Thompson, A.J., Miller, D.H., 2004. Abnormalities of cerebral perfusion in multiple sclerosis. J Neurol Neurosurg Psychiatry 75, 1288-1293.

Raz, N., Lindenberger, U., Rodrigue, K.M., Kennedy, K.M., Head, D., Williamson, A., Dahle, C., Gerstorf, D., Acker, J.D., 2005. Regional brain changes in aging healthy adults: general trends, individual differences and modifiers. Cereb Cortex 15, 1676-1689.

Reed, B.R., Eberling, J.L., Mungas, D., Weiner, M., Jagust, W.J., 2001. Frontal lobe hypometabolism predicts cognitive decline in patients with lacunar infarcts. Arch Neurol 58, 493-497.

Restom, K., Bangen, K.J., Bondi, M.W., Perthen, J.E., Liu, T.T., 2007. Cerebral blood flow and BOLD responses to a memory encoding task: a comparison between healthy young and elderly adults. Neuroimage 37, 430-439.

Restom, K., Perthen, J.E., Liu, T.T., 2008. Calibrated fMRI in the medial temporal lobe during a memory-encoding task. Neuroimage 40, 1495-1502.

Roberts, D.A., Detre, J.A., Bolinger, L., Insko, E.K., Leigh, J.S., Jr., 1994. Quantitative magnetic resonance imaging of human brain perfusion at 1.5 T using steady-state inversion of arterial water. Proc Natl Acad Sci U S A 91, 33-37.

Roberts, D.A., Rizi, R., Lenkinski, R.E., Leigh, J.S., Jr., 1996. Magnetic resonance imaging of the brain: blood partition coefficient for water: application to spin-tagging measurement of perfusion. J Magn Reson Imaging 6, 363-366.

Roman, G.C., Erkinjuntti, T., Wallin, A., Pantoni, L., Chui, H.C., 2002. Subcortical ischaemic vascular dementia. Lancet Neurol 1, 426-436.

Rosen, B.R., Belliveau, J.W., Aronen, H.J., Kennedy, D., Buchbinder, B.R., Fischman, A., Gruber, M., Glas, J., Weisskoff, R.M., Cohen, M.S., et al., 1991a.

Susceptibility contrast imaging of cerebral blood volume: human experience. Magn Reson Med 22, 293-299; discussion 300-293.

Rosen, B.R., Belliveau, J.W., Buchbinder, B.R., McKinstry, R.C., Porkka, L.M., Kennedy, D.N., Neuder, M.S., Fisel, C.R., Aronen, H.J., Kwong, K.K., et al., 1991b. Contrast agents and cerebral hemodynamics. Magn Reson Med 19, 285-292.

Rosen, B.R., Buckner, R.L., Dale, A.M., 1998. Event-related functional MRI: past, present, and future. Proc Natl Acad Sci U S A 95, 773-780.

Ross, M.H., Yurgelun-Todd, D.A., Renshaw, P.F., Maas, L.C., Mendelson, J.H., Mello, N.K., Cohen, B.M., Levin, J.M., 1997. Age-related reduction in functional MRI response to photic stimulation. Neurology 48, 173-176.

Rostrup, E., Law, I., Blinkenberg, M., Larsson, H.B., Born, A.P., Holm, S., Paulson, O.B., 2000. Regional differences in the CBF and BOLD responses to hypercapnia: a combined PET and fMRI study. Neuroimage 11, 87-97.

Roy, C.S., Sherrington, C.S., 1890. On the Regulation of the Blood-supply of the Brain. J Physiol 11, 85-158 117.

Sabri, O., Ringelstein, E.B., Hellwig, D., Schneider, R., Schreckenberger, M., Kaiser, H.J., Mull, M., Buell, U., 1999. Neuropsychological impairment correlates with hypoperfusion and hypometabolism but not with severity of white matter lesions on MRI in patients with cerebral microangiopathy. Stroke 30, 556-566.

Sasse, S.A., Berry, R.B., Nguyen, T.K., Light, R.W., Mahutte, C.K., 1996. Arterial blood gas changes during breath-holding from functional residual capacity. Chest 110, 958-964.

Schmidt, R., Enzinger, C., Ropele, S., Schmidt, H., Fazekas, F., 2006. Subcortical vascular cognitive impairment: similarities and differences with multiple sclerosis. J Neurol Sci 245, 3-7.

Schmidtke, K., Hull, M., 2005. Cerebral small vessel disease: how does it progress? J Neurol Sci 229-230, 13-20.

Schroeter, M.L., Cutini, S., Wahl, M.M., Scheid, R., Yves von Cramon, D., 2007. Neurovascular coupling is impaired in cerebral microangiopathy--An event-related Stroop study. Neuroimage 34, 26-34.

Schwarzbauer, C., Morrissey, S.P., Haase, A., 1996. Quantitative magnetic resonance imaging of perfusion using magnetic labeling of water proton spins within the detection slice. Magn Reson Med 35, 540-546.

Stefanovic, B., Warnking, J.M., Pike, G.B., 2004. Hemodynamic and metabolic responses to neuronal inhibition. Neuroimage 22, 771-778.

Takada, H., Nagata, K., Hirata, Y., Satoh, Y., Watahiki, Y., Sugawara, J., Yokoyama, E., Kondoh, Y., Shishido, F., Inugami, A., et al., 1992. Age-related decline of cerebral oxygen metabolism in normal population detected with positron emission tomography. Neurol Res 14, 128-131.

Thesen, S., Heid, O., Mueller, E., Schad, L.R., 2000. Prospective acquisition correction for head motion with image-based tracking for real-time fMRI. Magn Reson Med 44, 457-465.

Thomason, M.E., Foland, L.C., Glover, G.H., 2007. Calibration of BOLD fMRI using breath holding reduces group variance during a cognitive task. Hum Brain Mapp 28, 59-68.

Thulborn, K.R., Chang, S.Y., Shen, G.X., Voyvodic, J.T., 1997. High-resolution echo-planar fMRI of human visual cortex at 3.0 tesla. NMR Biomed 10, 183-190.

Tofts, P.S., 2003. Quantitative MRI of the Brain - Measuring changes caused by disease.

Tourdias, T., Rodrigo, S., Oppenheim, C., Naggara, O., Varlet, P., Amoussa, S., Calmon, G., Roux, F.X., Meder, J.F., 2008. Pulsed arterial spin labeling applications in brain tumors: practical review. J Neuroradiol 35, 79-89.

Uludag, K., 2008. Transient and sustained BOLD responses to sustained visual stimulation. Magn Reson Imaging 26, 863-869.

Uludag, K., Dubowitz, D.J., Yoder, E.J., Restom, K., Liu, T.T., Buxton, R.B., 2004. Coupling of cerebral blood flow and oxygen consumption during physiological activation and deactivation measured with fMRI. Neuroimage 23, 148-155.

Viswanathan, A., Freeman, R.D., 2007. Neurometabolic coupling in cerebral cortex reflects synaptic more than spiking activity. Nat Neurosci 10, 1308-1312.

Wardlaw, J.M., 2008. What is a lacune? Stroke 39, 2921-2922.

Watson, N.A., Beards, S.C., Altaf, N., Kassner, A., Jackson, A., 2000. The effect of hyperoxia on cerebral blood flow: a study in healthy volunteers using magnetic resonance phase-contrast angiography. Eur J Anaesthesiol 17, 152-159.

Wenz, F., Rempp, K., Brix, G., Knopp, M.V., Guckel, F., Hess, T., van Kaick, G., 1996. Age dependency of the regional cerebral blood volume (rCBV) measured with dynamic susceptibility contrast MR imaging (DSC). Magn Reson Imaging 14, 157-162.

Wilkinson, J.L., 1992. Neuroanatomy for medical students.

Williams, D.S., Detre, J.A., Leigh, J.S., Koretsky, A.P., 1992. Magnetic resonance imaging of perfusion using spin inversion of arterial water. Proc Natl Acad Sci U S A 89, 212-216.

Wolf, R.L., Detre, J.A., 2007. Clinical neuroimaging using arterial spin-labeled perfusion magnetic resonance imaging. Neurotherapeutics 4, 346-359.

Wolff, S.D., Balaban, R.S., 1989. Magnetization transfer contrast (MTC) and tissue water proton relaxation in vivo. Magn Reson Med 10, 135-144.

Wong, E.C., Buxton, R.B., Frank, L.R., 1997. Implementation of quantitative perfusion imaging techniques for functional brain mapping using pulsed arterial spin labeling. NMR Biomed 10, 237-249.

Woolrich, M.W., Chiarelli, P., Gallichan, D., Perthen, J., Liu, T.T., 2006. Bayesian inference of hemodynamic changes in functional arterial spin labeling data. Magn Reson Med 56, 891-906.

Yacoub, E., Duong, T.Q., Van De Moortele, P.F., Lindquist, M., Adriany, G., Kim, S.G., Ugurbil, K., Hu, X., 2003. Spin-echo fMRI in humans using high spatial resolutions and high magnetic fields. Magn Reson Med 49, 655-664.

Yamaguchi, T., Kanno, I., Uemura, K., Shishido, F., Inugami, A., Ogawa, T., Murakami, M., Suzuki, K., 1986. Reduction in regional cerebral metabolic rate of oxygen during human aging. Stroke 17, 1220-1228.

Yang, Y., Engelien, W., Pan, H., Xu, S., Silbersweig, D.A., Stern, E., 2000. A CBF-based event-related brain activation paradigm: characterization of impulse-response function and comparison to BOLD. Neuroimage 12, 287-297.

Yang, Y., Gu, H., Stein, E.A., 2004. Simultaneous MRI acquisition of blood volume, blood flow, and blood oxygenation information during brain activation. Magn Reson Med 52, 1407-1417.

Ye, F.Q., Mattay, V.S., Jezzard, P., Frank, J.A., Weinberger, D.R., McLaughlin, A.C., 1997. Correction for vascular artifacts in cerebral blood flow values measured by using arterial spin tagging techniques. Magn Reson Med 37, 226-235.

Yen, Y.F., Field, A.S., Martin, E.M., Ari, N., Burdette, J.H., Moody, D.M., Takahashi, A.M., 2002. Test-retest reproducibility of quantitative CBF measurements using FAIR perfusion MRI and acetazolamide challenge. Magn Reson Med 47, 921-928.

Zappe, A.C., Uludag, K., Oeltermann, A., Ugurbil, K., Logothetis, N.K., 2008. The influence of moderate hypercapnia on neural activity in the anesthetized nonhuman primate. Cereb Cortex 18, 2666-2673.

Zhang, W., Silva, A.C., Williams, D.S., Koretsky, A.P., 1995. NMR measurement of perfusion using arterial spin labeling without saturation of macromolecular spins. Magn Reson Med 33, 370-376.

Zhou, J., Wilson, D.A., Ulatowski, J.A., Traystman, R.J., van Zijl, P.C., 2001. Two-compartment exchange model for perfusion quantification using arterial spin tagging. J Cereb Blood Flow Metab 21, 440-455.

Zysset, S., Muller, K., Lohmann, G., von Cramon, D.Y., 2001. Color-word matching stroop task: separating interference and response conflict. Neuroimage 13, 29-36.

Zysset, S., Schroeter, M.L., Neumann, J., Yves von Cramon, D., 2007. Stroop interference, hemodynamic response and aging: An event-related fMRI study. Neurobiol Aging 28, 937-946.